Award Number: W81XWH-13-1-0129

TITLE: Maximizing PTH Anabolic Osteoporosis Therapy

PRINCIPAL INVESTIGATOR: JOSEPH BIDWELL

CONTRACTING ORGANIZATION:

TRUSTEES OF INDIANA UNIVERSITY
INDIANAPOLIS IN 46202-5130

REPORT DATE: September 2016

TYPE OF REPORT: Annual

PREPARED FOR: U.S. Army Medical Research and Materiel Command
Fort Detrick, Maryland 21702-5012

REPORT DOCUMENTATION PAGE

Form Approved
OMB No. 0704-0188

1. REPORT DATE	**2. REPORT TYPE**	**3. DATES COVERED**
September 2016	Annual	15 Aug 2015 - 14 Aug 2016

4. TITLE AND SUBTITLE

Maximizing PTH Anabolic Osteoporosis Therapy

5a. CONTRACT NUMBER

5b. GRANT NUMBER
W81XWH-13-1-0129

5c. PROGRAM ELEMENT NUMBER

6. AUTHOR(S)

Joseph Bidwell

E-Mail: jbidwell@iupui.edu

5d. PROJECT NUMBER

5e. TASK NUMBER

5f. WORK UNIT NUMBER

7. PERFORMING ORGANIZATION NAME(S) AND ADDRESS(ES)

TRUSTEES OF INDIANA UNIVERSITY
980 INDIANA AVE RM 2232
INDIANAPOLIS IN 46202-5130

8. PERFORMING ORGANIZATION REPORT NUMBER

9. SPONSORING / MONITORING AGENCY NAME(S) AND ADDRESS(ES)
U.S. Army Medical Research and Materiel Command
Fort Detrick, Maryland 21702-5012

10. SPONSOR/MONITOR'S ACRONYM(S)

11. SPONSOR/MONITOR'S REPORT NUMBER(S)

12. DISTRIBUTION / AVAILABILITY STATEMENT
Approved for Public Release; Distribution Unlimited

13. SUPPLEMENTARY NOTES
This is revised report

14. ABSTRACT

The purpose of this study is to test the efficacy of parathyroid hormone (PTH) mono-therapy and PTH+ anti-catabolic combination therapies on *Nmp4*$^{-/-}$ and wild type (WT) mice. **The scope of** the research comprises the following specific aims: (i & ii) to determine the impact of Nmp4 on the efficacy of PTH mono- and combination therapies with various anti-catabolics in ovariectomized (ovx) mice; (iii) to determine the cell type-specific contributions to the enhanced response of the *Nmp4*$^{-/-}$ mouse to these osteoporosis therapies. **In Year 3** we determined that loss of Nmp4 increases bone marrow osteoprogenitor number and converts osteoprogenitors into super-secretor osteoblasts by elevated ribosome biogenesis and the expansion of the ER protein processing capacity. **The most significant findings during the YEAR 3 period include the following**:

- Key finding #1: *Nmp4*$^{-/-}$ *osteoprogenitors are differentially responsive to PTH+RAL and PTH+ZOL.*
- Key finding #2: *The Nmp4*$^{-/-}$ *mice exhibited higher levels of serum osteocalcin compared to WT mice*
- Key finding #3: *Loss of Nmp4 did not significantly alter bone resorption*
- Key finding #4: *Loss of Nmp4 did not significantly alter serum OPG/RANKL ratios.*
- Key finding #5: *Loss of Nmp4 did not significantly alter the number of bone marrow adipocytes*
- Key finding #6: *The Nmp4*$^{-/-}$ *osteoprogenitor is a super-secretor cell*
- Key finding #7: *The Nmp4*$^{-/-}$ *osteoprogenitor over-extended ER machinery is sensitized to ZOL-induced apoptosis.*

15. SUBJECT TERMS
Nmp4-knockout (KO) mice, osteoporosis, ovariectomy, PTH combination therapies

16. SECURITY CLASSIFICATION OF:			**17. LIMITATION OF ABSTRACT**	**18. NUMBER OF PAGES**	**19a. NAME OF RESPONSIBLE PERSON**
a. REPORT	**b. ABSTRACT**	**c. THIS PAGE**			USAMRMC
U	U	U	UU	45	**19b. TELEPHONE NUMBER** *(include area code)*

Table of Contents

INTRODUCTION: The **subject of this research** is the need for improved osteoporosis therapies. The **study purpose** is to test the efficacy of parathyroid hormone (PTH) mono-therapy and PTH+anti-catabolic combination therapies on ovariectomized (ovx) *Nmp4*$^{-/-}$ and wild type (WT) mice. We previously determined that Nmp4 represses bone response to osteoanabolics[1-3]. The **research scope** comprises the following goals: **Specific Aims #1 & #2**, determine Nmp4 impact on the efficacy of PTH mono- and combination therapies with bisphosphonates and raloxifene; **Specific Aim #3**, to determine the cell type-specific contributions to the enhanced response of the *Nmp4*$^{-/-}$ mouse to these osteoporosis therapies.

BODY:

TABLE I: SYNOPOSIS OF 3rd YEAR PROGRESS REPORT

REPORT FIGURE	SOW SUBTASK(S)	SOW TASK DESCRIPTION	RESULTS DESCRIBED IN FIGURE OR APPENDIX
FIGURE 1	Subtask 2.1.g.3 Subtask 2.2.e.3 Subtask 3.5.c	Obtain and analyze μCT samples from WT and *Nmp4*$^{-/-}$ mice upon completion of the following treatments VEH, ALN, ZOL, RAL, PTH, PTH+ALN, PTH+ZOL, & PTH+RAL	Summary of skeletal response to mono-therapies and combination treatments to place more recent findings in context
FIGURE 2	Subtask 2.1.g.2 Subtask 2.2.e.2 Subtask 3.5.b	Obtain and analyze BM and PBL samples from treatments including VEH-, PTH- and PTH+RAL-treated mice	Example of immunohistochemical micrographs of BM osterix-positive cells for counting osteoprogenitors
FIGURE 3	Subtask 2.1.g.2 Subtask 2.2.e.2 Subtask 3.5.b	Obtain and analyze BM and PBL samples from treatments including VEH-, PTH- RAL-, PTH+ZOL- and PTH+RAL-treated mice	BM osterix-positive cell counts and statistical analyses derived from immunohistochemical analyses
FIGURE 4	Subtask 2.1.g.2 Subtask 2.2.e.2 Subtask 3.5.b	Obtain and analyze BM and PBL samples from treatments including VEH-, PTH- and PTH+RAL-treated mice	Immunohistochemical micrographs of BM osteocalcin-positive cells for visually assessing bone anabolic activity
FIGURE 5	Subtask 2.1.g.1 Subtask 2.2.e.1 Subtask 3.5.a	Obtain and analyze DXA and serum samples from treatments including VEH-, PTH- RAL-, PTH+ZOL- and PTH+RAL-treated mice	Serum OCN measurements and statistical analysis for comparison of select treatment cohorts
FIGURE 6	Subtask 2.1.g.2 Subtask 2.2.e.2 Subtask 3.5.b	Obtain and analyze BM and PBL samples from treatments including VEH-, PTH- and PTH+RAL-treated mice	Immunohistochemical micrographs of BM TRAP-positive cells for counting osteoclast progenitors and osteoclasts
FIGURE 7	Subtask 2.1.g.2 Subtask 2.2.e.2 Subtask 3.5.b	Obtain and analyze BM and PBL samples from treatments including VEH-, PTH- RAL-, PTH+ZOL- and PTH+RAL-treated mice	BM TRAP+ S/BS and statistical analyses derived from immunohistochemical analyses
FIGURE 8	Subtask 2.1.g.1 Subtask 2.2.e.1 Subtask 3.5.a	Obtain and analyze DXA and serum samples from treatments including VEH-, PTH- RAL-, PTH+ZOL- and PTH+RAL-treated mice	Serum CTX measurements and statistical analysis for comparison of select treatment cohorts
FIGURE 9	Subtask 2.1.g.1 Subtask 2.2.e.1 Subtask 3.5.a	Obtain and analyze DXA and serum samples from treatments including VEH-, PTH- RAL-, PTH+ZOL- and PTH+RAL-treated mice	Serum OPG/RANKL measurements and statistical analysis for comparison of select treatment cohorts
FIGURE 10	Subtask 2.1.g.2 Subtask 3.5.b	Obtain and analyze BM and PBL samples from treatments including VEH-, PTH- and PTH+RAL-treated mice	Examples of immunohistochemical micrographs of BM adipocytes for counting fat cells
FIGURE 11	Subtask 2.1.g.2 Subtask 2.2.e.2 Subtask 3.5.b	Obtain and analyze BM and PBL samples from VEH-, PTH- RAL-, PTH+ZOL- and PTH+RAL-treated mice	BM adipocyte cell counts and statistical analyses derived from immunohistochemical analyses
FIGURE 12	Subtask 2.1.g.2 Subtask 6.2	Obtain and analyze BM and PBL samples and culture/expand both WT & *Nmp4*$^{-/-}$ MSPCs	MTT assay showing differential sensitivity of *Nmp4*$^{-/-}$ and WT BM osteoprogenitors to ZOL and RAL
FIGURE 13	Subtask 4.2.a Subtask 4.3.a	Breed *Nmp4*$^{fl/fl}$ 3.6Col-Cre+ & *Nmp4*$^{fl/fl}$-Cre– mice; Breed *Nmp4*$^{fl/fl}$ Cat K-Cre+ & *Nmp4*$^{fl/fl}$-Cre–	Map of Nmp4 (Zfp384) floxed construct
Appendix Manuscript 1	Subtask 2.1.g.2 Subtask 6.2	Obtain and analyze BM and PBL samples from treatments (VEH) and expand both WT & *Nmp4*$^{-/-}$ MSPCs for phenotype analysis	Published study describes molecular basis of BM osteoprogenitors as having enhanced capacity for secretion
Appendix Manuscript 2	Subtask 2.1.a-2.1.g.3 Subtask 6.2	Conduct PTH mono-therapy experiments and analyze bone (μCT), BM, and serum. Expand WT & *Nmp4*$^{-/-}$ MSPCs for phenotype analysis.	Published study describes improved response of ovariectomized *Nmp4*$^{-/-}$ mice to PTH mono-therapy and alterations in *Nmp4*$^{-/-}$ BM osteoprogenitors

Abbreviations in Table I and SOW:

ALN:	Alendronate
BM:	Bone Marrow
CTX:	C-terminal telopeptides
DXA:	Dual X-ray absorptiometry
µCT:	Micro-computed tomography
MSC:	Mesenchymal stem cell
MSPC:	Mesenchymal stem/progenitor cell
Nmp4$^{-/-}$:	global knockout (KO) of *nuclear matrix protein 4*
OCN:	Osteocalcin
OPG:	Osteoprotegerin
PBL:	Peripheral blood
PTH:	parathyroid hormone
RAL:	Raloxifene (abbreviated RALOX in the original SOW)
RANKL:	Receptor activator of nuclear factor-κB ligand
TRAP+:	tartrate-resistant acid phosphatase
TRAP+ S/BS:	TRAP-positive cell surface/bone surface
VEH:	Vehicle control
WT:	Wild type
ZOL:	Zolendronate

Overview of Scientific Discoveries To Date:

- **Year 1** we determined that the exaggerated response to anabolic doses of PTH observed in healthy *Nmp4*$^{-/-}$ mice[1-3] was preserved in ovx *Nmp4*$^{-/-}$ mice but that disabling this transcription factor did not protect them from ovx-induced bone loss without therapy[4].
- **Year 2** we ascertained that PTH+RAL added the most bone in WT and *Nmp4*$^{-/-}$ mice followed by PTH+ZOL with synergistic drug interactions (PTH x anti-catabolic) in both therapies. Loss of Nmp4 enhanced increases in femoral BV/TV under PTH mono-therapy (genotype x treatment interaction), PTH+RAL, and PTH+ZOL but did not augment the anti-catabolic mono-therapies. The *Nmp4*$^{-/-}$ mice showed an enhanced vertebral trabeculae thickening and an increased responsiveness of this parameter to multiple treatments.
- **Year 3** *we focused on analyzing the bone marrow of the Nmp4*$^{-/-}$ *mice and the mesenchymal stem/progenitor cells (MSPCs)/osteoprogenitors because these cells appear to be driving the enhanced bone formation under anabolic therapies*. We determined that loss of Nmp4 increased the number of bone marrow osteoprogenitors and converts them into super-secretor osteoblasts as a result of enhanced protein production and secretion mediated by elevated ribosome biogenesis and the expansion of the endoplasmic reticulum (ER) protein processing capacity, respectively. The enhanced protein secretion appears to be via alterations in the unfolded protein response (UPR)[5]. However, this escalated secretory activity comes at a cost. *Nmp4*$^{-/-}$ osteoprogenitors are more vulnerable to UPR-induced apoptosis compared to WT cells[5]. This may explain our finding that co-treatment with ZOL significantly attenuated the PTH-induced increase in the *Nmp4*$^{-/-}$ bone marrow osteoprogenitor pool and that co-treatment with RAL enhanced hormone-mediated expansion of this osteogenic reserve. WT mice did not show this dichotomy. Bisphosphonates trigger UPR-induced ER stress in multiple cell types via their inhibition of farnesyl pyrophosphate synthase activity[6]. Therefore challenge with ZOL may further stress the already over-extended *Nmp4*$^{-/-}$ ER machinery whereas RAL does not. *This has considerable clinical significance because it may explain why the PTH+RAL therapy typically outperformed the PTH+ZOL treatment in the null mice. Understanding how disabling Nmp4 enhances osteoprogenitor/osteoblast capacity for making bone matrix will provide information on designing Nmp4-based adjuvant therapies for osteoporosis treatment*.

SUMMARY OF KEY FINDINGS FOR YEAR 3:

- **Key finding #1:** *Nmp4*$^{-/-}$ mice harbored more osteoprogenitors under the PTH+RAL therapy than under the PTH+ZOL treatment. ZOL appeared to significantly attenuate PTH-induced expansion of the *Nmp4*$^{-/-}$ osteogenic reserve. WT mice did not show this dichotomy.
  - Figures: 2 & 3
  - Tasks: Subtasks 2.1.g.2, 2.2.e.2, & 3.5.b

- **Key finding #2:** The *Nmp4*$^{-/-}$ mice exhibited higher levels of serum osteocalcin compared to WT mice.
  - Figures: Figures 4 & 5
  - Tasks: Subtasks 2.1.g.1, 2.1.g.2, 2.2.e.1, 2.2.e.2, 3.5.a, 3.5.b

- **Key finding #3:** Loss of Nmp4 did not significantly alter bone resorption activity under the various treatments as evaluated by immunohistochemistry (TRAP+ surface/bone surface) and serum analysis (C-terminal telopeptide, CTX].
  - Figures: 6, 7, 8
  - Tasks: Subtasks 2.1.g.1, 2.1.g.2, 2.2.e.1, 2.2.e.2, 3.5.a, 3.5.b

- **Key finding #4:** Loss of Nmp4 did not significantly alter the serum OPG/RANKL ratio
  - Figure: 9
  - Tasks: Subtasks 2.1.g.1, 2.2.e.1, 3.5.a

- **Key finding #5:** Loss of Nmp4 did not significantly alter the number of bone marrow adipocytes. Treatment of mice with PTH mono-therapy or the PTH+anti-catabolic combination therapies significantly reduced marrow adipogenesis.
  - Figures: 10 & 11
  - Tasks: Subtasks 2.1.g.2, 2.2.e.2, 3.5.b

- **Key finding #6:** Our analysis of the WT and *Nmp4*$^{-/-}$ BM revealed that loss of Nmp4 converted the MSPCs/osteprogenitors to super-secretor cells[4,5]. These cells produce and release more bone matrix than WT osteoblasts. This unique MSPC/osteoprogenitor phenotype was determined to be the result of elevated ribosome biogenesis and an expanded capacity of the endoplasmic reticulum (ER) to process and fold proteins destined for the bone matrix. This enhanced ER capacity was a result of select alterations in the unfolded protein response (UPR)[4,5].
  - Appendix: Manuscript #1, Young et al., 2016; Manuscript #2, Childress et al., 2015
  - Tasks: Subtasks 2.1.g.2 & 6.2

- **Key finding #7:** The escalated secretory activity of the *Nmp4*$^{-/-}$ cells comes at a cost. In Manuscript #1 (Appendix) we demonstrated that the *Nmp4*$^{-/-}$ MSPC is sensitized to pharmacological ER stress[5]. Specifically, the *null* cells were more susceptible to tunicamycin-induced apoptosis than the WT cells. Tunicamycin antagonizes the cell protein-folding machinery causing ER stress and ultimately apoptosis. We interpret these results to mean that the already extended *Nmp4*$^{-/-}$ ER machinery in these super-secretor cells cannot manage added demand. We propose that this contributes to ZOL suppression of PTH-induced increases in *Nmp4*$^{-/-}$ bone marrow osteoprogenitors (Figure 3). Bisphosphonates, including ZOL trigger UPR-induced ER stress in multiple cell types via their inhibition of farnesyl pyrophosphate synthase activity[6]. Preliminary MTT assays show that bone marrow *Nmp4*$^{-/-}$ MSPCs are more sensitive to ZOL-induced apoptosis than WT cells. Conversely, *Nmp4*$^{-/-}$ MSPCs are more responsive to RAL-induced proliferation than WT cells.
  - Figure 12:
  - Appendix: Manuscript #1, Young et al., 2016
  - Tasks: Subtasks 2.1.g.2 & 6.2

EXPERIMENTAL THERAPIES:

- WT and *Nmp4*$^{-/-}$ mice were ovx'ed at 12wks of age
- At 16wks of age the mice were treated with the following therapies for 8wks:
  - Vehicle (VEH) control
  - Alendronate [ALN, 1µg/kg/d]
  - Zolendronate [ZOL, 80µg/kg 1X dose]
  - Raloxifene [RAL, 1mg/kg/d]
  - hPTH(1-34) [PTH, 30µg/kg/d]
  - Combination PTH+ALN
  - Combination PTH+ZOL
  - Combination PTH+RAL

To place **Year 3** data in context **Figure 1** summarizes a key finding from **Year 2**, showing that disabling Nmp4 enhanced PTH-, PTH+RAL-, and PTH+ZOL-induced increases in femoral BV/TV.

A. Femoral BV/TV, 24wks

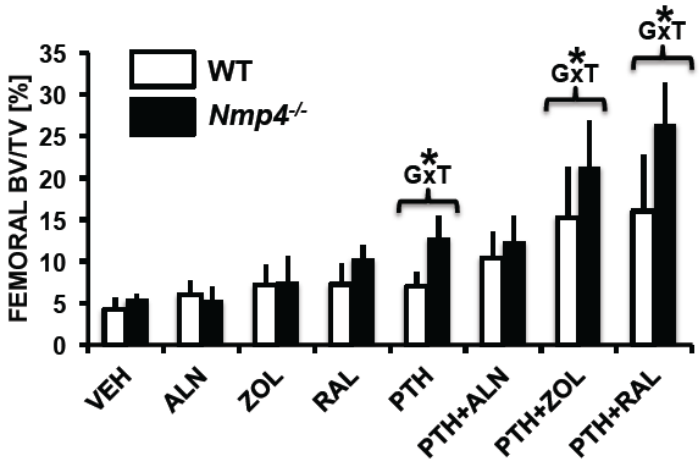

B. Genotype effect [p<0.0001]
Student's t post hoc

LEVEL		MEAN
Nmp4$^{-/-}$	A	12.71
WT	B	9.19

Levels not connected by same letter are significantly different

C. Treatment effect [p<0.0001]
Tukey-Kramer post-hoc

LEVEL		MEAN
PTH+RAL	A	21.72
PTH+ZOL	A	18.31
PTH+ALN	B	11.41
PTH	BC	9.94
RAL	BCD	8.81
ZOL	CDE	7.31
ALN	DE	19.76
VEH	E	19.65

D. Genotype x treatment effect [p<0.0001]
Tukey-Kramer post hoc

LEVEL		MEAN
Nmp4$^{-/-}$ PTH+RAL	A	26.48
Nmp4$^{-/-}$ PTH+ZOL	AB	21.38
WT PTH+RAL	BC	16.06
WT PTH+ZOL	CD	15.25
Nmp4$^{-/-}$ PTH	CDE	12.86
Nmp4$^{-/-}$ PTH+ALN	CDEF	12.36
WT PTH+ALN	DEFG	10.45
Nmp4$^{-/-}$ RAL	CDEFG	10.38
Nmp4$^{-/-}$ ZOL	EFGH	7.48
WT RAL	EFGH	7.25
WT ZOL	EFGH	7.14
WT PTH	FGH	7.03
WT ALN	GH	6.04
Nmp4$^{-/-}$ VEH	GH	5.46
Nmp4$^{-/-}$ ALN	GH	5.31
WT VEH	H	4.25

Figure 1: **TASKS: Subtasks 2.1.g.3, 2.2.e.3, 3.5.c** Femoral BV/TV (24wks of age) for WT and *Nmp4*$^{-/-}$ mice under all treatment groups [A] The bar graph represents the means of femoral BV/TVs for all the experimental cohorts. The data were analyzed using a 2W ANOVA using genotype and treatment as the independent variables. [B] There was a significant genotype effect ($p<0.0001$). A Student's t post hoc test showed that the *Nmp4*$^{-/-}$ mice as a group exhibited a higher femoral BV/TV than the WT mice. [C] There was a significant treatment effect ($p<0.0001$). A Tukey-Kramer HSD post hoc test revealed the differences between all the means of the treatment cohorts combing WT and *Nmp4*$^{-/-}$ mice. The mice under the PTH+RAL and PTH+ZOL therapies had the highest femoral BV/TV. The PTH and RAL mono-therapies were the only single drug treatments to significantly enhance BV/TV femoral over the VEH cohorts. [D] There was a strong genotype x treatment (G x T) interaction. A Tukey-Kramer HSD post hoc test revealed that loss of Nmp4 improved the PTH+RAL-, PTH+ZOL-, and PTH-induced gain in femoral BV/TV. The data represents average ± SD, n=7-12 mice/group.

KEY FINDING #1: *Nmp4*$^{-/-}$ mice harbor more osteoprogenitors than WT mice. *Nmp4*$^{-/-}$ mice harbor more osteoprogenitors under PTH+RAL therapy than the PTH+ZOL treatment. WT mice don't show this dichotomy.

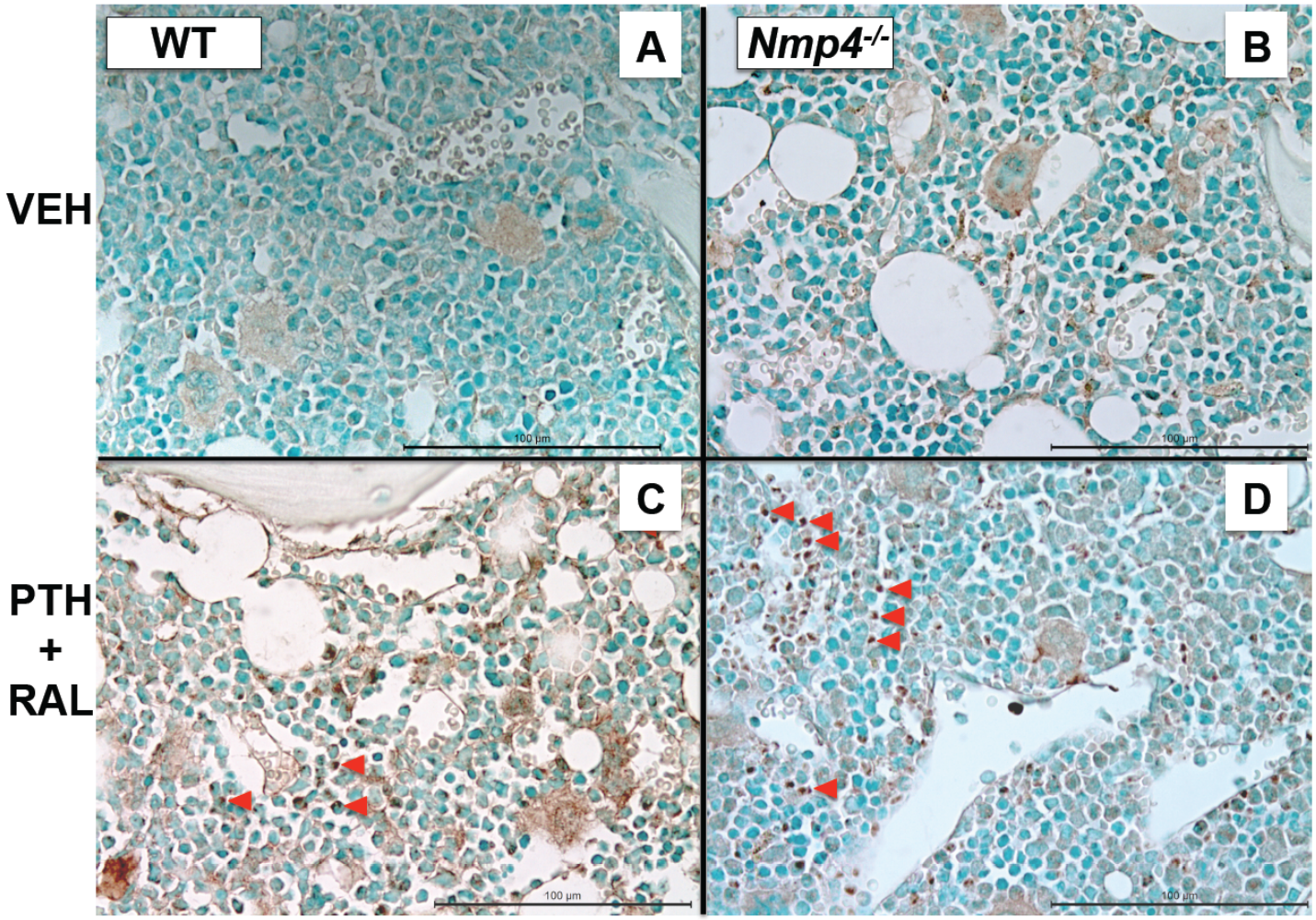

Figure 2: **TASKS: Subtasks 2.1.g.2, 2.2.e.2, 3.5.b** Immunohistochemical micrographs of bone marrow sections from the experimental cohorts [A] WT vehicle control (VEH); [B] *Nmp4*$^{-/-}$ VEH; [C] WT PTH+RAL treatment and [D] *Nmp4*$^{-/-}$ PTH+RAL. Cells exhibiting a brown nucleus (red arrowheads) were counted as positive for osterix, a marker for marrow osteoprogenitors (see text for details). The data represents typical image obtained from n=4-6 mice/group.

To interrogate the basis underlying the improved response of *Nmp4*$^{-/-}$ mice over the WT animals to PTH+RAL and PTH+ZOL we assessed the number of bone marrow osteoprogenitor cells in these cohorts. Immunohistochemical analysis was used to identify cells expressing the osteoblast-specific transcription factor osterix[7], (see Figure 2). Osterix was detected on formalin-fixed, paraffin-embedded sections by using a primary antibody from AbCam (human anti-SP7/osterix, #ab 94744). We followed the protocol described by Nissenson and colleagues with some modifications[8,9]. Briefly, slides were de-paraffinized at room temperature in Coplin jars in three washes of xylene, and rehydrated in a decreasing ethanol gradient. Endogenous peroxidases were deactivated with 3% H_2O_2 for 5 min, and sections were blocked in PBS supplemented with 1.5% goat serum (Gibco BRL) for 30 min at room temperature. Sections were incubated with primary antibody (1:25 dilution) in blocking solution overnight at 4°C. Sections were then washed in PBS and incubated with the biotinylated goat anti-rabbit IgG for 45 min at room temperature. After washing with PBS, sections were incubated with VECTASTAIN® ABC Reagent for 30 min at room temperature, followed by washing in buffer for 5 minutes. Incubating sections in peroxidase substrate solution according to the manufacturer's instructions achieved color development. Finally, counterstaining was accomplished by staining with 0.2% methyl green for 60-90 seconds, followed by dehydration in a series of ethanol and xylene changes and mounted using coverslips with xylene-based mounting media.

The osterix-positive cells exhibited a strong nuclear brown stain (Figure 2). We used a semiautomatic analysis system (Bioquant OSTEO 7.20.10, Bioquant Image Analysis Co., Nashville, TN, USA) to count

osteoprogenitors. The number of osterix-positive cells were counted in a 1mm² area approximately 1mm below the growth plate of the distal femur.

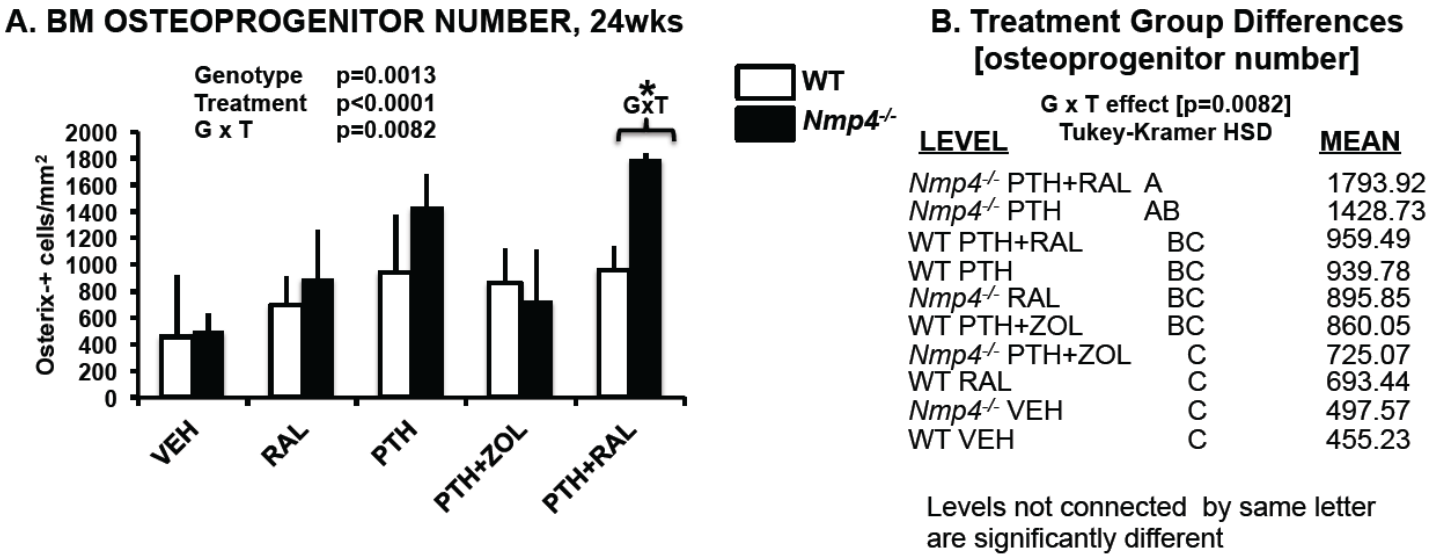

Figure 3: TASKS: Subtasks 2.1.g.2, 2.2.e.2, 3.5.b. The number of BM osterix-positive cells and serum osteocalcin in WT and *Nmp4*$^{-/-}$ mice under 5 of the 8 different therapies. [A] Bar graphs showing osterix-positive cells counts. The data were analyzed employing a 2W ANOVA using genotype and treatment as the independent variables followed by a Tukey-Kramer HSD post-hoc test. There was a significant genotype effect demonstrating that the *Nmp4*$^{-/-}$ marrow exhibited more osterix-positive cells than the WT marrow. There was a significant treatment effect ($p<0.0001$) and a strong G x T interaction ($p=0.0082$). [B] A Tukey-Kramer HSD post hoc test revealed the differences between all the means of the treatment cohorts using the connecting letter format. The mice under the PTH+RAL had the highest number of osteoprogenitors and had significantly more than the WT PTH+RAL cohort. The *Nmp4*$^{-/-}$ PTH+ZOL cohort had significantly fewer bone marrow osterix-positive cells that these mice under PTH mono-therapy or PTH+RAL, whereas the WT mice did not exhibit any difference in osterix-positive cell number between these three therapies. The data represents average ± SD, n=4-6 mice/group.

The cell counts were compared using a 2W ANOVA with genotype and treatment as independent variables. *Nmp4*$^{-/-}$ mice typically harbored more osteoprogenitors than WT mice (genotype effect, Figure 3A). There was a strong treatment effect and a genotype x treatment interaction (Figure 3A). A Tukey-Kramer HSD post hoc test revealed that the *Nmp4*$^{-/-}$ PTH+RAL cohort harbored significantly more bone marrow osteoprogenitors than the other treatment groups, with the exception of the *Nmp4*$^{-/-}$ PTH mono-therapy group (Figure 3B). The PTH+RAL therapy showed a genotype x treatment interaction. *Nmp4*$^{-/-}$ mice harbored significantly more bone marrow osteoprogenitors under the PTH+RAL therapy than under the PTH+ZOL treatment. These results suggest that co-treatment with ZOL significantly attenuated the PTH-induced increase in the *Nmp4*$^{-/-}$ bone marrow osteoprogenitor pool and that co-treatment with RAL enhanced hormone-mediated expansion of this osteogenic reserve. These dichotomous effects were much weaker in the WT mice (Figure 3A & 3B).

KEY FINDING #2: The *Nmp4*$^{-/-}$ mice exhibited higher levels of serum osteocalcin compared to WT mice.

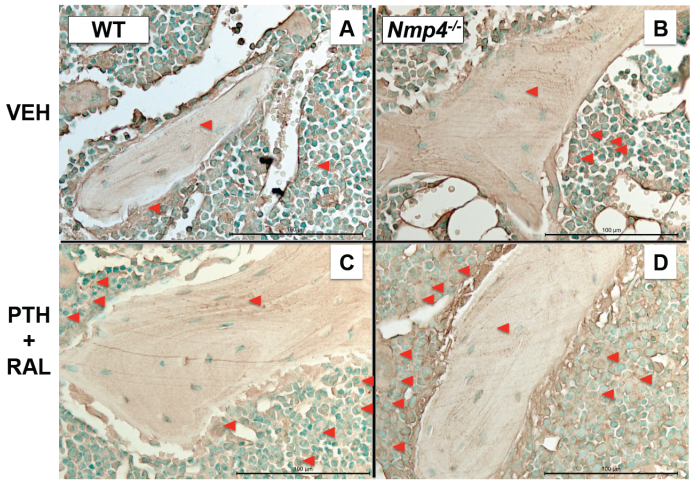

Figure 4: TASKS: Subtask 2.1.g.2, 2.2.e.2, 3.5.b. Immunohistochemical micrographs of bone marrow sections from the experimental cohorts [A] WT vehicle control (VEH); [B] *Nmp4*$^{-/-}$ VEH; [C] WT PTH+RAL treatment and [D] *Nmp4*$^{-/-}$ PTH+RAL. The brown stain within and surrounding the cells (red arrowheads) indicate examples of osteocalcin-positive cells in the marrow from WT and *Nmp4*$^{-/-}$ mice. An increase in staining was observed in mice under the therapies that included PTH. See text for experimental details. These data represents typical image obtained from n=4-6 mice/group.

We performed immunohistochemical staining for the bone matrix protein osteocalcin as an indicator of local anabolic activity (Figure 4). We also evaluated serum osteocalcin as a marker for global bone formation (Figure 5, see next page). Osteocalcin was detected on formalin-fixed, paraffin-embedded sections as described above for osterix with the exceptions that the osteocalcin primary antibody was from Takara (mouse osteocalcin, #M173). Also antigen retrieval was

necessary and was performed using 0.5% trypsin for 30 min at 37°C in a humidified chamber. Finally, sections were incubated with primary antibody 1:200 dilution in blocking solution overnight at 4°C. Sections were then washed in PBS and incubated with the biotinylated goat anti-rabbit IgG (VectaStain® Elite ABC Kit, Vector Laboratories, Inc. Burlingame, CA) for 45 min at room temperature.

The immunohistochemical analysis showed osteocalcin as a brown stain within bone marrow cells and/or surrounding these cells as a halo (Figure 4, previous page). Osteocalcin was also apparent in the trabecular bone as a light brown stain. Bone marrow tissue samples obtained from WT and *Nmp4*$^{-/-}$ mice under the PTH+RAL therapy stained more intensely for osteocalcin than those bone sections derived from animals maintained under the vehicle-control treatment (Figure 4, previous page).

Serum osteocalcin was evaluated at 24wks of age as a global bone formation marker using the ELISA BTI Mouse Osteocalcin EIA kit (Biomedical Technologies, Inc., Stoughton MA) following the manufacturers instructions. Serum osteocalcin levels were compared using a 2W ANOVA with genotype and treatment as independent variables (Figures 5A & 5B). *Nmp4*$^{-/-}$ mice as a group showed modest but significantly higher serum osteocalcin levels than WT mice (genotype effect, Figure 5A). There was a strong treatment effect but no genotype x treatment interaction (Figure 5A). A Tukey-Kramer HSD post hoc test of the treatment groups (combining WT and *Nmp4*$^{-/-}$ cohorts) revealed that PTH, PTH+ZOL, and PTH+RAL therapies elevated serum osteocalcin as compared to the VEH and RAL cohorts (Figure 5B).

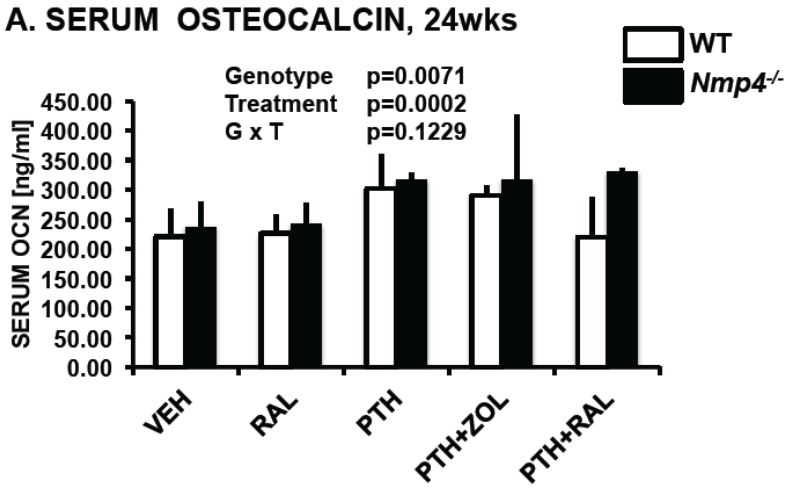

B. Treatment Group Differences [serum osteocalcin]

Treatment effect [p=0.0082]

LEVEL	Tukey-Kramer HSD	MEAN
PTH	A	309.53
PTH+ZOL	A	303.42
PTH+RAL	AB	275.21
RAL	B	233.86
VEH	B	229.40

Levels not connected by same letter are significantly different

Figure 5: **TASKS: Subtasks 2.1.g.1, 2.2.e.1, 3.5.a.** Serum osteocalcin in WT and *Nmp4*$^{-/-}$mice at the end of the indicated treatments (24wks of age). [A] The bar graph represents the means of serum osteocalcin for 10 of the experimental cohorts. The data were analyzed using a 2W ANOVA using genotype and treatment as the independent variables. There were significant genotype (G) and treatment (T) effects but no GxT interactions. [B] A Tukey-Kramer HSD post hoc test revealed the differences between all the means of the treatment cohorts, combing WT and *Nmp4*$^{-/-}$ mice (no GxT interaction). The PTH, PTH+RAL, and PTH+ZOL elevated serum osteocalcin. The data represents average±SD, n=5-7 mice/group. See text for details

KEY FINDING #3: Loss of Nmp4 did not significantly alter bone resorption activity under the various treatments as evaluated by immunohistochemistry (TRAP+ surface/bone surface) and serum analysis (C-terminal telopeptide, CTX].

Nmp4 is expressed in all tissues throughout the body[10], but its global loss appears to primarily impact bone and sporadically spermatogenesis[11]. The *Nmp4*$^{-/-}$ mice employed in these experiments are global knockouts and thus our analyses of the bone marrow of this model (Subtasks 2.1.g.2, 2.2.e.2, 3.5.b) must include the bone resorption arm.

To evaluate whether loss of Nmp4 influenced bone marrow osteoclasts we used histochemical staining to assess the surface of tartrate-resistant acid phosphatase (TRAP)-positive cells/bone surface (TRAP+ S/BS). The protocol outlined by Erlebacher and Derynchk[12] with some minor modifications was employed. Briefly, de-paraffinized slides were rehydrated with sequential ethanol washes. After equilibration in 0.2 M sodium acetate, 50 mM sodium tartrate, pH 5.0, for 20 min at room temperature, sections were incubated for 60 min at 37°C in the same buffer containing 0.5 mg/ml naphthol AS-MX phosphate (Sigma Chem. Co., St. Louis, MO) and 1.1 mg/ml fast red TR salt (Sigma). Sections were counterstained with toluidine blue. Finally the slides were dried for 24 hours. Aqueous-base mounting media was added on top of the sample and coverslip was applied.

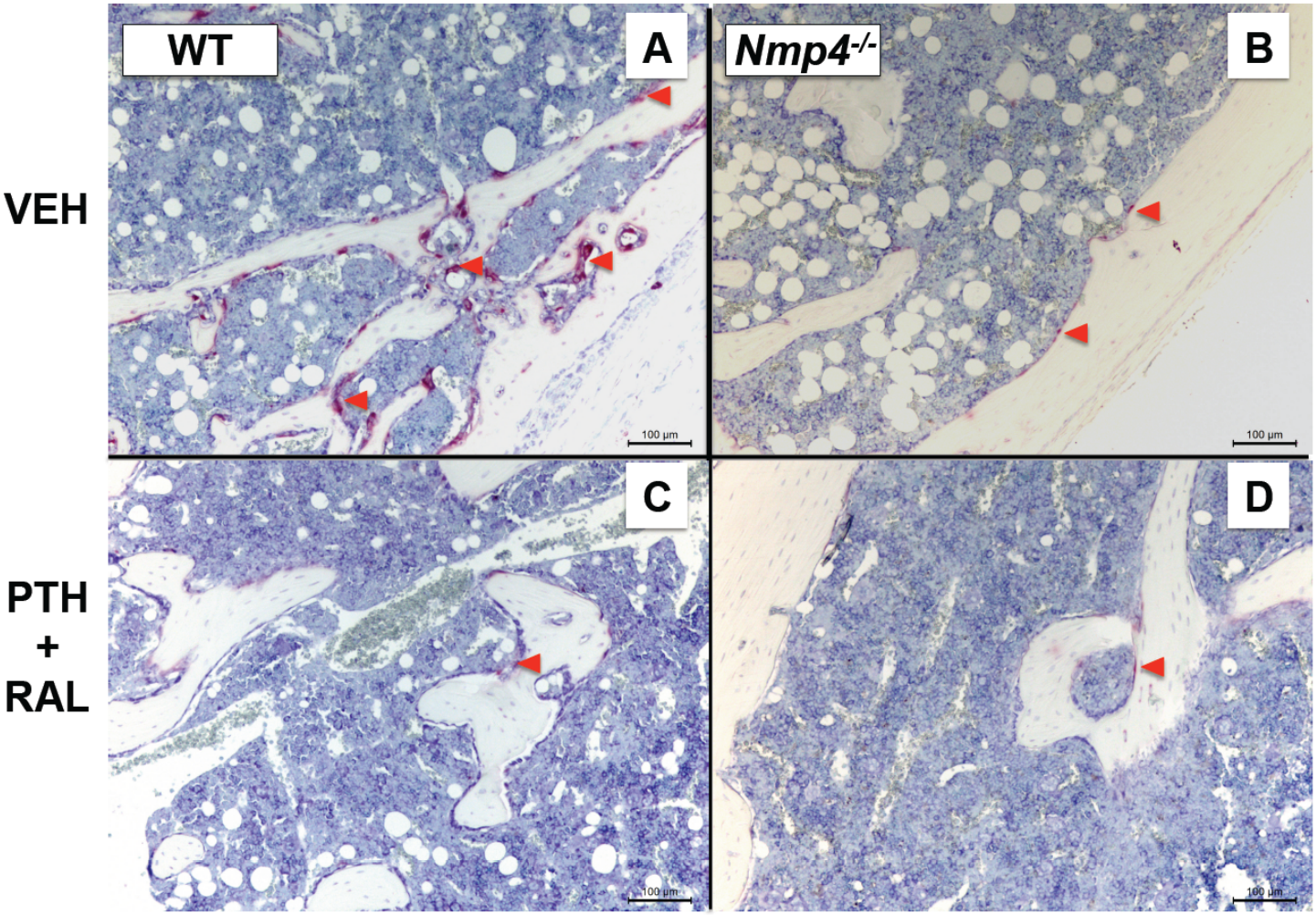

Figure 6: **TASKS: Subtasks 2.1.g.2, 2.2.e.2, 3.5.b.** Immunohistochemical micrographs of bone marrow sections from the experimental cohorts [A] WT vehicle control (VEH); [B] *Nmp4*$^{-/-}$ VEH; [C] WT PTH+RAL treatment and [D] *Nmp4*$^{-/-}$ PTH+RAL. Cells exhibiting a red staining (red arrowheads) were counted as positive for TRAP, a marker for marrow osteoclast progenitors or osteoclasts (see text for details). The data represents typical image obtained from n=7 mice/group.

The bone marrow sections from the vehicle-treated cohorts showed several TRAP+ cells along the bone trabeculae (Figures 6A & 6B). The slides derived from the PTH+RAL cohorts showed somewhat fewer TRAP+ cells than the vehicle controls (Figures 6C & 6D).

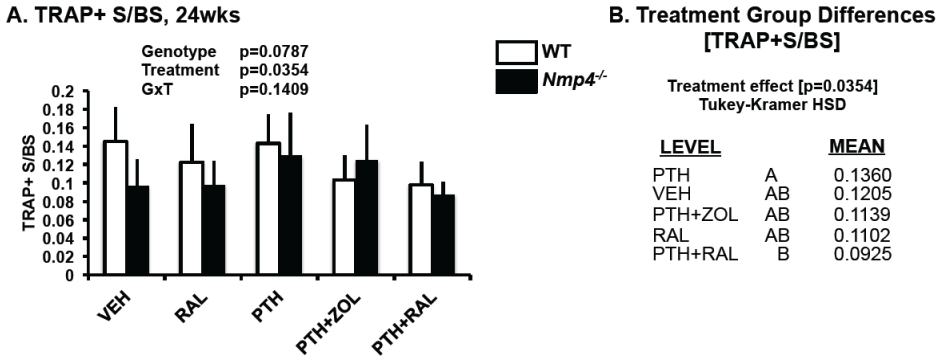

Figure 7: **TASKS: Subtask 2.1.g.2, 2.2.e.2, 3.5.b** TRAP+ S/BS in WT and *Nmp4*$^{-/-}$ mice under 5 of the 8 different therapies. [A] Bar graphs showing TRAP+ S/BS. The data were analyzed with a 2W ANOVA using genotype (G) and treatment (T) as independent variables followed by a Tukey-Kramer HSD post-hoc test. There was no genotype effect or G x T interaction. There was a treatment effect (p=0.0354) [B] The post hoc test revealed the differences between all the means of the treatment cohorts combing WT and *Nmp4*$^{-/-}$ mice. Statistically there was no difference between most of the treatment groups except for the PTH mono-therapy, which had the highest TRAP+S/BS and PTH+RAL, which had the lowest value. The data represents average ± SD, n=7 mice/group.

The parameter of TRAP+ S/BS in the various treatment cohorts was compared using a 2W ANOVA with genotype and treatment as independent variables. Loss of Nmp4 did not impact TRAP+ S/BS (no genotype effect, Figure 7A). There was a treatment effect but no genotype x treatment interaction (Figure 7A). A Tukey-Kramer HSD post hoc test revealed that the differences in TRAP+ S/BS between the treatment groups were modest (Figure 7B).

Serum C-terminal telopeptides (CTX) was assessed as an indicator for resorption using the RatLaps™ ELISA following the

manufacturer's instructions (Immunodiagnostic System Inc., Scottsdale, AZ). Serum CTX levels were compared using a 2W ANOVA with genotype and treatment as independent variables (Figures 8A & 8B). There was no significant difference in serum CTX levels between WT and *Nmp4*$^{-/-}$ mice (no genotype effect, Figure 6A). There was a strong treatment effect but no genotype x treatment interaction (Figure 8A). A Tukey-Kramer HSD post hoc test of the treatment groups (combining WT and *Nmp4*$^{-/-}$ cohorts) revealed that PTH+RAL sustained the highest serum CTX although this was not significantly different than the PTH-mono-therapy (Figure 8B). Intermittent hormone enhances the rate of remodeling and thus elevates both bone formation and resorption[13]. Interestingly, the PTH+ZOL treatment exhibited modest but significantly lower serum CTX (Figures 8A & 8B), suggestive that remodeling was somewhat attenuated compared to the PTH+RAL therapy.

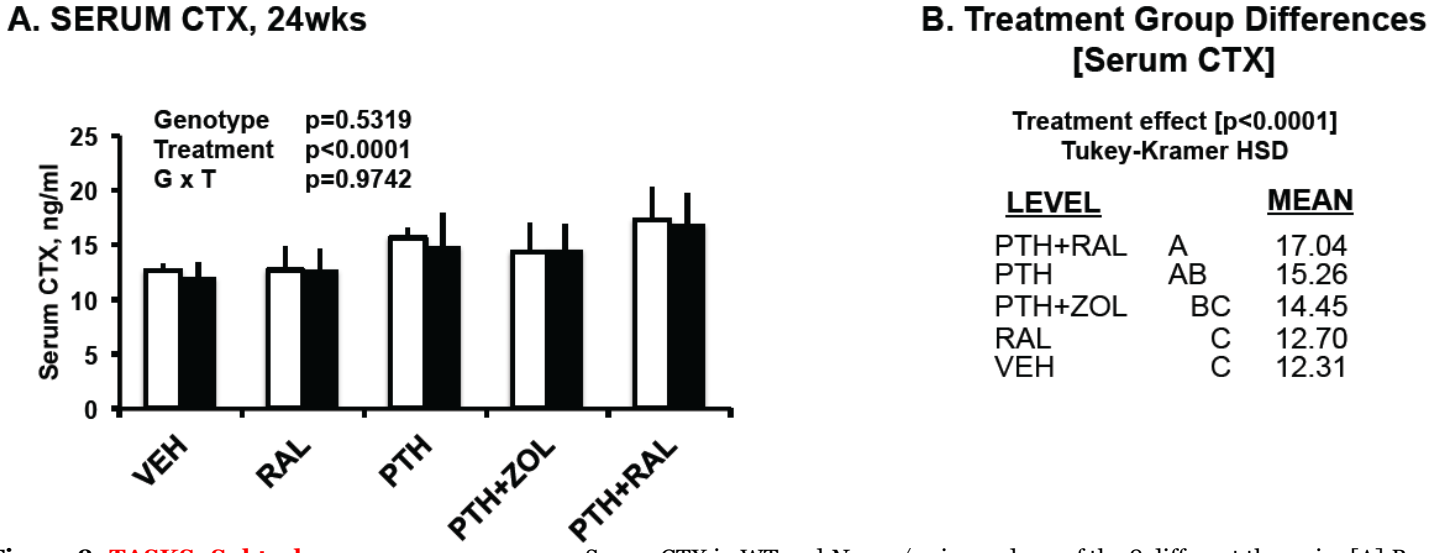

Figure 8: **TASKS: Subtasks 2.1.g.1, 2.2.e.1, 3.5.a** Serum CTX in WT and *Nmp4*$^{-/-}$ mice under 5 of the 8 different therapies [A] Bar graphs showing serum CTX levels. The data were analyzed employing a 2W ANOVA using genotype and treatment as the independent variables followed by a Tukey-Kramer HSD post-hoc test. There was no genotype effect or G x T interaction. There was a strong and significant treatment effect ($p<0.0001$). [B] A Tukey-Kramer HSD post hoc test revealed the differences between all the means of the treatment cohorts combing WT and *Nmp4*$^{-/-}$ mice. The mice under the PTH+RAL therapy had the most elevated serum CTX levels followed closely by PTH. The data represents average ± SD, n=6-7 mice/group.

Key finding #4: Loss of Nmp4 did not significantly alter the serum OPG/RANKL ratio

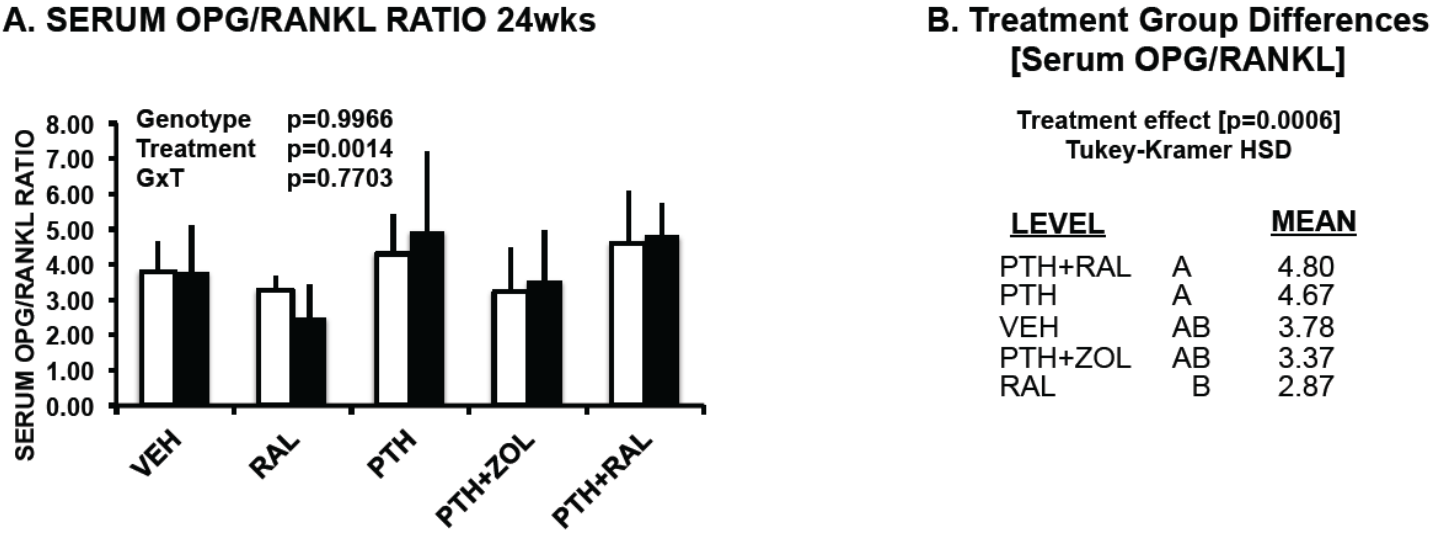

Figure 9: **TASKS: Subtasks 2.1.g.1, 2.2.e.1, 3.5.a.** Serum OPG/RANKL ratio in WT and *Nmp4*$^{-/-}$ mice under 5 of the 8 different therapies. [A] Bar graphs showing serum OPG/RANKL ratios. The data were analyzed employing a 2W ANOVA using genotype and treatment as the independent variables followed by a Tukey-Kramer HSD post-hoc test. There was no genotype effect or G x T interaction. There was a treatment effect. [B] A Tukey-Kramer HSD post hoc test revealed the differences between all the means of the treatment cohorts combing WT and *Nmp4*$^{-/-}$ mice. The PTH+RAL treatment showed the most elevated ratio and the RAL cohorts showed the lowest. The data represents average ± SD, n=6-7 mice/group.

KEY FINDING# 5: Loss of Nmp4 did not significantly alter bone marrow adipocytes. Treatment of mice with PTH mono-therapy or the PTH+anti-catabolic combination therapies significantly reduced marrow adipogenesis.

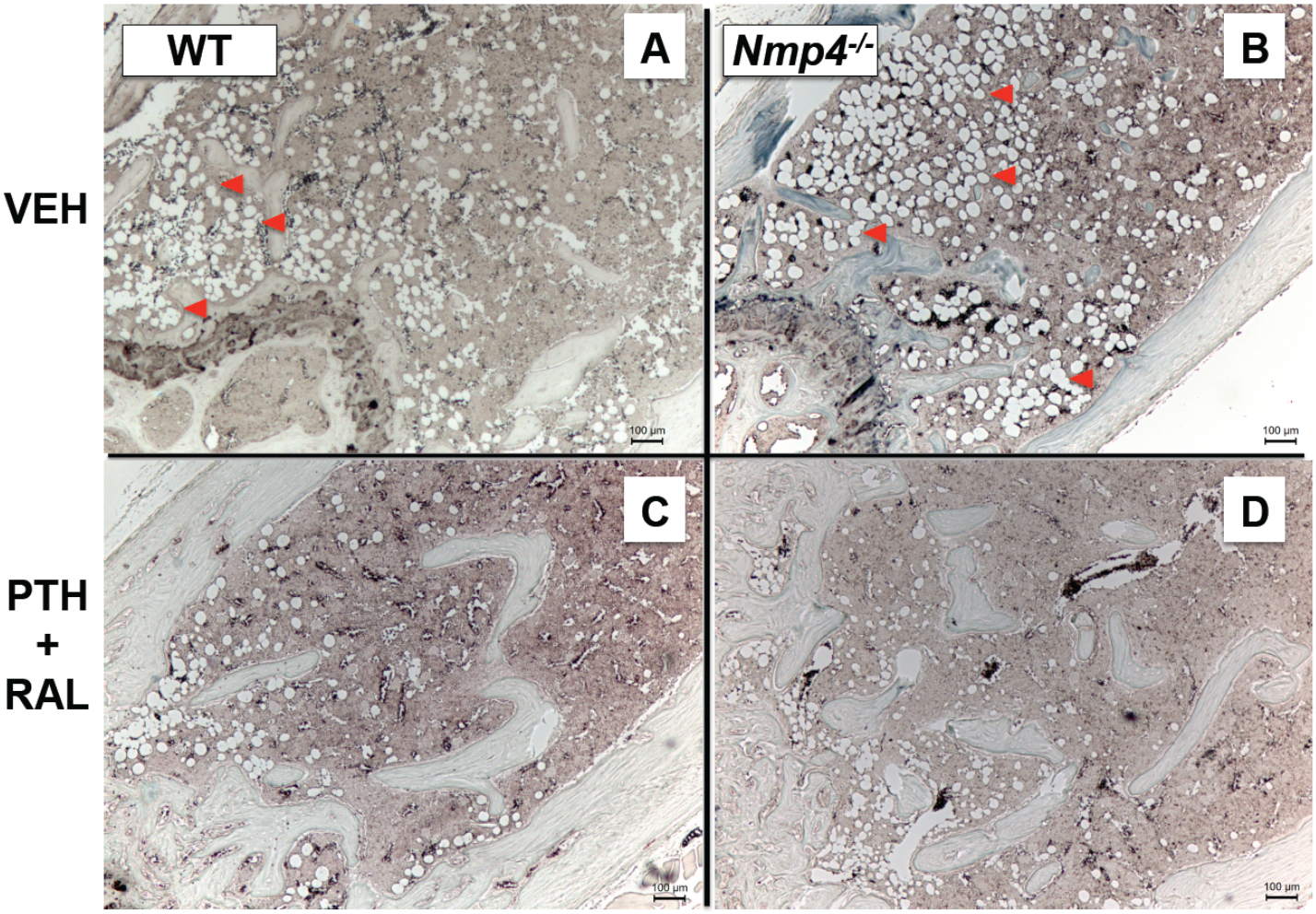

Figure 10: TASKS: Subtasks 2.1.g.2, 3.5.b Immunohistochemical micrographs of bone marrow sections from the experimental cohorts [A] WT vehicle control (VEH); [B] *Nmp4*$^{-/-}$ VEH; [C] WT PTH+RAL treatment and [D] *Nmp4*$^{-/-}$ PTH+RAL. The vacant cells (>30µm in size) with membrane positively stained with Sudan Black (red arrowheads) were counted and then normalized with the area selected (see text for details). The data represents typical image obtained from n=7 mice/group

Mesenchymal stem progenitor cells (MSPCs) are multipotent precursors that are capable of differentiating into osteoblasts and adipocytes, which until recently were considered two mutually exclusive events[14-17]. We therefore counted the number of bone marrow adipocytes in select cohorts. Slides were deparaffinized followed by rehydration via sequential ethanol washes. The slides were then incubated in Sudan Black B solution for 3 hours. Subsequently, the slides were rinsed thoroughly in two changes of 70% isopropyl alcohol followed by six changes of distilled water. Slides were counterstained in nuclear fast red solution for 10 minutes and rinsed again with two changes of distilled water. Glycerin jelly was added on top of the sample and coverslip was applied.

A cursory view of the Sudan Black B-stained slides showed a striking decrease in the number of fat cells in those mice treated with PTH or a combination of PTH+anti-catabolic (Figure 10). Therefore we used the Bioquant OSTEO system described above for enumerating the bone marrow adipoctyes. For this protocol we counted the number of Sudan Black B-stained cells in a 2mm^2 area directly below the growth plate of the distal femur.

Counter to the increase in bone marrow osteoprogenitor number with PTH and PTH+RAL therapies, the number of bone marrow adipocytes decreased in mice treated with PTH, PTH+RAL, or PTH+ZOL (Figures 11A & 11B, next page). The adipocyte counts in the various treatment cohorts was compared using a 2W ANOVA with genotype and treatment as independent variables. Loss of Nmp4 did not impact adipocyte number (no genotype effect, Figure 11A). There was a strong treatment effect but no genotype x treatment interaction (Figure 11A). A Tukey-Kramer HSD post hoc test revealed that the differences in adipocyte number

were greatest between those treatments receiving PTH as either a mono-therapy or combination therapy and those treatments not receiving hormone (Figure 11B).

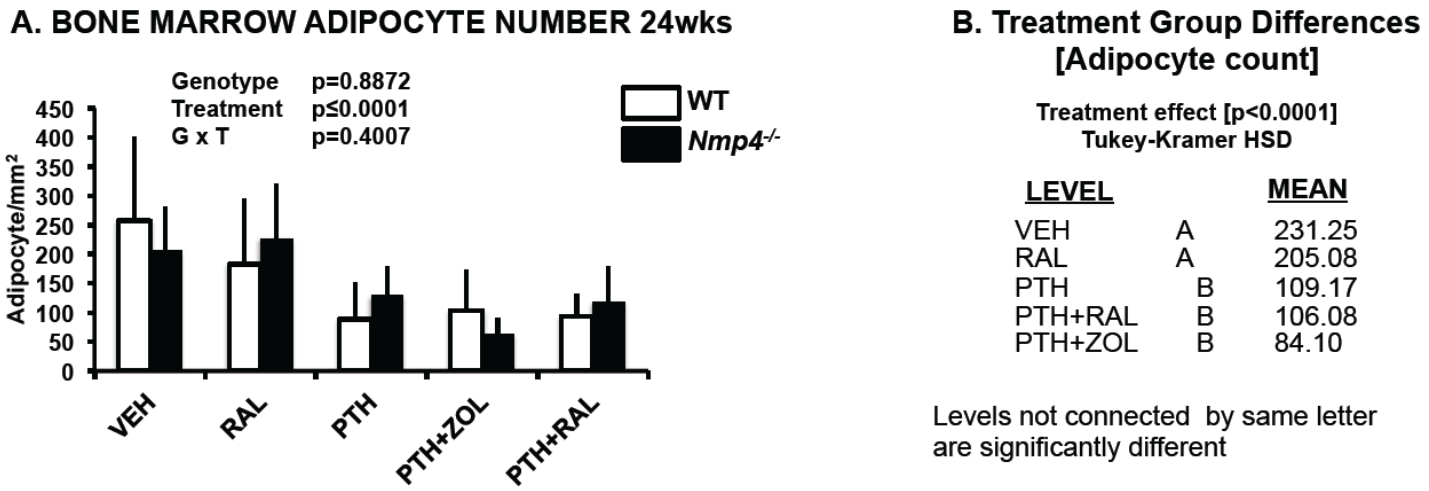

Figure 11: **TASKS: Subtasks 2.1.g.2, 2.2.e.2, 3.5.b** Bone marrow adipocyte number in WT and *Nmp4*$^{-/-}$ mice under 5 of the 8 different therapies. [A] Bar graphs showing bone marrow adipocyte number. The data were analyzed employing a 2W ANOVA using genotype and treatment as the independent variables followed by a Tukey-Kramer HSD post-hoc test. There was no genotype effect or G x T interaction. There was a strong treatment effect (p,0.0001) [B] A Tukey-Kramer HSD post hoc test revealed the differences between all the means of the treatment cohorts combing WT and *Nmp4*$^{-/-}$ mice. The VEH and RAL cohorts exhibited the most bone marrow adipocytes whereas those therapies that included PTH had the fewest number of adipocytes. The data represents average ± SD, n=7 mice/group.

Key finding #6: Our analysis of the WT and *Nmp4*$^{-/-}$ BM (**Subtasks 2.1.g.2 & 6.2**) revealed that loss of Nmp4 converted the MSPCs/osteprogenitors to super-secretor cells[4,5]. These cells produce and release more bone matrix than WT osteoblasts. This unique MSPC/osteoprogenitor phenotype was determined to be the result of elevated ribosome biogenesis and an expanded capacity of the endoplasmic reticulum (ER) to process and fold proteins destined for the bone matrix. This enhanced ER capacity was a result of select alterations in the unfolded protein response (UPR)[4,5].

A key aim of this DOD grant is to *determine the cell type-specific contributions to the enhanced response of the Nmp4*$^{-/-}$ *mouse to these osteoporosis therapies*. The experimental approach for accomplishing this aim includes the evaluation of the phenotypes of the *Nmp4*$^{-/-}$ bone marrow cells. As indicated above loss of Nmp4 increased the number of the osteoprogenitors (Figures 2 & 3). Further analysis of these cells revealed that disabling Nmp4 resulted in elevated transcription of bone matrix genes, a significant rise in ribosome biogenesis and mRNA translation[4,5]. Additionally, we showed that the ER capacity of the Nmp4 MSPCs is expanded via the enhanced expression of GADD34 and other proteins of the UPR allowing the processing of a large protein client load required for producing more bone[5]. The details of these studies are described in our published papers included in this Appendix.

Appendix Manuscript #1: Young et al., 2016:

- FIGURE 2. Deletion of Nmp4 in MSPCs increases ribosome biogenesis and protein synthesis [**Subtasks 2.1.g.2 & 6.2**]
- FIGURE 3. Deletion of Nmp4 facilitates maintenance of global translation during activation of the UPR [**Subtasks 2.1.g.2 & 6.2**]
- FIGURE 4. Deletion of Nmp4 sensitizes MSPCs to pharmacological induction of ER stress [**Subtasks 2.1.g.2 & 6.2**]
- FIGURE 5. Model for Nmp4 regulation of ribosome biogenesis and the UPR [**Subtasks 2.1.g.2 & 6.2**]

Appendix Manuscript #2: Childress et al., 2015:

- TABLE 1. Bone loss data. The % change body weight, uterine weight, and µCT of distal femur and L5 vertebra from WT and *Nmp4*$^{-/-}$ mice after ovx or sham operation 4-week postop [**Subtask 2.1.e**]
- FIGURE 2. Disabling Nmp4 enhances PTH restorative therapy in the distal femur of ovx *Nmp4*$^{-/-}$ mice. [**Subtasks 2.1.a-2.1.g.3**]
- TABLE 2. Table 2. PTH-Induced Bone Gain Data [**Subtasks 2.1.a-2.1.g.3**]

- FIGURE 3. The exaggerated response to anabolic PTH persists in the L5 vertebra of ovx *Nmp4*$^{-/-}$ mice. [**Subtasks 2.1.a-2.1.g.3**]
- TABLE 3. Histomorphometry and Serum Analyses [**Subtasks 2.1.g.1, 2.1.g.4, 2.1.g.5**]
- FIGURE 4. Ovx does not abrogate the expanded population of osteoprogenitors and CD8^{+} T cells in *Nmp4*$^{-/-}$ mice [**Subtasks 2.1.g.2**]
- FIGURE 5. Expanded *Nmp4*$^{-/-}$ MSPCs exhibit enhanced proliferation and mineralization in culture [**Subtasks 2.1.g.2, 6.2**]
- FIGURES 9 & 10. Comparison of mRNA expression profiles derived from nondifferentiating (d 3) and osteogenic-differentiating (d 5–16) WT and *Nmp4-/-* cells [**Subtasks 2.1.g.2, 6.2**]
- **Note:** FIGURES 6-8 and TABLE 4 were part of a related project supported by Eli Lilly

Key finding #7: Key finding #7: The escalated secretory activity of the *Nmp4*$^{-/-}$ cells comes at a cost. In Manuscript #1 (Appendix) we demonstrated that the *Nmp4*$^{-/-}$ MSPC is sensitized to pharmacological ER stress[5]. Specifically, the *null* cells were more susceptible to tunicamycin-induced apoptosis than the WT cells. Tunicamycin antagonizes the cell protein-folding machinery causing ER stress and ultimately apoptosis. We interpret these results to mean that the already extended *Nmp4*$^{-/-}$ ER machinery in these super-secretor cells cannot manage added demand. We propose that this contributes to ZOL suppression of PTH-induced increases in *Nmp4*$^{-/-}$ bone marrow osteoprogenitors (Figure 3). Bisphosphonates, including ZOL trigger UPR-induced ER stress in multiple cell types via their inhibition of farnesyl pyrophosphate synthase activity[6]. Preliminary MTT assays show that bone marrow *Nmp4*$^{-/-}$ MSPCs are more sensitive to ZOL-induced apoptosis than WT cells. Conversely, *Nmp4*$^{-/-}$ MSPCs are more responsive to RAL-induced proliferation than WT cells.

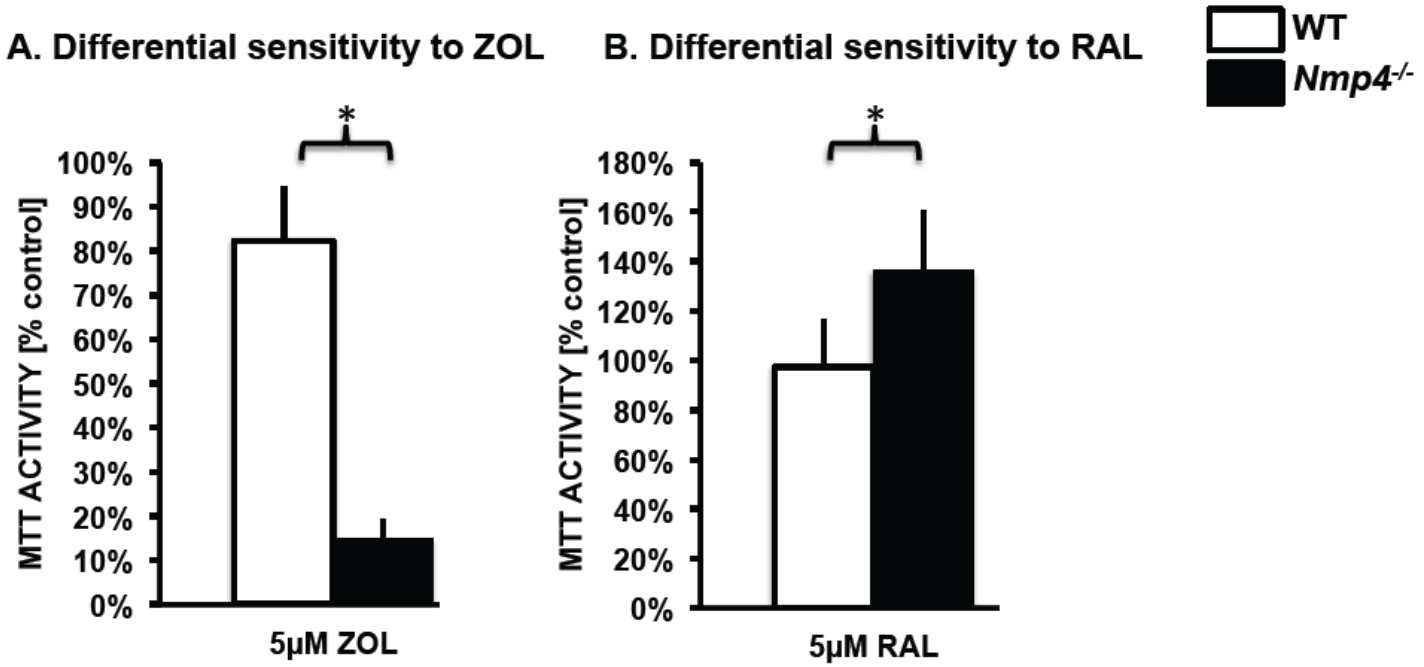

Figure 12: **Tasks: Subtasks 2.1.g.2 & 6.2** MTT assays [A] WT and *Nmp4*$^{-/-}$ MSPCs were exposed to ZOL or vehicle control for 3 days before evaluated for MTT activity. The *Nmp4*$^{-/-}$ MPSCs exhibited a dramatic decrease in MTT activity (~80% cell death) compared to WT cells [B] *Nmp4*$^{-/-}$ and WT MSPCs were exposed to RAL or vehicle control for 24hrs before evaluated for MTT activity. The MSPCs from the *Nmp4*$^{-/-}$ bone marrow exhibited a significant increase in MTT activity compared to WT cells. The data were analyzed using a Student's t test and represents average ± SD, n=4 wells of cell/group.

Our *in vivo* results suggest that co-treatment with ZOL significantly attenuated the PTH-induced increase in the *Nmp4*$^{-/-}$ bone marrow osteoprogenitor pool and that co-treatment with RAL enhanced hormone-mediated expansion of this osteogenic reserve. These effects were much weaker in the WT mice (Figures 3A & 3B). To address whether loss of Nmp4 alters MSPC/osteoprogenitor sensitivity to the osteoporosis anti-catabolics ZOL or RAL, we exposed cultures of expanded bone marrow MSPC/osteoprogenitor cells to various concentrations of these drugs. We are using MTT assays to monitor the response of the WT and *Nmp4*$^{-/-}$ MSPC/osteoprogenitor cells to these anti-catabolics (Figures 12A & 12B). The MTT assay is a colorimetric test for evaluating cell metabolic activity and is routinely used to reflect the number

of viable cells present in a culture system[18]. MTT activity was measured using CellTiter 96 well non-radioactive cell proliferation assay (Promega) as we have recently described[5] and this published study is included in the Appendix of this report (Publication #1). We have described the methods for harvesting and expanding these cells[4] and this published study is included in the Appendix of this report (Publication #2).

Our preliminary MTT data showed that the WT and *Nmp4*$^{-/-}$ cells exhibited a differential sensitivity to the ZOL and RAL (Figures 12A & 12B), which paralleled that of our in vivo observations (Figures 2 & 3). Over 80% of the *Nmp4*$^{-/-}$ MSPCs underwent cell death, likely via apoptosis, upon a 3 day challenge with ZOL (5µM) whereas only about 20% of the WT cells showed this response. Exposure to RAL (5µM, 24hrs) resulted in a significant increase in MTT activity in the null cells but not the WT MSPCs. We are presently optimizing and expanding these experiments in order to test the hypothesis that the *Nmp4*$^{-/-}$ osteoprogenitor while a hyper-anabolic super-secretor cell is more susceptible to bisphosphonate-induced apoptosis due to its already over-extended ER activity. *This has considerable clinical significance because it may explain why the PTH+RAL therapy typically outperformed the PTH+ZOL treatment in the null mice. Understanding how disabling Nmp4 enhances osteoprogenitor/osteoblast capacity for making bone matrix will provide information on designing Nmp4-based adjuvant therapies for osteoporosis treatment*.

ADDITIONAL RESEARCH ACTIVITIES: We have received a NO COST EXTENSION to complete the following experiments from the original SOW

Breeding of conditional knockout (KO) mice [**TASKS: Subtasks 4.2.a and 4.3.a**]

- The objectives for subtasks 4.2.a and 4.3.a are the breeding of *Nmp4*$^{fl/fl}$ *3.6Col-Cre+*, *Nmp4*$^{fl/fl}$ *Cathepsin K-Cre+*, and *Nmp4*$^{fl/fl}$*-Cre–* mice. Our initial attempt to flox Nmp4 using the Indiana University School of Medicine Mouse Core yielded chimeric mice that underwent partial recombination of the targeting construct. Specifically, the 3' loxP site was successfully and correctly incorporated into intron 7, but the 5' loxP site was excluded from the recombination event within intron 3 despite being included in the targeting construct. As both loxP sites are required for conditional gene inactivation experiments, we have recently decided to use the Nmp4 (Zfp384) floxed construct from the EUCOMM consortium to make the conditional knockout mice (Figure 13). TransViragen Inc, has guaranteed delivery of an F1 mouse containing this construct in the germline. NO FUNDS FROM THE DOD have been used to make this animal model. This approach, which is already in progress, will allow us to finish the floxed mouse and continue with our studies.

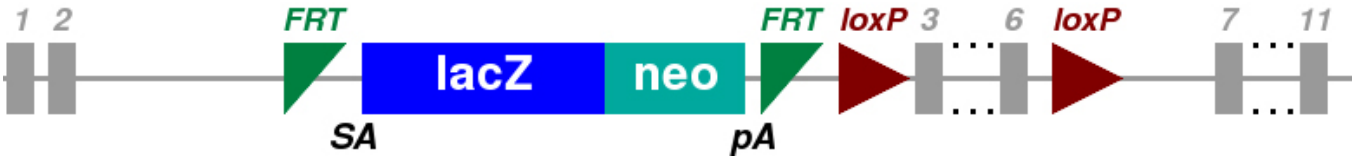

Figure 13: TASKS: Subtasks 4.2.a and 4.3.a EUCOMM Nmp4 (Zfp384) floxed construct used in our conditional knockout mice

Biomechanical testing and bone histmorphometry [**TASKS: Subtasks 2.1.g.4-2.1.g.6 and 2.1.e.4-2.1.e.6, 3.5.d-3.5.f**]

- The biomechanical testing and histomorphometry analyses for bones from the various treatments are underway

CD8+ T cell impact on the Nmp4$^{-/-}$ *bone phenotype* [**TASKS: Subtasks 5.4-5.5**].

- The CD8+ T cell ablation experiments are ongoing

Bone marrow transplantation experiments [**TASKS: Subtasks 6.3-6.6**]

- The bone marrow transplantation experiments comparing the capacities of *null* and WT MSPCs to restore trabecular architecture will be completed.

KEY RESEARCH ACCOMPLISHMENTS FOR 3rd YEAR:

- **Key finding #1:** *Nmp4*$^{-/-}$ osteoprogenitors are differentially responsive to PTH+RAL and PTH+ZOL.
- **Key finding #2:** The *Nmp4*$^{-/-}$ mice exhibited higher levels of serum osteocalcin compared to WT mice
- **Key finding #3:** Loss of Nmp4 did not significantly alter bone resorption
- **Key finding #4:** Loss of Nmp4 did not significantly alter serum OPG/RANKL ratios.
- **Key finding #5:** Loss of Nmp4 did not significantly alter the number of bone marrow adipocytes
- **Key finding #6:** The *Nmp4*$^{-/-}$ osteoprogenitor is a super-secretor cell
- **Key finding #7:** The *Nmp4*$^{-/-}$ osteoprogenitor over-extended ER machinery is sensitized to ZOL-induced apoptosis.

REPORTABLE OUTCOMES:
Presentations in which the DOD support was acknowledged:

- Invited seminar: 11/18/15; Richard L Roudebush VA Medical Center Title: *Boosting Bone Anabolism: Engineering a Super Secretory Osteoblast*
- Invited seminar: 12/11/15: IUPUI Department of Biology Title: *Boosting Bone Anabolism: Engineering a Super Secretory Osteoblast*
- Invited seminar: 01/14/16: IUSM Title: *Engineering a Super Secretory Osteoblast*
- National meeting: American Society for Bone & Mineral Research, September 16-19, 2016, Atlanta, GA, Title: Engineering a hyper-anabolic, super-secreting osteoblast
- Manuscript accepted: Childress P, Stayrook KR, Alvarez MB, Wang Z, Shao Y, Hernandez-Buquer S, Mack JK, Grese ZR, He Y, Horan D, Pavalko FM, Warden SJ, Robling AG, Yang FC, Allen MR, Krishnan V, Liu Y, Bidwell JP. 2015 Genome-Wide Mapping and Interrogation of the Nmp4 Antianabolic Bone Axis. Mol Endocrinol. 29(9):1269-85. [See Appendix]
- Manuscript accepted: Young SK, Shao Y, Bidwell JP, Wek RC. 2016 Nuclear Matrix Protein 4 Is a Novel Regulator of Ribosome Biogenesis and Controls the Unfolded Protein Response via Repression of Gadd34 Expression. J Biol Chem. 2016 291(26):13780-8.

Funding applied for based on work supported by this award:
Agency: NIH
Program: NIAMS
Title: The Nmp4 Anti-Anabolic Bone Axis
Date submitted: 10/05/2015
Annual direct costs: $308,277
Score: 31 PERCENTILE. The reviews were very positive. We are planning to re-submit a revised proposal

Agency: NIH
Program: MGB
Title: The Nmp4-UPR control of proteostasis
Date submitted: 06/05/2016
Annual direct costs: $250,000
Score: In review

CONCLUSION: Key experimental discovery for 3rd year of DOD study
Our key discovery was that disabling Nmp4 enhanced the PTH-induced increase in bone marrow osteoprogenitors (the osteogenic reserve) and converts these cells and descendant osteoblasts into super-secretors. This escalated secretory activity comes at a cost. The $Nmp4^{-/-}$ MSPC/osteoprogenitor is sensitized to pharmacological ER stress. We propose that this accounts for the diminished osteoprogenitor osteogenic reserve in the $Nmp4^{-/-}$ mice treated with PTH+ZOL compared to those null mice under the PTH+RAL therapy.
"So what?"
Women comprise the fastest growing group of the US veterans contributing to the looming osteoporosis epidemic within the veteran population. The Veterans Affairs (VA) health care system will be in high demand by female veterans of Operation Enduring Freedom and Operation Iraqi Freedom. PTH is the only FDA-approved anabolic osteoporosis therapy and adds significant amounts of bone to the osteoporotic skeleton. Therefore, this drug has the potential to restore the bone lost in a variety of VA clinical settings. However, a drawback to PTH use is that potency declines within 2 years and thus it is not suitable as a long-term therapy, which is problematic in treating a chronic degenerative disease. Clinicians have attempted to improve PTH therapy by adding an anti-catabolic (e.g. raloxifene or a bisphosphonate) to the treatment. This has not met with success. The present discovery supports our contention that disabling Nmp4 or some component of its pathway will unlock the block on PTH combination therapies and enhance/extend regeneration of osteoporotic bone in post-menopausal female veterans. We have made significant advances this year in understanding the molecular mechanisms that support the Nmp4 phenotype. This research will lead to identifying new pharmacological targets for boosting bone anabolism in the VA patient population.

REFERENCES:

1 Robling, A. G. *et al.* Nmp4/CIZ suppresses parathyroid hormone-induced increases in trabecular bone. *Journal of cellular physiology* **219**, 734-743, doi:10.1002/jcp.21717 (2009).

2 Childress, P. *et al.* Nmp4/CIZ suppresses the response of bone to anabolic parathyroid hormone by regulating both osteoblasts and osteoclasts. *Calcified tissue international* **89**, 74-89, doi:10.1007/s00223-011-9496-y (2011).

3 He, Y. *et al.* Nmp4/CIZ suppresses the parathyroid hormone anabolic window by restricting mesenchymal stem cell and osteoprogenitor frequency. *Stem cells and development* **22**, 492-500, doi:10.1089/scd.2012.0308 (2013).

4 Childress, P. *et al.* Genome-Wide Mapping and Interrogation of the Nmp4 Antianabolic Bone Axis. *Molecular endocrinology* **29**, 1269-1285, doi:10.1210/me.2014-1406 (2015).

5 Young, S. K., Shao, Y., Bidwell, J. P. & Wek, R. C. Nuclear Matrix Protein 4 is a Novel Regulator of Ribosome Biogenesis and Controls the Unfolded Protein Response Via Repression of Gadd34 Expression. *The Journal of biological chemistry*, doi:10.1074/jbc.M116.729830 (2016).

6 Chen, J. C., Wu, M. L., Huang, K. C. & Lin, W. W. HMG-CoA reductase inhibitors activate the unfolded protein response and induce cytoprotective GRP78 expression. *Cardiovascular research* **80**, 138-150, doi:10.1093/cvr/cvn160 (2008).

7 Nakashima, K. *et al.* The novel zinc finger-containing transcription factor osterix is required for osteoblast differentiation and bone formation. *Cell* **108**, 17-29 (2002).

8 Hsiao, E. C. *et al.* Osteoblast expression of an engineered Gs-coupled receptor dramatically increases bone mass. *Proceedings of the National Academy of Sciences of the United States of America* **105**, 1209-1214, doi:10.1073/pnas.0707457105 (2008).

9 Wattanachanya, L. *et al.* Assessing the osteoblast transcriptome in a model of enhanced bone formation due to constitutive Gs-G protein signaling in osteoblasts. *Experimental cell research* **333**, 289-302, doi:10.1016/j.yexcr.2015.02.009 (2015).

10 Thunyakitpisal, P. *et al.* Cloning and functional analysis of a family of nuclear matrix transcription factors (NP/NMP4) that regulate type I collagen expression in osteoblasts. *Journal of bone and mineral research : the official journal of the American Society for Bone and Mineral Research* **16**, 10-23, doi:10.1359/jbmr.2001.16.1.10 (2001).

11 Nakamoto, T. *et al.* Impaired spermatogenesis and male fertility defects in CIZ/Nmp4-disrupted mice. *Genes to cells : devoted to molecular & cellular mechanisms* **9**, 575-589, doi:10.1111/j.1356-9597.2004.00746.x (2004).

12 Erlebacher, A. & Derynck, R. Increased expression of TGF-beta 2 in osteoblasts results in an osteoporosis-like phenotype. *J Cell Biol* **132**, 195-210 (1996).

13 Jilka, R. L. Molecular and cellular mechanisms of the anabolic effect of intermittent PTH. *Bone* **40**, 1434-1446, doi:10.1016/j.bone.2007.03.017 (2007).

14 Chen, Y. H. *et al.* EZH2 and HDAC9c regulate age-dependent mesenchymal stem cell differentiation into osteoblasts and adipocytes. *Stem cells (Dayton, Ohio)*, doi:10.1002/stem.2400 (2016).

15 Gimble, J. M., Zvonic, S., Floyd, Z. E., Kassem, M. & Nuttall, M. E. Playing with bone and fat. *Journal of cellular biochemistry* **98**, 251-266, doi:10.1002/jcb.20777 (2006).

16 Worthley, D. L. *et al.* Gremlin 1 identifies a skeletal stem cell with bone, cartilage, and reticular stromal potential. *Cell* **160**, 269-284, doi:10.1016/j.cell.2014.11.042 (2015).

17 Chan, C. K. *et al.* Identification and specification of the mouse skeletal stem cell. *Cell* **160**, 285-298, doi:10.1016/j.cell.2014.12.002 (2015).

18 Mosmann, T. Rapid colorimetric assay for cellular growth and survival: application to proliferation and cytotoxicity assays. *Journal of immunological methods* **65**, 55-63 (1983).

APPENDIX:

Note: Copies of two published manuscripts are included in this year's appendix.

- Young SK, Shao Y, Bidwell JP, Wek RC. 2016 Nuclear Matrix Protein 4 Is a Novel Regulator of Ribosome Biogenesis and Controls the Unfolded Protein Response via Repression of Gadd34 Expression. J Biol Chem. 291(26):13780-8.
- Childress P, Stayrook KR, Alvarez MB, Wang Z, Shao Y, Hernandez-Buquer S, Mack JK, Grese ZR, He Y, Horan D, Pavalko FM, Warden SJ, Robling AG, Yang FC, Allen MR, Krishnan V, Liu Y, Bidwell JP. 2015 Genome-Wide Mapping and Interrogation of the Nmp4 Antianabolic Bone Axis. Mol Endocrinol. 29(9):1269-85.

THE JOURNAL OF BIOLOGICAL CHEMISTRY VOL. 291, NO. 26, pp. 13780–13788, June 24, 2016

Nuclear Matrix Protein 4 Is a Novel Regulator of Ribosome Biogenesis and Controls the Unfolded Protein Response via Repression of *Gadd34* Expression*

Received for publication, March 28, 2016, and in revised form, April 18, 2016 Published, JBC Papers in Press, April 29, 2016, DOI 10.1074/jbc.M116.729830

Sara K. Young[‡], **Yu Shao**[§], **Joseph P. Bidwell**[¶1], **and Ronald C. Wek**[‡2]

From the [‡]*Department of Biochemistry and Molecular Biology,* [¶]*Department of Anatomy and Cell Biology, and* [§]*Department of Medical and Molecular Genetics, Indiana University School of Medicine, Indianapolis, Indiana 46202-5126*

The unfolded protein response (UPR) maintains protein homeostasis by governing the processing capacity of the endoplasmic reticulum (ER) to manage ER client loads; however, key regulators within the UPR remain to be identified. Activation of the UPR sensor PERK (EIFAK3/PEK) results in the phosphorylation of the α subunit of eIF2 (eIF2α-P), which represses translation initiation and reduces influx of newly synthesized proteins into the overloaded ER. As part of this adaptive response, eIF2α-P also induces a feedback mechanism through enhanced transcriptional and translational expression of *Gadd34* (*Ppp1r15A*), which targets type 1 protein phosphatase for dephosphorylation of eIF2α-P to restore protein synthesis. Here we describe a novel mechanism by which *Gadd34* expression is regulated through the activity of the zinc finger transcription factor NMP4 (ZNF384, CIZ). NMP4 functions to suppress bone anabolism, and we suggest that this occurs due to decreased protein synthesis of factors involved in bone formation through NMP4-mediated dampening of *Gadd34* and *c-Myc* expression. Loss of *Nmp4* resulted in an increase in *c-Myc* and *Gadd34* expression that facilitated enhanced ribosome biogenesis and global protein synthesis. Importantly, protein synthesis was sustained during pharmacological induction of the UPR through a mechanism suggested to involve GADD34-mediated dephosphorylation of eIF2α-P. Sustained protein synthesis sensitized cells to pharmacological induction of the UPR, and the observed decrease in cell viability was restored upon inhibition of GADD34 activity. We conclude that NMP4 is a key regulator of ribosome biogenesis and the UPR, which together play a central role in determining cell viability during endoplasmic reticulum stress.

Professional secretory cells balance the synthesis, folding, and trafficking of proteins to ensure optimal protein export. Upon differentiation and physiological cues, increased synthesis of polypeptides slated for secretion can lead to accumulation of unfolded proteins in the endoplasmic reticulum (ER)[3] that trigger the unfolded protein response (UPR) (1). The UPR features multiple sensory proteins, including PERK (EIF2AK3/PEK), IRE1 (ERN1), and ATF6, which are each situated in the ER and are activated by unfolded proteins in the ER (1). Induction of the UPR leads to a program of translational and transcriptional gene expression that collectively serve to expand the processing capacity of the ER to effectively manage an expanded ER client load (1).

In response to ER stress, PERK phosphorylates the α subunit of eIF2 (eIF2α-P), which represses global translation initiation that reduces influx of newly synthesized proteins into the overloaded ER (2, 3). Coincident with dampening of global protein synthesis, eIF2α-P leads to preferential translation of *Atf4*, encoding a transcription activator of UPR genes involved in nutrient import, metabolism, and alleviation of oxidative stress (4–6). ATF4 also directly induces the transcriptional expression of *Gadd34* (*Ppp1r15A*), which targets type 1 protein phosphatase for dephosphorylation of eIF2α-P (7–9). Translational expression of *Gadd34* is also enhanced by eIF2α-P, and the resulting increased GADD34 serves in feedback control that restores protein synthesis, allowing for translational expression of UPR gene transcripts (7, 10, 11).

UPR-directed transcription is also driven by IRE1, a riboendonuclease that facilitates splicing of *Xbp1* mRNA, leading to translation of an activated version of the XBP1 transcription factor. In response to ER stress, ATF6 is transported from the ER to Golgi for proteolytic cleavage that allows for release of the amino-terminal portion of ATF6 to enter the nucleus and direct transcription of targeted UPR genes (1). Oasis is another transcription factor closely related to ATF6 that is also activated via regulated intramembrane proteolysis during ER stress (12). Together the ATF4, XBP1, ATF6, and Oasis transcription factors serve to enhance expression of UPR genes involved in protein folding and assembly, vesicular transport, ER and Golgi expansion, and degradation of unfolded proteins (1, 12). Hence the UPR provides for key transcriptional, translational, and proteolytic processes that are central to professional secretory cells.

* This work was supported, in whole or in part, by National Institutes of Health Grant GM049164 (to R. C. W.). This work was also supported by the Ralph W. and Grace M. Showalter Research Trust Fund (to R. C. W.) and Department of Defense Grant PR120563 (to J. P. B.). The content is solely the responsibility of the authors and does not necessarily represent the official views of the National Institutes of Health. The authors declare no conflicts of interest with the contents of this manuscript.

[1] To whom correspondence may be addressed: Dept. of Anatomy and Cell Biology, Indiana University School of Medicine, 635 Barnhill Dr., Indianapolis, IN 46202-5126. Tel.: 317-278-1142; Fax: 317-278-2040; E-mail: jbidwell@iu.edu.

[2] To whom correspondence may be addressed: Dept. of Biochemistry and Molecular Biology, 635 Barnhill Dr., Indiana University School of Medicine, Indianapolis, Indiana 46202-5126; Tel.: 317-274-0549; Fax: 317-274-4686; E-mail: rwek@iu.edu.

[3] The abbreviations used are: ER, endoplasmic reticulum; UPR, unfolded protein response; eIF2α-P, phosphorylation of the α subunit of eIF2; MSPC, mesenchymal stem progenitor cell; qPCR, quantitative PCR; MTT, 3-(4,5-dimethylthiazol-2-yl)-2,5-diphenyltetrazolium bromide.

Emphasizing the importance of the key UPR regulators in secretory cells, loss of function of *Perk*, *Atf4*, *Ire1*, *Xpb1*, or *Oasis*, disrupts the health and secretory functions of osteoblasts and subsequent bone formation (13–15). Treatment of precursor osteoblasts with bone morphogenetic protein BMP2 is suggested to activate each of the UPR branches, directing expression of target genes that contribute to secretion and bone formation (13, 14, 16). Given the central role of the UPR in protein homeostasis and expansion of secretory capacity, there is a growing consensus that the UPR functions in conjunction with additional regulators of bone development. For example, ATF4 is an essential regulator of osteoblast biology, and there are likely to be additional regulatory networks integrating the UPR to bone development (13, 17). We previously reported that the zinc finger transcription factor NMP4 (ZNF384, CIZ) functions to suppress bone anabolism, partially through the repression of genes such as *Plaur*, *Spp1*, and *Col1a1*, which play important roles in osteogenic lineage commitment and mineralization (18–20). Targeted deletion of *Nmp4* in mice enhances bone response to PTH and BMP2 and protects these animals from osteopenia. Furthermore, ChIP-Seq analyses of NMP4-binding sites in preosteoblasts, embryonic stem cells, and two blood cell lines suggest that NMP4 binds to the promoters of genes encoding UPR regulators and modulates their gene expression (20).

In this study we addressed the role of NMP4 in the regulation of the UPR and its control of transcription and protein synthesis processes. Our analysis indicates that NMP4 regulates protein synthesis through transcriptional repression of both *c-Myc* and *Gadd34*. Loss of *Nmp4* results in an increase in *c-Myc* and *Gadd34* expression, enhancing ribosome biogenesis and global protein synthesis. Importantly, protein synthesis is sustained during pharmacological induction of the UPR through a mechanism suggested to involve GADD34-mediated dephosphorylation of eIF2α-P. Sustained protein synthesis sensitizes cells to pharmacological induction of the UPR. Furthermore, the observed decrease in cell viability upon activation of the UPR is restored upon inhibition of GADD34 activity. These results emphasize the importance of appropriate regulation of *Gadd34* expression and its role in the maintenance of cellular homeostasis through regulation of eIF2α-P.

Experimental Procedures

Mice—WT and *Nmp4*$^{-/-}$ mice are as previously described (20). The local Institutional Animal Care and Use Committee approved all husbandry practices and experimental procedures.

Cell Culture—Mesenchymal stem progenitor cells (MSPCs) were isolated from bone marrow using a Ficoll gradient as described (20, 22) and were cultured in Mesencult Media with Mesencult Stimulatory Supplement (StemCell Technologies).

Immunoblot Analysis—MSPCs were treated with 2 μM tunicamycin for up to 9 h, 10 μM salubrinal for 6 h, or left untreated. Spleen, liver, and bone marrow tissues were isolated from *Nmp4*$^{+/+}$ and *Nmp4*$^{-/-}$ mice, and protein lysates were collected and quantified from the tissues and MSPCs followed by immunoblot analyses as previously described (10). Antibodies used for immunoblot analyses are listed in Table 1.

TABLE 1
Description of antibodies used for immunoblots in this study

Protein of interest	Supplier and catalog number
NMP4	Sigma #HPA004051
GADD34	Proteintech #10449-1-AP
CReP	Proteintech #14634-1-AP
ATF4	Santa Cruz #sc-22800
eIF2α~P	Abcam #ab32157
RPS6~P ribosomal protein	Cell Signaling #2211
RPS6 total ribosomal protein	Cell Signaling #2317
RPL11 ribosomal protein	Cell Signaling #18163
c-MYC	Cell Signaling #5605
β-actin	Sigma #A5441
eIF2α total	Monoclonal antibody kindly provided by Dr. Scott Kimball (Pennsylvania State University College of Medicine, Hershey, PA)

mRNA Measurement by qPCR—RNA was isolated from MSPCs and tissues using TRIzol reagent (Invitrogen), and single-strand cDNA synthesis was conducted with the TaqMan reverse transcriptase kit (Applied Biosystems) following the manufacturer's instructions. Transcript levels were quantified by qPCR using SYBR Green (Applied Biosystems) on a Realplex2 Master Cycler (Eppendorf). $\Delta\Delta$CT values were calculated for each transcript in which β-actin levels were used for normalization. Primers used for qPCR analysis are listed in Table 2.

Plasmid Constructs and Luciferase Assays—The DNA segments containing 1 kb of the human *Gadd34* and *Crep* promoters were inserted between KpnI and BglII in a pGL3 basic backbone. The *Gadd34* promoter-Luc and *CReP* promoter-Luc constructs were transiently co-transfected with a *Renilla* reporter plasmid into WT or *Nmp4*$^{-/-}$ MSPCs for 24 h followed by a 6-h 2 μM tunicamycin treatment. Lysates were collected, and Firefly and *Renilla* luciferase activities were measured as described (5). At least three independent biological experiments were conducted for each luciferase measurement, and relative values are represented with S.D. indicated.

Total RNA and DNA Measurement—RNA and DNA was isolated from MSPCs using TRIzol reagent (Invitrogen) following the manufacturer's instructions. Quantification of RNA and DNA was determined by absorbance measurement at 260 and 280 nm by nanodrop.

Polysome Profiling and Sucrose Gradient Ultracentrifugation—MSPCs were treated with 2 μM tunicamycin or 10 μM salubrinal for 6 h or left untreated. Lysates were collected, sheared, and layered on top of 10–50% sucrose gradients as described (10). Whole-cell lysate polysome profiles were measured with a Piston Gradient Fractionator (BioComp) and a 254-nm UV monitor with Data Quest Software.

Cell Viability Assays—MTT and Caspase 3/7 assays were conducted by seeding cells at 5000 cells/well in a 96-well plate. For MTT time course analysis, cells were cultured for 24 h followed by up to 24 h of treatment with 2 μM tunicamycin alone or in combination with either 10 μM salubrinal or 250 nM torin 1 (Tocris) for an additional 24 h, and MTT activity was measured using CellTiter 96 well non-radioactive cell proliferation assay (Promega). For Caspase 3/7 assays, cells were seeded, cultured for 24 h, and treated in the presence or absence of 2 μM tunicamycin for an additional 24 h, and Caspase 3/7 activity was measured using the Caspase-Glo 3/7 Assay System (Promega).

Statistical Analyses—Values indicate the mean ± S.D. and represent at least three independent experiments. Statistical significance was calculated using the two-tailed Student's *t* test. Differences between multiple groups were analyzed using a two-way analysis of variance followed by a post hoc Tukey HSD test. For the statistical analyses, genotype and treatment were set as fixed factors, and StatPlus software was used to calculate significance. p values <0.05 were considered statistically significant with differences between treatment groups indicated by asterisks (*) and differences between genotypes indicated by a number (#) symbol.

TABLE 2
Description of primers used for qPCR in this study

Primer name	Primer sequence
Gadd34 forward	5′-AGGACCCCGAGATTCCTCTA-3′
Gadd34 reverse	5′-CCTGGAATCAGGGGTAAGGT-3′
Crep forward	5′-GGCTACAGTGGCCTTCTCTG-3′
Crep reverse	5′-CATCCATCCCTTGCAAATTC-3′
c-Myc forward	5′-GAAAACGACAAGAGGCGGAC-3′
c-Myc reverse	5′-AATGGACAGGATGTAGGCGG-3′
45S rRNA forward	5′-TTTTTGGGGAGGTGGAGAGTC-3′
45S rRNA reverse	5′-CTGATACGGGCAGACACAGAA-3′
Rpl11 forward	5′-CCTCAATATCTGCGTCGGGG-3′
Rpl11 reverse	5′-TTCCGCAACTCATACTCCCG-3′
Rps6 forward	5′-CAGGACCAAAGCACCCAAGA-3′
Rps6 reverse	5′-CAGTGAGGACAGCCTACGTC-3′
β-Actin forward	5′-TGTTACCAACTGGGACGACA-3′
β-Actin reverse	5′-GGGGTGTTGAAGGTCTCAAA-3′

Results

Genome-wide analyses of NMP4-binding sites in multiple cell lines, including preosteoblast MC3T3-E1, embryonic cell line ES-E14, B cell lymphoma Ch12, and murine erythroleukemia cells, suggest that NMP4 binds to specific regions in the *Gadd34* promoter at the described NMP4 binding consensus sequence (AAAAAAAAA) (see the UCSC Genome Bioinformatics website and Ref. 20). The reported NMP4-binding site in the *Gadd34* promoter in MC3T3-E1 cells is illustrated in Fig. 1*A* (20), and we posited that NMP4 alters transcriptional expression of *Gadd34* mRNA. To address this idea we used qPCR to measure *Gadd34* mRNA in tissues involving bone and blood homeostasis, including bone marrow, spleen, and liver, from wild-type (WT) mice and those containing a whole body deletion of *Nmp4*. In either bone marrow or spleen, loss of *Nmp4* led to >2-fold induction in *Gadd34* mRNA, whereas there was a trend toward an increase, although not significant, in the *Nmp4*$^{-/-}$ liver tissues (Fig. 1*B*). These findings suggest that NMP4 can serve as a repressor of *Gadd34* mRNA expression in multiple tissues, although likely to different extents.

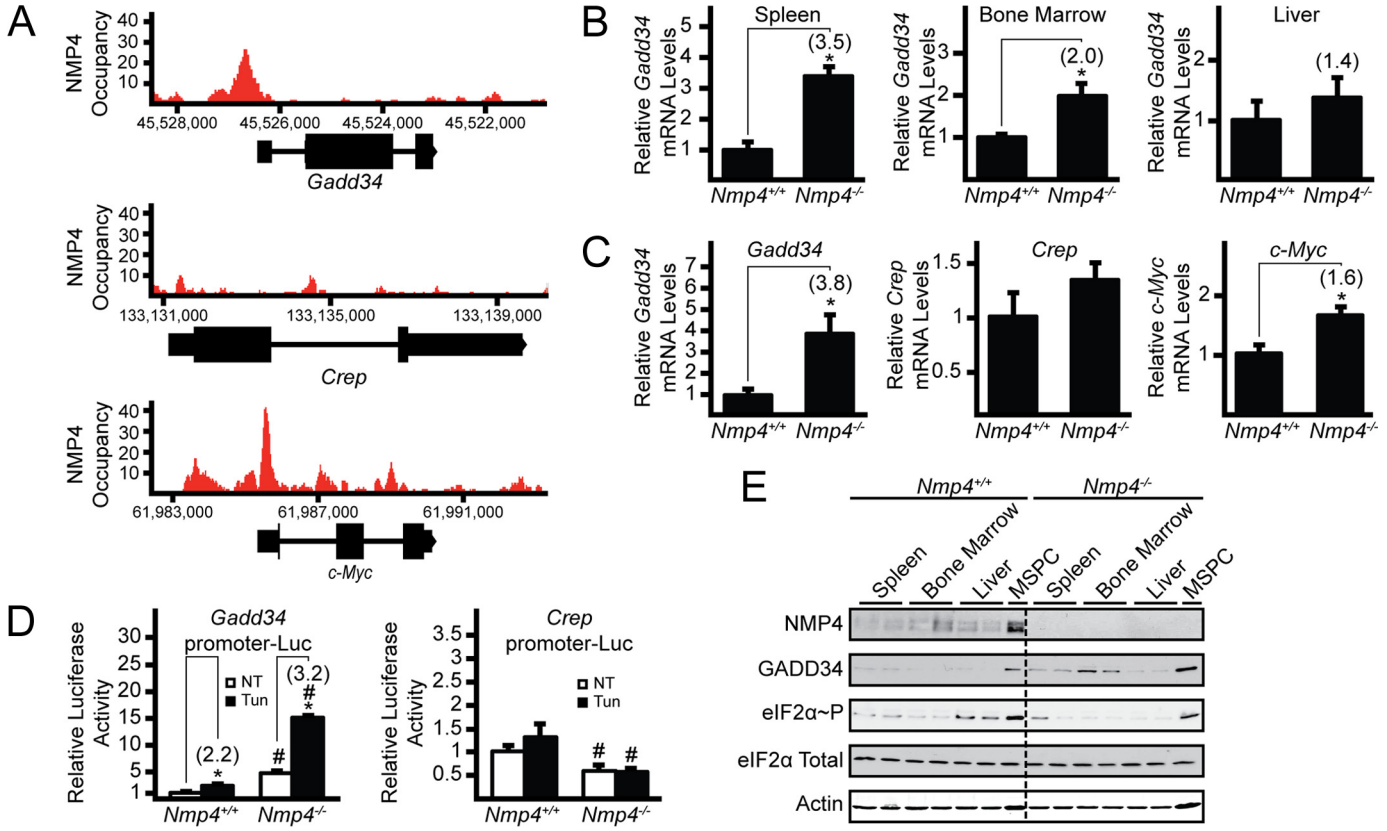

FIGURE 1. **Expression of *Gadd34* is increased upon deletion of *Nmp4*.** *A*, NMP4 occupancy on the genomic loci corresponding to sequences encoding *Gadd34*, *Crep*, and *c-Myc* genes that were reported in the genome-wide ChIP-Seq analysis (20). NMP4 occupancy (read count) is indicated on the *y* axis. *Boxes* indicate exonic sequences encoding *Gadd34*, *Crep*, and *c-Myc* mRNAs, and *horizontal lines* indicate intronic regions. *B*, total RNA was collected from spleen, bone marrow, and liver tissues from *Nmp4*$^{+/+}$ and *Nmp4*$^{-/-}$, mice and relative levels of *Gadd34* mRNA were measured by qRT-PCR. *C*, levels of *Gadd34*, *Crep*, and *c-Myc* mRNA were also measured in WT and *Nmp4*$^{-/-}$ MSPCs. *D*, *Gadd34* and *Crep* transcriptional control was measured in WT or *Nmp4*$^{-/-}$ MSPCs in the presence or absence of tunicamycin (*Tun*) via Dual-Luciferase assay. *E*, the indicated proteins were measured in the indicated *Nmp4*$^{+/+}$ and *Nmp4*$^{-/-}$ tissues and MSPCs by immunoblot. *Panel A* is representative of three independent biological experiments, and relative values are represented as histograms with the S.D. indicated in *panels B*, *C*, and *D*. *Panel E* is representative of three independent biological experiments. Differences between treatment groups are indicated by asterisks (*), and differences between genotypes are indicated by number (#) symbols. *NT*, not treated.

Given the diversity of cell types in bone marrow and spleen, we next prepared MSPCs from bone marrow from the WT and *Nmp4*-deleted mice and measured *Gadd34* mRNA in these cultured primary cells. Consistent with our bone marrow measurements, there was almost a 4-fold increase in *Gadd34* mRNA levels in the *Nmp4*-depleted cells compared with WT (Fig. 1*C*). By comparison there was minimal difference between the WT and mutant MSPCs for the amount of *Crep* (*Ppp1r15B*) mRNA (Fig. 1*C*), which encodes a constitutively expressed targeting subunit for dephosphorylation of eIF2α-P (23).

To determine whether NMP4 serves to repress transcription of the *Gadd34* gene, we transfected luciferase reporter constructs with transcriptional expression directed by the *Gadd34* or *Crep* promoters. There was a >4-fold increase in *Gadd34* promoter activity in the MSPCs deleted for *Nmp4* compared with WT (Fig. 1*D*). ATF4 and CHOP are both known to directly increase the transcriptional expression of the *Gadd34* gene in response to ER stress, and the *Gadd34* promoter luciferase reporter also contains the ATF4 and CHOP-binding sites that are at locations distinct from NMP4 (8, 24). In both WT and $Nmp4^{-/-}$ cells, luciferase activity was sharply increased upon the addition of tunicamycin, an inhibitor of *N*-linked glycosylation and potent inducer of ER stress. However, *Nmp4*-deleted cells showed the greatest extent of *Gadd34* promoter activity upon ER stress, with a >6-fold increase compared with WT (Fig. 1*D*). By comparison, luciferase expressed from the *Crep* promoter showed a 40% decrease in reporter activity compared with WT, and as expected, *Crep* promoter activity was not significantly changed upon tunicamycin treatment.

Next we measured GADD34 protein in bone marrow, spleen, and liver from WT mice and MSPCs and their *Nmp4* knock-out counterparts. Levels of GADD34 protein were increased in $Nmp4^{-/-}$ tissues and MSPCs, with the most significant changes observed in bone marrow and MSPCs (Fig. 1*E*). Elevated levels of GADD34 protein would be expected to lead to lowered levels of eIF2α-P even in conditions not subject to overt stress, and this finding was confirmed in our immunoblot analyses (Fig. 1*E*). NMP4 was also present in all tissues analyzed as well as MSPCs, although the levels were varied, with NMP4 being the most abundant in MSPCs. These findings suggest that NMP4 can serve as a major regulator of *Gadd34* expression in multiple cell types.

Loss of Nmp4 in MSPCs Increases Protein Synthesis—Phosphorylation of eIF2α represses global translation by lowering the levels of eIF2-GTP available for delivery of aminoacylated initiator tRNA to ribosomes (25). Therefore, elevated levels of GADD34 and the consequential reduction of eIF2α-P would be predicted to enhance global protein synthesis. Lysates prepared from WT and $Nmp4^{-/-}$ MSPCs were analyzed by sucrose gradient ultracentrifugation to visual the amounts of translated mRNAs in polysomes (Fig. 2*A*). There was a sharp increase in large polysomes upon loss of *Nmp4* in the MPSCs, indicative of much higher levels of protein synthesis. Interestingly there was also an increase in free 40S and 60S ribosomal subunits and monosomes in the $Nmp4^{-/-}$ cells, suggesting that the enhanced translation was also accompanied by an increase the amount of ribosomes.

To test the idea that increased global translation in $Nmp4^{-/-}$ cells is a consequence of elevated GADD34 activity, we treated the MSPCs with salubrinal, a small molecule inhibitor of GADD34, and CReP-targeted dephosphorylation of eIF2α-P (26). Treatment of the *Nmp4*-deleted cells led to a marked reduction in large polysomes, indicating that the inhibition of GADD34 and CReP lowered global protein synthesis (Fig. 2*B*). By comparison, salubrinal did not appreciably change the polysome profile in WT MSPCs. In conjunction, we also measured the levels of eIF2α-P in WT and $Nmp4^{-/-}$ MSPCs left untreated, treated individually, or treated in combination with salubrinal or tunicamycin (Fig. 2*C*). Levels of eIF2α-P in the WT MSPCs remained largely unchanged with salubrinal treatment alone but were increased with tunicamycin treatment that was further elevated with combined drug treatment. Measurement of eIF2α-P was largely decreased in the $Nmp4^{-/-}$ MSPCs due to increased *Gadd34* expression; however, there was a modest increase in eIF2α-P with either salubrinal or tunicamycin treatment alone that was further exacerbated with the combined drug treatment (quantified in Fig. 2*C*). We conclude that elevated *Gadd34* expression in the $Nmp4^{-/-}$ MSPCs contributes to a portion of the observed increase in global protein synthesis.

Deletion of Nmp4 in MSPCs Increases Ribosome Biogenesis—Given that more ribosomes are suggested to be present in the $Nmp4^{-/-}$ cells, we carried out sucrose gradient ultracentrifugation using lysates depleted for Mg^{2+}, a condition that leads to release of ribosomes from mRNAs. There were significant increases in both free 40S and 60S ribosomal subunits in the $Nmp4^{-/-}$ cells compared with WT (Fig. 2*D*). Equal amounts of total RNA, as determined by absorbance at 260 nm, were applied to the sucrose gradients, and we noted that there were consistently more RNA in the MSPCs deleted for *Nmp4* compared with equal numbers of WT cells. We confirmed this key finding by purifying and measuring total RNA and DNA from equal numbers of the MSPCs. Although there were similar amounts of DNA between the $Nmp4^{-/-}$ and WT cells, there was 2-fold more total RNA in the *Nmp4*-deleted cells compared with WT (Fig. 2*E*). The majority of total RNA in cells consists of rRNA, and these results support the idea that there is increased ribosome biogenesis in the MSPCs upon deletion of *Nmp4*.

We next sought to understand the underlying basis for increased ribosomes in the MSPCs deleted for *Nmp4*. mTORC1 and c-MYC are potent inducers of ribosome biogenesis (27, 28), and prior ChIP-Seq analyses indicated that NMP4 can bind to the promoter of the *c-Myc* gene (Fig. 1*A*) (20). There were increased levels of *c-Myc* mRNA in the $Nmp4^{-/-}$ cells as compared with WT (Fig. 1*C*). Furthermore, there were elevated c-MYC protein levels in the $Nmp4^{-/-}$ cells, whereas levels of phosphorylated S6, a measure of mTORC1 activity, were similar between the *Nmp4*-depleted cells and WT (Fig. 3*B*). We note that total S6 protein levels were significantly increased in the $Nmp4^{-/-}$ cells, consistent with increased ribosome biogenesis. These results suggest that increased expression of *c-Myc* in the MSPCs deleted for *Nmp4* is an underlying reason for increased ribosomes. To address this idea, we used qPCR to measure expression levels of c-MYC target genes in WT and *Nmp4*-deleted MSPCs. Consistent with our measurements of

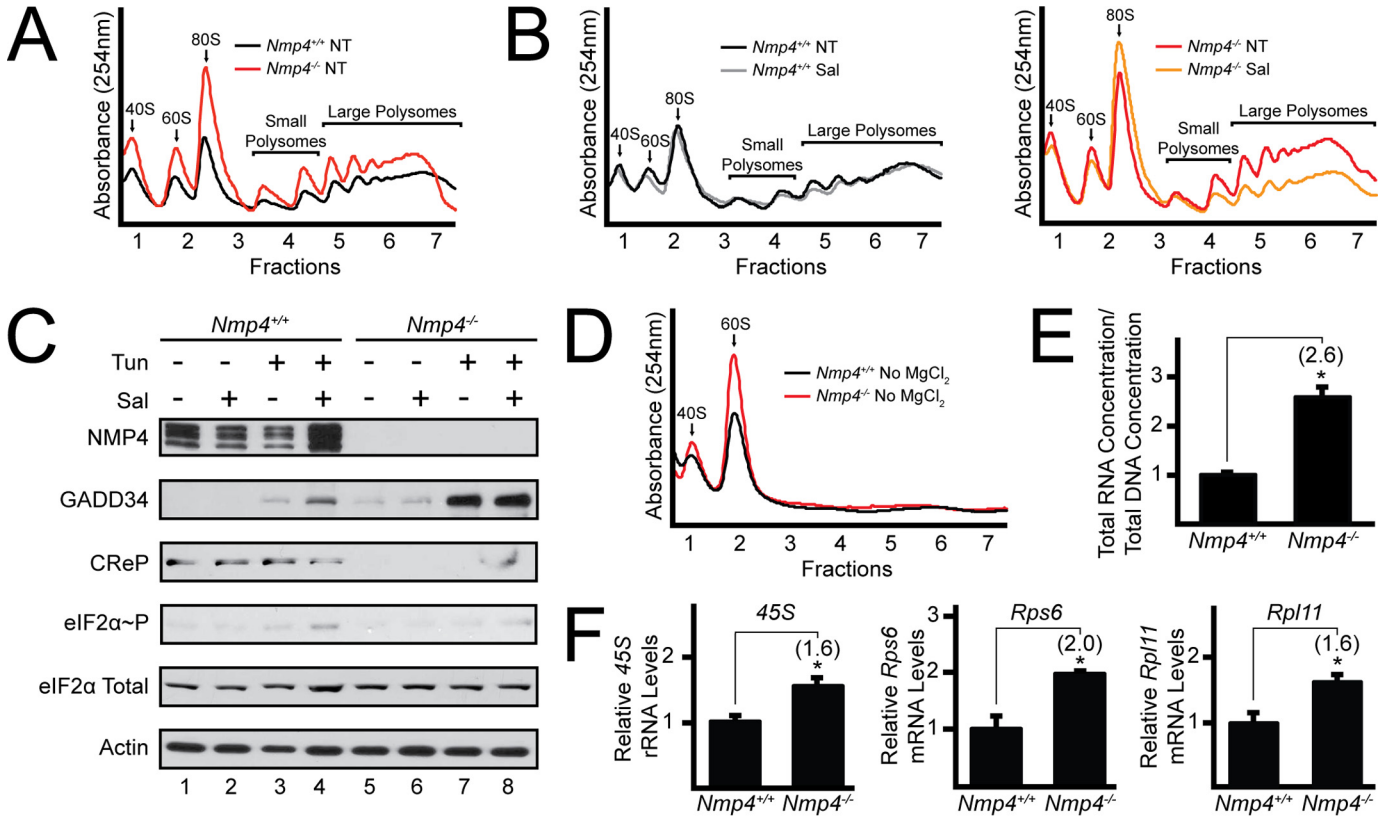

FIGURE 2. **Deletion of *Nmp4* in MSPCs increases ribosome biogenesis and protein synthesis.** *A*, lysates were collected from WT and *Nmp4*$^{-/-}$ MSPCs, and equal amounts of total RNA were layered on top of 10–50% sucrose gradients followed by ultracentrifugation and analysis of whole-lysate polysome profiles at 254 nm. *B*, polysome profiles were conducted as in *panel A* with the addition of treatment of WT and *Nmp4*$^{-/-}$ cells with salubrinal for 6 h or no treatment (*NT*). *C*, WT and *Nmp4*$^{-/-}$ MSPCs were treated individually or in combination with salubrinal and tunicamycin for 6 h as indicated, and the indicated proteins were measured by immunoblot. Quantification of eIF2α~P was conducted using ImageJ software. Values feature the lane number in the immunoblot, with the first lane on the left designated as *lane 1*, followed by quantification of eIF2α-P in parentheses: 1(1); 2(1); 3(1.6); 4(3.3); 5(0.6); 6(0.8); 7(1.3); 8(2.4). *D*, levels of 40S and 60S ribosomal subunits were measured as in *panel A* with the exception that $MgCl_2$ was omitted in the lysis and sucrose gradients. *E*, total DNA and total RNA lysates were quantified from WT and *Nmp4*$^{-/-}$ MSPCs. *F*, the *45S* rRNA and *Rps6* and *Rpl11* mRNAs were measured by qRT-PCR in WT and *Nmp4*$^{-/-}$ MSPCs. *Panels A*, *B*, *C*, and *D* are representative of three independent biological experiments. Relative values of three biological replicates are represented as histograms with the S.D. indicated for *panels E* and *F*. Differences between treatment groups are indicated by *.

increased 40S and 60S ribosomal subunits, there was a 1.6-fold increase in expression of *45S* rRNA and *Rpl11* mRNA and a 2-fold increase in *Rps6* mRNA (Fig. 2*F*). These results support that idea that ribosome biogenesis is increased in MSPCs deleted for *Nmp4* by a mechanism involving c-MYC.

Deletion of Nmp4 Sensitizes MSPCs to Chronic ER Stress—In the UPR, expression of *Gadd34* is induced transcriptionally via ATF4 and translationally in response to eIF2α-P (8, 10). Consistent with this idea, we observed a >8-fold increase in the level of *Gadd34* transcript upon treatment of WT cells with tunicamycin (Fig. 3*A*). A similar induction of *Gadd34* mRNA was also observed upon tunicamycin treatment of *Nmp4*$^{-/-}$ cells; however, given that *Nmp4*-deleted cells have much higher basal levels of *Gadd34* transcripts, there was about a 4-fold increase in *Nmp4*$^{-/-}$ cells exposed to tunicamycin compared with similarly stress WT MSPCs. Analysis of *Gadd34* mRNA levels also resulted in a statistically significant two-way analysis of variance for genotype × treatment interactions. These patterns of induction of GADD34 protein were also observed in the WT and *Nmp4*$^{-/-}$ cells (Fig. 3*B*). Together these results are consistent with the idea that NMP4 serves to lower *Gadd34* transcription expression during both basal and stressed conditions.

Upon ER stress in WT cells there was induced eIF2α-P, with a maximum ~6 h of tunicamycin treatment. By 9 h of ER stress, increased expression of endogenous *Gadd34* led to feedback dephosphorylation of eIF2α-P (Fig. 3*B*). The greater levels of GADD34 protein in the *Nmp4*$^{-/-}$ cells culminated in minimal induction of eIF2α-P during ER stress, which led to lowered levels of ATF4 expression and largely sustained protein synthesis during tunicamycin treatment (Fig. 3, *B* and *C*). Of interest, *Nmp4*$^{-/-}$ cells showed a sharp reduction in the amounts of CReP protein. Despite being designated a constitutively expressed targeting subunit for type 1 protein phosphatase dephosphorylation of eIF2α-P, *Crep* expression was reported to be sharply reduced upon overexpression of GADD34 (10), suggesting that there can be cross-regulation between the *Crep* and *Gadd34* genes.

We next measured mTORC1 activity and expression of *c-Myc* in the MSPCs subjected to ER stress. Consistent with prior reports (29), mTORC1 was repressed by ER stress in WT cells as illustrated by lowered phosphorylation of RPS6 during the time course of tunicamycin treatment (Fig. 3*B*). A similar reduction in RPS6 phosphorylation during ER stress also occurred in the *Nmp4*-deleted cells. We did note that total RPL11 levels as well as RPS6 were increased in the

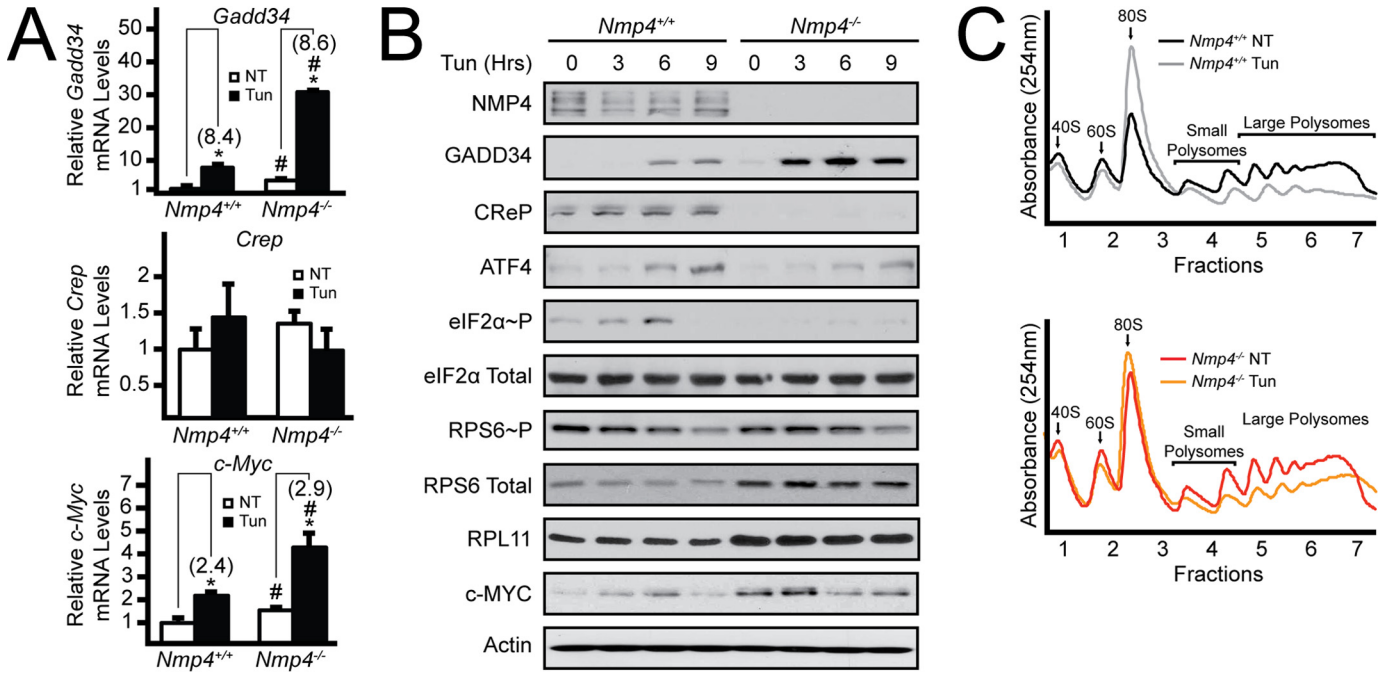

FIGURE 3. **Deletion of *Nmp4* facilitates maintenance of global translation during activation of the UPR.** *A*, *Gadd34*, *Crep*, and c-*Myc* mRNAs were measured by qRT-PCR in WT and *Nmp4*$^{-/-}$ MSPCs that were treated with tunicamycin (*Tun*) for 6 h or left untreated. *NT*, not treated. *B*, WT and *Nmp4*$^{-/-}$ MSPCs were treated with tunicamycin for 3, 6, or 9 h or left untreated, and the indicated proteins were measured by immunoblot. *C*, lysates were collected from WT and *Nmp4*$^{-/-}$ MSPCs treated with tunicamycin for 6 h or left untreated, and equal amounts of total RNA were layered on top of 10–50% sucrose gradients followed by ultracentrifugation and analysis of whole-lysate polysome profiles at 254 nm. Relative values of three biological replicates are represented as histograms with the S.D. indicated for *Panel A*. *Panels B* and *C* are representative of three independent biological experiments. Differences between treatment groups are indicated by asterisks (*), and differences between genotypes are indicated by a number # symbols.

Nmp4$^{-/-}$ cells independent of ER stress, which further supports the idea that there are increased amounts of ribosomes upon deletion of *Nmp4*. Levels of c-MYC protein were higher in *Nmp4*$^{-/-}$ cells compared with WT in the absence of stress (Fig. 3*B*). However, with longer exposure to ER stress the *Nmp4*-deleted cells showed some lowering of c-MYC protein.

Phosphorylation of eIF2α can provide for protection against acute ER stress (1, 30, 31). Given that *Nmp4*$^{-/-}$ cells exhibit elevated *Gadd34* expression concomitant with lower eIF2α-P, we measured the viability of WT and *Nmp4*-deleted cells exposed to tunicamycin for up to 24 h. WT cells were largely resistant to ER stress, with only a modest 10% reduction in cell viability as measured by MTT assay (Fig. 4*A*). By comparison, *Nmp4*$^{-/-}$ cells showed a striking sensitivity to the ER stress, culminating in a 60% reduction of cells by 24 h of tunicamycin treatment. Furthermore, there was increased caspase 3/7 activity in the *Nmp4*-deleted cells upon ER stress, which was absent in similarly treated WT cells (Fig. 4*B*). Finally, we addressed the role of increased *Gadd34* expression in the sensitization of *Nmp4*$^{-/-}$ cells to acute ER stress. The WT and *Nmp4*-deleted cells were treated with tunicamycin in the presence or absence of salubrinal (Fig. 4*C*). Salubrinal treatment provided for cell resistance to tunicamycin in the *Nmp4*$^{-/-}$ cells. Furthermore, combination treatment with torin 1, a potent small molecule inhibitor of mTORC1 (32), did not significantly alter the sensitivity of the *Nmp4*$^{-/-}$ cells to the ER stress. These findings indicate that increased *Gadd34* expression resulting from loss of *Nmp4* in MSPCs renders cells more sensitive to acute ER stress.

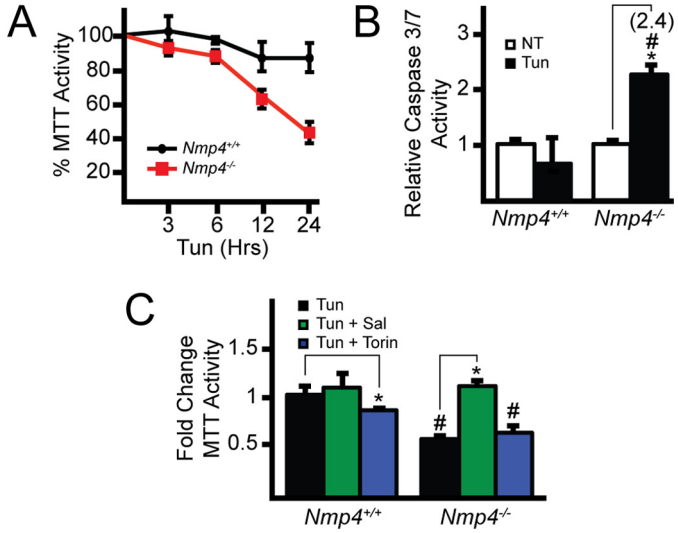

FIGURE 4. **Deletion of *Nmp4* sensitizes MSPCs to pharmacological induction of ER stress.** *A*, equal numbers of MSPCs were cultured for 24 h followed by treatment with or without tunicamycin for up to an additional 24 h. MTT activity was measured by the conversion of tetrazolium to formazan. *B*, caspase 3/7 activity was measured in MSPCs treated with tunicamycin for 24 h or no ER stress. *C*, MTT activity was measured in the MSPCs treated with tunicamycin or combined treatment with either salubrinal or torin 1. Relative values of three biological replicates are illustrated with the S.D. indicated for *panels A*, *B*, and *C*. Differences between treatment groups are indicated by *asterisks* (*), and differences between genotypes are indicated by a number (#) symbols.

Discussion

In this study we showed that NMP4 represses *Gadd34* and *c-Myc* expression and that loss of *Nmp4* culminates in increased ribosome biogenesis and protein synthesis (Fig. 5).

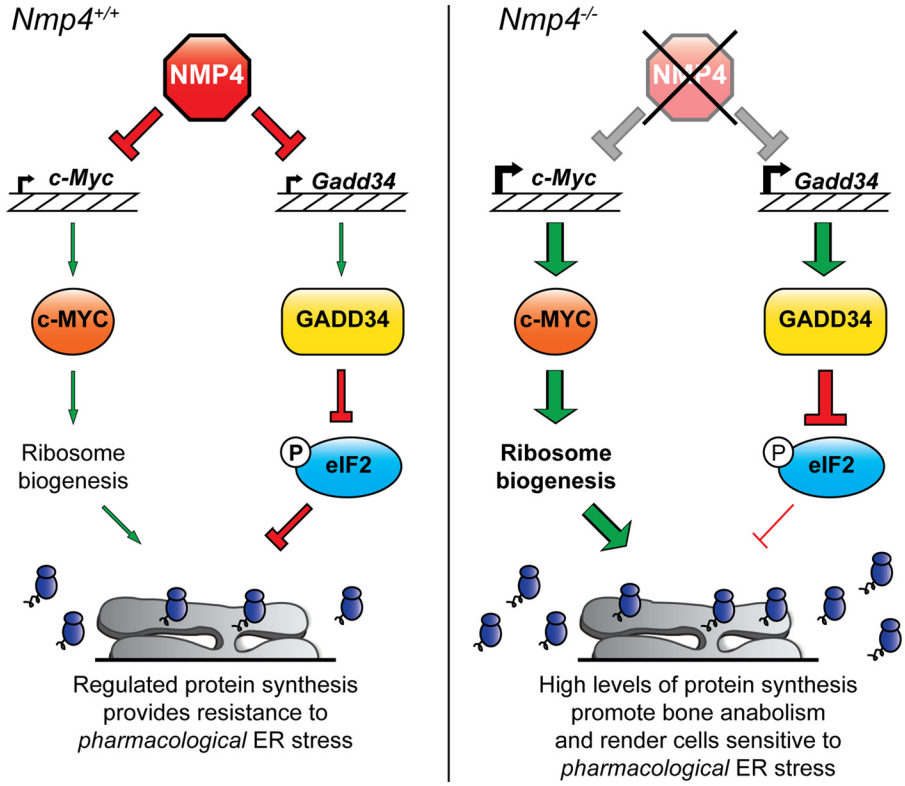

FIGURE 5. **Model for NMP4 regulation of ribosome biogenesis and the UPR.** NMP4 serves to dampen transcriptional expression of *c-Myc* and *Gadd34*, which are important for regulation of ribosome biogenesis and eIF2α-P and the UPR, respectively. ER stress and induction of the UPR in *Nmp4*$^{+/+}$ cells results in decreased protein synthesis that promotes stress alleviation, partially through the regulated expression of *c-Myc* and *Gadd34*. However, in *Nmp4*$^{-/-}$ cells there are high levels of *c-Myc* and *Gadd34* expression and subsequent elevation of ribosome biogenesis and translation initiation through GADD34-mediated dephosphorylation of eIF2α-P. As a consequence, heightened levels of synthesized proteins slated to be retained in the cytosol and those directed into the ER for secretion are maintained during pharmacological induction of the UPR, thwarting stress adaptation that renders cells sensitive to the acute ER stress. Loss of *Nmp4* has also been shown to increase bone anabolism in mice, which is likely due, at least in part, to increased c-MYC- and GADD34-mediated protein synthesis and secretion.

Translational control is central to the maintenance of cellular homeostasis and is critical for the implementation of the UPR, especially in professional secretory cells. In the UPR, eIF2α-P is central for resistance to acute ER stress, and premature resumption of translation can reduce cell viability (24, 33, 34). This idea is illustrated by the finding that pharmacological induction of ER stress resulted in decreased cell viability of *Nmp4*$^{-/-}$ MSPCs that was ameliorated upon inhibition of GADD34 and CReP activity. Furthermore, we showed that loss of *Nmp4* increases ribosome biogenesis by a process suggested to involve c-MYC, contributing to further increases in protein synthesis (Fig. 5). Combined, these results suggest a prominent role for NMP4-mediated dampening of translational control in the UPR, which is critical in the ability of cells to appropriately sense and respond to ER stress. A model for NMP4-mediated regulation of *c-Myc* and *Gadd34* expression and subsequent translation control is presented in Fig. 5. NMP4 serves to repress both *c-Myc* and *Gadd34* expression, helping to maintain appropriate regulation of ribosome biogenesis and translation initiation through eIF2α-P (Fig. 5). Loss of *Nmp4* results in heightened *c-Myc* and *Gadd34* expression that contributes to increases in ribosome biogenesis and translation initiation, likely facilitating enhanced bone matrix deposition in mice. However, high levels of protein synthesis incurred through the loss of *Nmp4* rendered cells sensitive to acute ER stress induced by pharmacological agents, such as tunicamycin, due to an inability to appropriately regulate translation and activate some of the adaptive features of the UPR (Fig. 5).

Previous work suggested that activation of the UPR plays a significant and obligatory role in osteoblast differentiation, proliferation, and function, supporting the idea that the UPR promotes cellular homeostasis in highly secretory cells by regulating changes in gene expression and protecting cells from defects in protein folding (1, 13, 35). Emphasizing the importance of the key UPR regulators in secretory cells, loss of function of *Perk*, *Atf4*, *Ire1*, *Xpb1*, or *Oasis* disrupts the health and secretory functions of osteoblasts and subsequent bone formation (13–15). Here we show that NMP4 also plays a role in the appropriate regulation of the UPR through repression of the expression of *Gadd34*. Loss of *Nmp4* resulted in a GADD34-mediated increase in protein synthesis basally that was largely sustained during pharmacological induction of ER stress, which then sensitized cells to the underlying stress. This finding emphasizes the role of NMP4 in maintaining the cell in a homeostatic state in which protection from proteotoxicity is balanced with the secretory requirements of the cell. In contrast to pharmacological stress, more mild, physiological stresses would likely result in maintenance of translation and some acceleration of protein secretion in the *Nmp4*$^{-/-}$ background without the toxicities associated with sustained pharmacological induction of ER stress. Indeed, targeted deletion of *Nmp4* in mice enhances bone response to PTH and BMP2 and protects

these animals from osteopenia likely through increased production and secretion of factors that facilitate bone formation (20).

The regulated expression and activity of NMP4 in response to pharmacological and physiological stresses also likely plays a role in NMP4-mediated regulation of ribosome biogenesis and the UPR. *Nmp4* mRNA was reported to be expressed in all major organs analyzed, although there were two distinct transcripts that were differentially expressed by a mechanism suggested to involve alternative mRNA splicing (36). Transcription of *Nmp4* is also mediated through the activity of two alternative promoters that both respond to PTH treatment and result in the production of *Nmp4* mRNAs with different transcription start sites (37). Collectively, these regulatory mechanisms result in the production of multiple NMP4 protein isoforms, some of which contain an in-frame amino-terminal extension and all of which contain Cys_2His_2 zinc finger binding domains, which can range from five to eight in number (36–38). Although we observed multiple NMP4 protein isoforms, we did not detect an appreciable change in the pattern of NMP4 expression in response to pharmacological induction of the UPR (Fig. 3*B*). This suggests that protein modifications identified in NMP4 (39, 40) or availability of NMP4 interacting proteins (36) may play a role in regulating the localization and activity of NMP4 in response to cellular cues to modulate protein production and secretion (21).

Of note is the decrease in CReP protein expression that was observed upon loss of *Nmp4* and overexpression of *Gadd34*. Despite being designated a constitutively expressed targeting subunit for type 1 protein phosphatase dephosphorylation of eIF2α-P, *Crep* expression was previously reported to be sharply reduced upon overexpression of GADD34 (10), suggesting an unexplored cross-regulation between the *Crep* and *Gadd34* genes. The changes in ribosome biogenesis and eIF2α-P described herein emphasize the importance of regulation of NMP4 in *Gadd34* and *c-Myc* expression in the maintenance of cellular homeostasis and provide a better understanding of the processes that maintain appropriate levels of protein synthesis in highly secretory tissues.

Author Contributions—S. K. Y. designed, performed, and analyzed the experiments and wrote the manuscript. Y. S. performed the experiments. R. C. W. and J. P. B. conceived and coordinated the study, designed and analyzed the experiments, and wrote the manuscript. All authors reviewed the results and approved the final version of the manuscript.

References

1. Walter, P., and Ron, D. (2011) The unfolded protein response: from stress pathway to homeostatic regulation. *Science* **334,** 1081–1086
2. Shi, Y., Vattem, K. M., Sood, R., An, J., Liang, J., Stramm, L., and Wek, R. C. (1998) Identification and characterization of pancreatic eukaryotic initiation factor 2α-subunit kinase, PEK, involved in translational control. *Mol. Cell. Biol.* **18,** 7499–7509
3. Harding, H. P., Zhang, Y., and Ron, D. (1999) Protein translation and folding are coupled by an endoplasmic-reticulum-resident kinase. *Nature* **397,** 271–274
4. Harding, H. P., Zhang, Y., Zeng, H., Novoa, I., Lu, P. D., Calfon, M., Sadri, N., Yun, C., Popko, B., Paules, R., Stojdl, D. F., Bell, J. C., Hettmann, T., Leiden, J. M., and Ron, D. (2003) An integrated stress response regulates amino acid metabolism and resistance to oxidative stress. *Mol. Cell* **11,** 619–633
5. Vattem, K. M., and Wek, R. C. (2004) Reinitiation involving upstream open reading frames regulates *ATF4* mRNA translation in mammalian cells. *Proc. Natl. Acad. Sci. U.S.A.* **101,** 11269–11274
6. Harding, H. P., Novoa, I., Zhang, Y., Zeng, H., Wek, R., Schapira, M., and Ron, D. (2000) Regulated translation initiation controls stress-induced gene expression in mammalian cells. *Mol. Cell* **6,** 1099–1108
7. Novoa, I., Zeng, H., Harding, H. P., and Ron, D. (2001) Feedback inhibition of the unfolded protein response by GADD34-mediated dephosphorylation of eIF2α. *J. Cell Biol.* **153,** 1011–1022
8. Ma, Y., and Hendershot, L. M. (2003) Delineation of a negative feedback regulatory loop that controls protein translation during endoplasmic reticulum stress. *J. Biol. Chem.* **278,** 34864–34873
9. Connor, J. H., Weiser, D. C., Li, S., Hallenbeck, J. M., and Shenolikar, S. (2001) Growth arrest and DNA damage-inducible protein GADD34 assembles a novel signaling complex containing protein phosphatase 1 and inhibitor 1. *Mol. Cell. Biol.* **21,** 6841–6850
10. Young, S. K., Willy, J. A., Wu, C., Sachs, M. S., and Wek, R. C. (2015) Ribosome reinitiation directs gene-specific translation and regulates the integrated stress response. *J. Biol. Chem.* **290,** 28257–28271
11. Lee, Y. Y., Cevallos, R. C., and Jan, E. (2009) An upstream open reading frame regulates translation of GADD34 during cellular stresses that induce eIF2α phosphorylation. *J. Biol. Chem.* **284,** 6661–6673
12. Kondo, S., Saito, A., Asada, R., Kanemoto, S., and Imaizumi, K. (2011) Physiological unfolded protein response regulated by OASIS family members, transmembrane bZIP transcription factors. *IUBMB life* **63,** 233–239
13. Saito, A., Ochiai, K., Kondo, S., Tsumagari, K., Murakami, T., Cavener, D. R., and Imaizumi, K. (2011) Endoplasmic reticulum stress response mediated by the PERK-eIF2α-ATF4 pathway is involved in osteoblast differentiation induced by BMP2. *J. Biol. Chem.* **286,** 4809–4818
14. Tohmonda, T., Miyauchi, Y., Ghosh, R., Yoda, M., Uchikawa, S., Takito, J., Morioka, H., Nakamura, M., Iwawaki, T., Chiba, K., Toyama, Y., Urano, F., and Horiuchi, K. (2011) The IRE1α-XBP1 pathway is essential for osteoblast differentiation through promoting transcription of Osterix. *EMBO Rep.* **12,** 451–457
15. Murakami, T., Saito, A., Hino, S., Kondo, S., Kanemoto, S., Chihara, K., Sekiya, H., Tsumagari, K., Ochiai, K., Yoshinaga, K., Saitoh, M., Nishimura, R., Yoneda, T., Kou, I., Furuichi, T., Ikegawa, S., Ikawa, M., Okabe, M., Wanaka, A., and Imaizumi, K. (2009) Signalling mediated by the endoplasmic reticulum stress transducer OASIS is involved in bone formation. *Nat. Cell Biol.* **11,** 1205–1211
16. Jang, W. G., Kim, E. J., Kim, D. K., Ryoo, H. M., Lee, K. B., Kim, S. H., Choi, H. S., and Koh, J. T. (2012) BMP2 protein regulates osteocalcin expression via Runx2-mediated Atf6 gene transcription. *J. Biol. Chem.* **287,** 905–915
17. Karsenty, G. (2008) Transcriptional control of skeletogenesis. *Annu. Rev. Genomics Hum. Genet.* **9,** 183–196
18. Childress, P., Philip, B. K., Robling, A. G., Bruzzaniti, A., Kacena, M. A., Bivi, N., Plotkin, L. I., Heller, A., and Bidwell, J. P. (2011) Nmp4/CIZ suppresses the response of bone to anabolic parathyroid hormone by regulating both osteoblasts and osteoclasts. *Calcif. Tissue Int.* **89,** 74–89
19. Robling, A. G., Childress, P., Yu, J., Cotte, J., Heller, A., Philip, B. K., and Bidwell, J. P. (2009) Nmp4/CIZ suppresses parathyroid hormone-induced increases in trabecular bone. *J. Cell. Physiol.* **219,** 734–743
20. Childress, P., Stayrook, K. R., Alvarez, M. B., Wang, Z., Shao, Y., Hernandez-Buquer, S., Mack, J. K., Grese, Z. R., He, Y., Horan, D., Pavalko, F. M., Warden, S. J., Robling, A. G., Yang, F. C., Allen, M. R., Krishnan, V., Liu, Y., and Bidwell, J. P. (2015) Genome-wide mapping and interrogation of the nmp4 antianabolic bone axis. *Mol. Endocrinol.* **29,** 1269–1285
21. Feister, H. A., Torrungruang, K., Thunyakitpisal, P., Parker, G. E., Rhodes, S. J., and Bidwell, J. P. (2000) NP/NMP4 transcription factors have distinct osteoblast nuclear matrix subdomains. *J. Cell. Biochem.* **79,** 506–517
22. Wu, X., Estwick, S. A., Chen, S., Yu, M., Ming, W., Nebesio, T. D., Li, Y., Yuan, J., Kapur, R., Ingram, D., Yoder, M. C., and Yang, F. C. (2006) Neurofibromin plays a critical role in modulating osteoblast differentiation of mesenchymal stem/progenitor cells. *Hum. Mol. Genet.* **15,** 2837–2845
23. Jousse, C., Oyadomari, S., Novoa, I., Lu, P., Zhang, Y., Harding, H. P., and

Ron, D. (2003) Inhibition of a constitutive translation initiation factor 2a phosphatase, CReP, promotes survival of stressed cells. *J. Cell Biol.* **163,** 767–775
24. Han, J., Back, S. H., Hur, J., Lin, Y. H., Gildersleeve, R., Shan, J., Yuan, C. L., Krokowski, D., Wang, S., Hatzoglou, M., Kilberg, M. S., Sartor, M. A., and Kaufman, R. J. (2013) ER-stress-induced transcriptional regulation increases protein synthesis leading to cell death. *Nat. Cell Biol.* **15,** 481–490
25. Baird, T. D., and Wek, R. C. (2012) Eukaryotic initiation factor 2 phosphorylation and translational control in metabolism. *Adv. Nutr.* **3,** 307–321
26. Boyce, M., Bryant, K. F., Jousse, C., Long, K., Harding, H. P., Scheuner, D., Kaufman, R. J., Ma, D., Coen, D. M., Ron, D., and Yuan, J. (2005) A selective inhibitor of eIF2α dephosphorylation protects cells from ER stress. *Science* **307,** 935–939
27. van Riggelen, J., Yetil, A., and Felsher, D. W. (2010) MYC as a regulator of ribosome biogenesis and protein synthesis. *Nat. Rev. Cancer* **10,** 301–309
28. Iadevaia, V., Liu, R., and Proud, C. G. (2014) mTORC1 signaling controls multiple steps in ribosome biogenesis. *Semin. Cell Dev. Biol.* **36,** 113–120
29. Preston, A. M., and Hendershot, L. M. (2013) Examination of a second node of translational control in the unfolded protein response. *J. Cell Sci.* **126,** 4253–4261
30. Scheuner, D., Song, B., McEwen, E., Liu, C., Laybutt, R., Gillespie, P., Saunders, T., Bonner-Weir, S., and Kaufman, R. J. (2001) Translational control is required for the unfolded protein response and *in vivo* glucose homeostasis. *Mol. Cell* **7,** 1165–1176
31. Harding, H. P., Zhang, Y., Bertolotti, A., Zeng, H., and Ron, D. (2000) Perk is essential for translational regulation and cell survival during the unfolded protein response. *Mol. Cell* **5,** 897–904
32. Thoreen, C. C., Kang, S. A., Chang, J. W., Liu, Q., Zhang, J., Gao, Y., Reichling, L. J., Sim, T., Sabatini, D. M., and Gray, N. S. (2009) An ATP-competitive mammalian target of rapamycin inhibitor reveals rapamycin-resistant functions of mTORC1. *J. Biol. Chem.* **284,** 8023–8032
33. Bernales, S., Papa, F. R., and Walter, P. (2006) Intracellular signaling by the unfolded protein response. *Annu. Rev. Cell Dev. Biol.* **22,** 487–508
34. Marciniak, S. J., Yun, C. Y., Oyadomari, S., Novoa, I., Zhang, Y., Jungreis, R., Nagata, K., Harding, H. P., and Ron, D. (2004) CHOP induces death by promoting protein synthesis and oxidation in the stressed endoplasmic reticulum. *Genes Dev.* **18,** 3066–3077
35. Wei, J., Sheng, X., Feng, D., McGrath, B., and Cavener, D. R. (2008) PERK is essential for neonatal skeletal development to regulate osteoblast proliferation and differentiation. *J. Cell. Physiol.* **217,** 693–707
36. Nakamoto, T., Yamagata, T., Sakai, R., Ogawa, S., Honda, H., Ueno, H., Hirano, N., Yazaki, Y., and Hirai, H. (2000) CIZ, a zinc finger protein that interacts with p130(cas) and activates the expression of matrix metalloproteinases. *Mol. Cell. Biol.* **20,** 1649–1658
37. Alvarez, M., Shah, R., Rhodes, S. J., and Bidwell, J. P. (2005) Two promoters control the mouse Nmp4/CIZ transcription factor gene. *Gene* **347,** 43–54
38. Thunyakitpisal, P., Alvarez, M., Tokunaga, K., Onyia, J. E., Hock, J., Ohashi, N., Feister, H., Rhodes, S. J., and Bidwell, J. P. (2001) Cloning and functional analysis of a family of nuclear matrix transcription factors (NP/NMP4) that regulate type I collagen expression in osteoblasts. *J. Bone Miner. Res.* **16,** 10–23
39. Sharma, K., D'Souza, R. C., Tyanova, S., Schaab, C., Winiewski, J. R., Cox, J., and Mann, M. (2014) Ultradeep human phosphoproteome reveals a distinct regulatory nature of Tyr and Ser/Thr-based signaling. *Cell Rep.* **8,** 1583–1594
40. Mertins, P., Yang, F., Liu, T., Mani, D. R., Petyuk, V. A., Gillette, M. A., Clauser, K. R., Qiao, J. W., Gritsenko, M. A., Moore, R. J., Levine, D. A., Townsend, R., Erdmann-Gilmore, P., Snider, J. E., Davies, S. R., *et al.* (2014) Ischemia in tumors induces early and sustained phosphorylation changes in stress kinase pathways but does not affect global protein levels. *Mol. Cell. Proteomics* **13,** 1690–1704

Genome-Wide Mapping and Interrogation of the Nmp4 Antianabolic Bone Axis

Paul Childress, Keith R. Stayrook, Marta B. Alvarez, Zhiping Wang, Yu Shao, Selene Hernandez-Buquer, Justin K. Mack, Zachary R. Grese, Yongzheng He, Daniel Horan, Fredrick M. Pavalko, Stuart J. Warden, Alexander G. Robling, Feng-Chun Yang, Matthew R. Allen, Venkatesh Krishnan, Yunlong Liu, and Joseph P. Bidwell

Department of Anatomy and Cell Biology (P.C., S.H.-B., D.H., A.G.R., M.R.A., J.P.B.), Indiana University School of Medicine, Indianapolis, Indiana 46202; Lilly Research Laboratories (K.R.S., J.K.M., Z.R.G., V.K.), Eli Lilly and Company, Indianapolis, Indiana 46202; Orthopaedic Surgery (M.B.A.), Indiana University School of Medicine; Department of Medical and Molecular Genetics (Z.W., Y.S., Y.L., J.P.B.), Indiana University School of Medicine; Center for Computational Biology and Bioinformatics (Z.W., Y.L.), Indiana University School of Medicine; Department of Pediatrics (Y.H., F.-C.Y.), Indiana University School of Medicine; Herman B Wells Center for Pediatric Research (Y.H., F.-C.Y.); Cellular and Integrative Physiology (F.M.P.); Center for Translational Musculoskeletal Research (S.J.W.), School of Health and Rehabilitation Sciences, Indiana University; and Department of Physical Therapy (S.J.W.), School of Health and Rehabilitation Sciences, Indiana University, Indianapolis, Indiana 46202

PTH is an osteoanabolic for treating osteoporosis but its potency wanes. Disabling the transcription factor nuclear matrix protein 4 (Nmp4) in healthy, ovary-intact mice enhances bone response to PTH and bone morphogenetic protein 2 and protects from unloading-induced osteopenia. These *Nmp4*$^{-/-}$ mice exhibit expanded bone marrow populations of osteoprogenitors and supporting CD8^{+} T cells. To determine whether the *Nmp4*$^{-/-}$ phenotype persists in an osteoporosis model we compared PTH response in ovariectomized (ovx) wild-type (WT) and *Nmp4*$^{-/-}$ mice. To identify potential Nmp4 target genes, we performed bioinformatic/pathway profiling on Nmp4 chromatin immunoprecipitation sequencing (ChIP-seq) data. Mice (12 w) were ovx or sham operated 4 weeks before the initiation of PTH therapy. Skeletal phenotype analysis included microcomputed tomography, histomorphometry, serum profiles, fluorescence-activated cell sorting and the growth/mineralization of cultured WT and *Nmp4*$^{-/-}$ bone marrow mesenchymal stem progenitor cells (MSPCs). ChIP-seq data were derived using MC3T3-E1 preosteoblasts, murine embryonic stem cells, and 2 blood cell lines. Ovx *Nmp4*$^{-/-}$ mice exhibited an improved response to PTH coupled with elevated numbers of osteoprogenitors and CD8^{+} T cells, but were not protected from ovx-induced bone loss. Cultured *Nmp4*$^{-/-}$ MSPCs displayed enhanced proliferation and accelerated mineralization. ChIP-seq/gene ontology analyses identified target genes likely under Nmp4 control as enriched for negative regulators of biosynthetic processes. Interrogation of mRNA transcripts in nondifferentiating and osteogenic differentiating WT and *Nmp4*$^{-/-}$ MSPCs was performed on 90 Nmp4 target genes and differentiation markers. These data suggest that Nmp4 suppresses bone anabolism, in part, by regulating IGF-binding protein expression. Changes in Nmp4 status may lead to improvements in osteoprogenitor response to therapeutic cues. **(*Molecular Endocrinology* 29: 1269–1285, 2015)**

Patients with severe osteoporosis are often treated with PTH, a potent osteoanabolic agent (1); however, the bone-building ability of this drug or its "anabolic window" wanes, likely due to latent increases in bone resorption (2–4). This limits its effectiveness to treat a chronic degenerative disease. Recent advances in bone-forming agents have shown that one can increase the extent of bone mass accrual with antisclerostin treatment compared with PTH (5). However, there may be unique pathways triggered by PTH, which allows for sustained targeting of early osteogenesis as evidenced by serum markers of bone formation such as N-terminal propeptide of type 1 procollagen (P1NP) and osteocalcin (OCN) (also known as bone gamma carboxyglutamate protein

ISSN Print 0888-8809 ISSN Online 1944-9917
Printed in USA

Received December 19, 2014. Accepted July 31, 2015.
First Published Online August 5, 2015

Abbreviations: AKT, thymoma viral proto-oncogene; BFR, bone formation rate; Bglap, bone gamma carboxyglutamate protein; BM, bone marrow; BMP2, bone morphogenetic protein 2; BV/TV, trabecular bone volume per total volume; ChIP-seq, chromatin immunoprecipitation sequencing; Conn.D, connectivity density; ΔΔCT, comparative threshold cycle; μCT, microcomputed tomography; CTX, C-terminal telopeptide; CXC, chemokine (C-X-C motif);

[Bglap]) (6, 7). In contrast to PTH, antisclerostin antibodies may have a limited capacity for targeting osteoprogenitors as evidenced by a relatively transient up-regulation of collagen-based markers such as P1NP (5). Therefore, given PTH's unique mode of action, therapies that could enhance PTH-mediated recruitment of osteoprogenitors may add value to some patients. How to achieve this enhancement is not clear. For example, attempts to extend and enhance PTH efficacy by combining treatment with antiresorptive medications have met with mixed success and have generally been underwhelming (8–10).

Blocking the activity of nuclear matrix protein 4 (Nmp4)/Cas-interacting zinc finger protein in mice dramatically enhanced their response to anabolic doses of PTH (11–13), suggesting a potential strategy for an adjuvant therapy (14). Intermittent exogenous doses of hormone stimulated equivalent new bone formation in wild-type (WT) and *Nmp4*$^{-/-}$ mice during the first 2 weeks of challenge, but at 3 weeks of treatment, the null mice exhibited greater than a 2-fold increase in new trabecular bone compared with their WT littermates (11). This augmented skeletogenesis in the *Nmp4*$^{-/-}$ mice was extended to 7 weeks of treatment and was observed in the femur, tibia, and vertebra. Serum OCN continued to rise at this time point in the *Nmp4*$^{-/-}$ mice but had decreased in the WT animals (11). However, the PTH response of the cortical compartment was equivalent throughout treatment in the WT and null mice (13). This suggests that disabling Nmp4 accelerates and enhances the response of bone to intermittent PTH (11).

Nmp4$^{-/-}$ bone may have a generalized accelerated and heightened response to systemic or local anabolic cues. For example, these mice also exhibited augmented bone morphogenetic protein 2 (BMP2)-induced ectopic bone formation compared with their WT littermates (15). The *Nmp4*-null mice showed an accelerated osseous regeneration after marrow ablation (15) and did not lose bone during hind limb unloading, which appeared to derive from an enhanced osteoblast activity (16).

Prerequisite for an adjuvant therapy target, disabling Nmp4 has little impact on the health, longevity, or global baseline phenotype of the mouse, with a few exceptions. The *Nmp4*$^{-/-}$ baseline skeletal phenotype (ie, bone mineral density and/or content and trabecular architecture) is generally equivalent compared with WT animals; although we have occasionally observed an unprovoked increase in bone properties in *Nmp4*$^{-/-}$ mice (11–13, 15). Similarly, male *Nmp4*$^{-/-}$ mice exhibit variable degrees of spermatogenic cell degeneration resembling germinal-cell aplasia with focal spermatogenesis resulting in *sporadic* infertility (17).

Our recent work suggests that the cellular basis of the osteoanabolic repressor function of Nmp4 is due to its effect on the bone marrow (BM)-derived stromal stem/progenitor cells also known as mesenchymal stem progenitor cells (MSPCs) (12). *Nmp4*$^{-/-}$ mice have significantly more osteoprogenitor cells in their marrow, which lie in wait to be quickly mobilized to differentiate into active osteoblasts upon stimulation with various osteoanabolic stimuli (12). There was no difference between WT and *Nmp4*$^{-/-}$ BM cellularity or profiles of several blood elements; however, the null mouse exhibited a 4-fold increase in CD45^{-}/CD105^{+}/nestin^{+}/CD146^{+} BM osteoprogenitor cells. These markers are a common hallmark to CFU-F cells with osteogenic potential (18, 19), and indeed, 4-fold more CFU-F$^{\text{Alk phos+}}$ and CFU-F$^{\text{Ob}}$ cells have been recovered from these mice compared with the WT animals (12, 15). A second, related phenomenon we have observed in *Nmp4*$^{-/-}$ mice is a 2-fold increase in the prevalence of CD8^{+} T cells in the femoral marrow, the lymphocyte population that provides potent input to induce MSPCs down the osteoblast differentiation pathway (12, 20–22). These blood cells express the parathyroid hormone 1 receptor and support the PTH anabolic response via the release of wingless-type MMTV integration site family, member 10B (Wnt10b) upon hormone challenge, which drives osteoprogenitor differentiation to preosteoblasts and mature matrix-producing bone cells (20–22).

There is little information on the molecular mechanisms and cellular pathways that mediate the antianabolic action of Nmp4. This transcription factor is a Cys_2His_2 zinc finger protein that primarily localizes to the nucleus although there is evidence for cytoplasmic activity (23, 24). The zinc fingers recognize the DNA minor groove of an AT-rich consensus sequence and 2 transactivation domains can suppress or activate transcription depending on the cellular context (24–28). The amino terminus of the rodent protein contains an src homology 3 domain-binding domain that associates with the adaptor signaling protein p130Crk-associated substrate (24), but the functional significance of this interaction remains unknown.

The *Nmp4*$^{-/-}$ progenitor cells and their progeny have an exaggerated stimulus response at the levels of tran-

CXCR4, CXC receptor 4; DAVID, Database for Annotation, Visualization, and Integrated Discovery; ENCODE, Encyclopedia of DNA Elements; FDR, false-discovery rate; FACS, fluorescence-activated cell sorting; GEM, genome wide event finding and motif discovery; GO, gene ontology; hPTH, human parathyroid hormone; Igfbp, Igf binding protein; KEGG, Kyoto Encyclopedia of Genes and Genomes; MAR, mineral apposition rate; MS/BS, mineralizing surface/bone surface; MSPC, mesenchymal stem progenitor cell; Nmp4, nuclear matrix protein 4; OCN, osteocalcin; ovx, ovariectomy; PBL, peripheral blood; P1NP, N-terminal propeptide of type 1 procollagen; preop, pre-operation; postop, postoperation; qRT-PCR, quantitative real-time PCR; SMI, structure model index; Tb.N, trabecular number; Tb.Sp, trabecular spacing; Tb.Th, trabecular thickness; *Thbs2*, thrombospondin 2; TLDA, TaqMan Low Density Array; TSS, transcription start site; Wnt10b, wingless-type MMTV integration site family; WT, wild-type; ZFP384, zinc finger protein 384 (mouse); ZNF384, zinc finger protein 384 (human).

scription and cell signaling (29–31). *Nmp4*-null BM stromal cells show an enhanced transcriptional response to PTH and BMP2 (26, 29, 30). The *Nmp4*$^{-/-}$-derived calvarial cells exhibit an increased load-induced phosphorylation of phosphatidylinositol 3-kinase and thymoma viral proto-oncogene (AKT) and β-catenin nuclear translocation (31). Analogous to heightened response to anabolic signals in *Nmp4*$^{-/-}$ osteolineage cells, osteoclast preparations from the null mice exhibited a heightened response to the remodeling signals of receptor activator of nuclear factor kappa-B ligand and macrophage colony-stimulating factor (11).

Two essential genotype-phenotype questions remaining to be addressed are 1) whether the *Nmp4*-null mouse is resistant to ovariectomy (ovx)-induced bone loss and 2) whether disabling Nmp4 improves PTH-based bone therapy in the ovx model. This is a focal preclinical extension of the *Nmp4*$^{-/-}$ phenotype necessary before this gene and its associated pathways can be considered potential targets for an adjuvant therapy. Additionally, we used expanded cultures of WT and *Nmp4*$^{-/-}$ MSPCs to probe the cell autonomous proliferative and mineralization activities of this cell population. To delineate the framework of the Nmp4 antianabolic network, we performed genome-wide chromatin immunoprecipitation sequencing (ChIP-seq) on MC3T3-E1 cells and combined these data with the data available for Nmp4 (also known as zinc finger protein 384 [ZFP384]) from the mouse Encyclopedia of DNA Elements (ENCODE) Consortium for transcription factors (32). Bioinformatic profiling, gene ontology (GO), and pathway analysis were performed on these datasets to infer a map of the negative regulation of bone anabolism under Nmp4 control. Interrogation of mRNA transcripts in nondifferentiating and osteogenic differentiating WT and *Nmp4*$^{-/-}$ MSPCs was performed on 90 Nmp4 target genes and differentiation markers to inaugurate validation of the Nmp4 antianabolic network.

Materials and Methods

Mice

Male and female *Nmp4*$^{-/-}$ mice, backcrossed onto a C57BL/6J background for 7 generations (11–13), and their WT littermates were produced and maintained in our colony at Indiana University Bioresearch Facility, Indiana University School of Dentistry. Our local Institutional Animal Care and Use Committee approved all husbandry practices and experimental procedures and regimens described in this investigation.

Bilateral ovx surgery

Twelve-week-old virgin mice were anesthetized using isoflurane inhalation followed by a mixture of xylazine and ketamine administered ip. A 1- to 2-cm dorsal incision was made in the midline below the level of the last rib and the skin bluntly dissected from the muscle on either side of the incision. Through the skin incision, the muscle wall was incised 1cm lateral to the midline 1–2cm below the last rib to enter the abdominal cavity. The periovarian fat pad was located and gently grasped and exteriorized. Care was taken not to directly handle the ovary to avoid abdominal implantation of ovarian tissue. Although holding the periovarian fat pad with forceps, the fallopian tube between the fat pad and uterus was clamped and crushed using mosquito hemostats. The crushed area was cut with scissors and the fat pad with ovary removed. The procedure was repeated on the contralateral side. The skin incision was closed with one or 2 surgical wound clips. The sham surgeries involved all the outlined steps except the crushing the fallopian tubes and the actual removal of the ovaries. To confirm the efficacy of ovx, uteri were weighed after euthanasia.

PTH treatment

At 16 weeks of age, ovx animals were sorted into 4 treatment groups based on equivalent mean-group-body weight. These 4 groups included 1) vehicle-treated WT; 2) PTH-treated WT; 3) vehicle-treated *Nmp4*$^{-/-}$; and 4) PTH-treated *Nmp4*$^{-/-}$ mice. Mice were injected sc with synthetic human PTH (hPTH) 1–34 acetate salt (Bachem Bioscience, Inc) at 30 μg/kg · d, daily or vehicle control (0.2% BSA and 1.0μN HCl in saline; Abbott Laboratory) for the length of time indicated.

Cell culture

Cells from ATCC (MC3T3-E1 subclone 4) were maintained in α-MEM supplemented with 100-IU/mL penicillin, 100-μg/mL streptomycin, 25-μg/mL amphotericin, 2mM L-glutamine (Gibco BRL), ascorbic acid (50 μg/mL; Sigma-Aldrich), and 10% fetal bovine serum (Sigma-Aldrich). Expanded MSPC cultures were established as previously described (33). Briefly, long BM was isolated from euthanized mice 6–8 weeks of age, and the BM mononuclear cells were isolated using a Ficoll gradient. These cells were plated in Mesencult Media + Mesencult Stimulatory Supplement (StemCell Technologies) and maintained in culture for 3–4 weeks without passage and fed every 5–7 days by removing 50% of the old media and adding 50% fresh media, very gently so as not to disturb the cells. At approximately 80% confluence, the cells were passaged at 1:3 dilution for 2 more passages before use or were frozen for storage. Cells were used for experiments between passages 5–10. For comparing cell proliferation rates between WT and *Nmp4*$^{-/-}$ MSPCs, the cells were transferred to α-MEM without the ascorbic acid in 12-well plates at 5000 cells/well (d 0). Cells were counted on days 2, 4, and 6 after seeding before refreshing the medium for the remaining cells. To evaluate mineralizing capacity cells were transferred to osteogenic differentiation medium and after 48 hours (d 0), which was comprised of α-MEM supplemented with ascorbic acid (5–50 μg/mL; Sigma-Aldrich), dexamethasone (0nM–10nM; Sigma-Aldrich), and 10mM glycerol 2-phosphate disodium salt hydrate (BGP) (Sigma-Aldrich). For controls, cells were passaged into fresh MesenCult medium without the osteogenic/mineralization supplements. Cells were stained for alkaline phosphatase activity using naphthol AS-MX phosphate and fast red violet B salt following the manufacturer's instructions (catalog 85L3R-1KT; Sigma) or for mineralization using alizarin red.

To compare mRNA expression profiles of select genes in nondifferentiating and osteogenic-differentiating WT and *Nmp4*$^{-/-}$ MSPCs, cells were seeded into 12-well plates at either 10 000 or 25 000 cells/well in Mesencult Media + Mesencult Stimulatory Supplement. Those cells at the lower seeding density were harvested on day 3 after seeding (nondifferentiating). The remaining cells were transferred to osteogenic differentiation medium 48 hours after seeding and harvested on days 5, 7, 9, and 16.

Flow cytometry

Cellular surface marker profiles from BM and peripheral blood (PBL) were assessed as previously described (12). The antibodies employed for flow cytometry were obtained from BD Biosciences. Stained cells were analyzed on an FACSCalibur (BD Biosciences) and results were quantified using FlowJo Version 8.8.6 software (TreeStar, Inc).

Microcomputed tomography (μCT)

Trabecular bone architecture was analyzed as we have previously described (11, 12). Briefly, femurs and L5 vertebra were excised from the WT and *Nmp4*$^{-/-}$ mice after euthanasia, the muscle and connective tissue removed, and the bones transferred to 10% buffered formalin, 4°C for 48 hours, after which the bones were placed in 70% ethanol (4°C) until analyzed. For femur analysis, a 2.6-mm span (~5 mm^3 of medullary space) of the excised distal femoral metaphysis was scanned in 70% ethanol on a desktop μCT (μCT 35; Scanco Medical AG) at 10-μm resolution using 55-kVp tube potential and 400-millisecond integration time, to measure 3-dimensional morphometric properties. The entire vertebra (L5) were scanned using standard methods (Skyscan 1172). Bones were reconstructed and analyzed using the manufacturer's software. The trabecular bone between the 2 growth plates was isolated from the cortical shell via manual tracing and assessed for trabecular architecture. From the 3-dimensional reconstructions the next parameters were obtained using the Scanco and Skyscan software analyses: trabecular bone volume per total volume (BV/TV) (%), connectivity density (Conn.D) (mm^{-3}), structure model index (SMI), trabecular number (Tb.N) (mm^{-1}), trabecular thickness (Tb.Th) (mm), and trabecular spacing (Tb.Sp) (mm) (34).

Bone histomorphometry

All histomorphometric parameters were obtained as previously described (11) following the ASBMR guidelines (35). Briefly, mice were administered ip injections of calcein green (20 mg/kg; Sigma-Aldrich) and alizarin red (25 mg/kg; Sigma-Aldrich) 6 and 3 days before euthanasia, respectively. The femur marrow cavity was exposed via cutting the anterior face of the epiphyseal plate. Bones were embedded in methyl-methacrylate subsequent to dehydration with graded alcohols, sectioned (4 μm) with a Leica RM2255 microtome (Leica Microsystems), and mounted unstained on microscope slides and imaged under fluorescent light with a microscope system (11). Bone formation rate (BFR), mineral apposition rate (MAR), and mineralizing surface/bone surface (MS/BS) were obtained from a 0.03-mm^2 metaphyseal region of interest from 250 to 1750 μm below the growth plate using ImagePro 3.1 software (Media Cybernetics).

Serum biochemistry

We analyzed serum P1NP to evaluate global bone formation in our experimental mice using the Rat/Mouse P1NP enzyme immuno-assay from IDS Immunodiagnostic Systems following the manufacturer's instructions. To follow bone resorption we analyzed serum C-terminal telopeptides (CTXs) with the RatLaps ELISA (Immunodiagnostic Systems, Inc) (11).

Quantitative real-time PCR (qRT-PCR) analysis

ChIP-quantitative PCR was used to authenticate select ChIP-seq profiles employing SYBR Green assays and SYBR Green Supermix (Bio-Rad). qRT-PCRs were carried out in triplicate on specific genomic regions. The resulting signals were normalized for primer efficiency by carrying out qRT-PCRs for each primer pair using Input DNA.

To evaluate gene expression in nondifferentiating and in osteogenic-differentiating WT and *Nmp4*$^{-/-}$ MPSCs, RNA was isolated with RNAeasy columns according to the manufacturer's instructions (QIAGEN). The RNA was reverse transcribed via the High-Capacity cDNA Reverse Transcription kit (Applied Biosystems). RNA expression profiling was performed on 3–4 replicates per time point for both genotypes over the 16-day culture period. Individual cDNAs were quantified by qRT-PCR using a custom TaqMan Low Density Array (TLDA) system (Format 96a; Applied Biosystems) designed for 96 genes, including Nmp4 target genes identified by our genome-wide ChIP-seq profiling, osteogenic differentiation marker genes, and candidate normalizer genes. All experiments were performed in biological quadruplicate or triplicate with TaqMan fast advanced master mix (Applied Biosystems) on a QuantStudio 7 Flex Real-Time PCR System. The probes used are listed in Supplemental Table 1. We used the ExpressionSuite v1.0.4 analysis software (Applied Biosystems) to analyze these data. This software uses the comparative threshold cycle ($\Delta\Delta$CT) method to quantify relative gene expression across a large number of genes and samples. The software provides options to normalize expression data using either global normalization or endogenous controls and calculates fold changes with *P* values. Gene expression data were normalized to 5 endogenous controls (*18S*, *Gusb*, *Rplp2*, *B2m*, and *Hprt*), although we report *Gusb* and *Rplp2* data here. In all experiments, the CT upper limit was set to 40, meaning that all mRNA detectors with a CT value greater than or equal to 40 were excluded. The multiple-comparisons correction (Benjamini-Hochberg method for false-discovery rate [FDR]) was applied to the data and $P \leq .05$ was considered significant. Additionally, individual qRT-PCRs were performed to monitor the expressions of *Sp7* (osterix, Mm00504574_m1) and *Bglap* (OCN, Mm03413826_mH) using *Rplp2* as the normalizer (Mm03059047_gH). The prepared cDNA was used to set up qRT-PCRs using FastStart Universal Probe Master mix (Rox) (Roche Life Science).

ChIP-seq and ChIP analysis

Cells from ATCC (MC3T3-E1 subclone 4) were seeded into 21 150-mm plates at an initial density of 50 000 cells/plate (320 cells/cm^2) and maintained in α-MEM complete medium + ascorbic acid. On day 14 after seeding, cells were treated with 25nM hPTH (1–34) or vehicle control for 1 hour before harvest. Subsequent to treatment cells were fixed with 1% formaldehyde for 15 minutes and quenched with 0.125M glycine. Cell pellets

were frozen in an ethanol dry ice bath and shipped to Active Motif for FactorPath analysis. The chromatin was isolated from the pellets by adding lysis buffer followed by disruption with a Dounce homogenizer. Lysates were sonicated and the DNA sheared to an average length of 300–500 bp. Genomic DNA (Input) was prepared by treating aliquots of chromatin with ribonuclease, proteinase K and heat for decross-linking, followed by ethanol precipitation. Pellets were resuspended and the resulting DNA was quantified on a NanoDrop spectrophotometer. Extrapolation to the original chromatin volume allowed quantitation of the total chromatin yield. An aliquot of chromatin (30 μg) was precleared with protein A agarose beads (Invitrogen, Thermo Fisher Scientific). Genomic DNA regions of interest were isolated using 4-μg antibody against ZNF384 (lot A57874; Sigma HPA004051). Complexes were washed, eluted from the beads with SDS buffer, and subjected to ribonuclease and proteinase K treatment. Cross-links were reversed by incubation overnight at 65°C, and ChIP DNA was purified by phenol-chloroform extraction and ethanol precipitation.

ChIP-seq (Illumina)

ChIP and Input DNAs were prepared for amplification by converting overhangs into phosphorylated blunt ends and adding an adenine to the 3′-ends. Illumina genomic adapters were ligated and the sample was size-fractionated (200–300 bp) on an agarose gel. After a final PCR amplification step (18 cycles), the resulting DNA libraries were quantified and sequenced on HiSeq 2000. Sequences (50nt reads, single end) were aligned to the mouse genome (mm10) using the Burrows-Wheeler algorithm. Alignments were extended in silico at their 3′-ends to a length of 150 bp, which is the average genomic fragment length in the size-selected library, and assigned to 32-nt bins along the genome. The resulting histograms (genomic "signal maps") were stored in BAR and bigWig files. ZFP384 peak locations were determined using the MACS algorithm (v1.4.2) with a cutoff of P = 1e-7 (36).

Bioinformatic profiling

In addition to generating our own Nmp4 ChIP-seq data from the MC3T3-E1 cells we used Nmp4 (Znf384) ChIP-seq data from murine embryonic stem cell line (ES-E14) and the B cell lymphoma cell lines Ch12 and MEL from the ENCODE Consortium for transcription factors 2011 Freeze datasets in NarrowPeak format (37). To assign an Nmp4 peak to a promoter region it had to be within −5 to +2 kb from a transcription start site (TSS). To assign a peak to an intragenic region it had to be located within the range defined by the TSS and the transcription end site, and not within the promoter range of the same gene. To assign a peak to an intergenic region, it had to be −10 000 kb from the TSS and +10 000 kb from the transcription end site, and not within the promoter range of the same gene. A peak could be assigned to multiple functional regions in an area of the genome harboring multiple genes. A common example of this is an area with genes on both strands. A peak may not fit any of these definitions and was assigned to the classification "other." This methodology yielded 34 317 functional assignments for the peaks in the MC3T3-E1 cells.

Genome wide event finding and motif discovery (GEM) analysis

GEM (38) was used to derive the Nmp4 consensus sequence. The latest mouse genome build (mm10) was employed together with the GEM default ChIP-seq read distribution file and a minimal k-mer width of 6 and maximum of 20.

Gene ontology

GO analysis was conducted using Database for Annotation, Visualization, and Integrated Discovery (DAVID) (39), and terms summarized using REVIGO (40). The ENCODE ChIP-Seq Significance Tool was employed to identify enriched transcription factors in our Nmp4 gene target list (41). Additionally some functional analysis was also generated through the use of QIAGEN's ingenuity pathway analysis (QIAGEN Redwood City; www.qiagen.com/ingenuity).

Bone phenotype statistical analysis

Statistical evaluations were processed using the program JMP version 7.0.1 (SAS Institute). The animal studies employed a two-way ANOVA using genotype and treatment as the independent variables followed by either a Tukey's honest significant difference or LS Means post hoc test if a genotype × treatment interaction was indicated. Statistical significance was set at $P \leq .05$. To compare growth rates of the WT and *Nmp4*$^{-/-}$ MSPCs derived from various experimental mice, we evaluated the slopes of log-transformed cell counts regressed onto experimental day using a t test. The numbers of mice per treatment group and replicates/treatment for the cell studies are indicated in the appropriate figures and tables.

Results

Nmp4$^{-/-}$ mice are not protected from ovx-induced bone loss

To determine whether genetically disabling Nmp4 activity protects mice from ovx-induced bone loss as it does from unloading-associated osteopenia (16), we removed the ovaries or performed sham operations on both WT and *Nmp4*$^{-/-}$ mice (Figure 1). Both the ovx WT and ovx *Nmp4*$^{-/-}$ mice experienced significant weight gain at 4-week postoperation (postop) (Table 1) consistent with previous mouse studies (42). Additionally, ovx resulted in

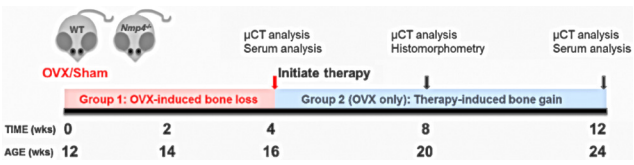

Figure 1. Schematic of treatment regimen for WT and *Nmp4*$^{-/-}$ mice; group 1 mice were subjected to ovx or sham operation at 12 weeks of age and evaluated for bone loss 4-week postop (16 wk of age). Group 2 mice were ovx at 12 weeks of age and began PTH or vehicle therapy at 16 weeks of age for a duration of 4 and 8 weeks. Endpoint analyses included μCT, serum analysis for P1NP and CTXs, and dynamic histomorphometry.

Table 1. Bone Loss Data

	WT		*Nmp4*$^{-/-}$		Two-Way ANOVA *P* Values		
	Sham	ovx	Sham	ovx	Genotype	Treatment	Gene × Treat
%Δ body weight	2.48 ± 7.73	8.65 ± 5.48	4.14 ± 4.70	5.66 ± 2.94	.69	0.03	.17
Uterine weight (g)	0.10 ± 0.05	0.04 ± 0.02	0.10 ± 0.02	0.05 ± 0.02	.30	<0.0001	.34
Distal femur							
BV/TV	0.019 ± 0.004	0.012 ± 0.004	0.038 ± 0.011	0.021 ± 0.010	<.0001	<0.0001	.06
SMI	3.818 ± 0.250	4.055 ± 0.357	3.387 ± 0.263	3.810 ± 0.294	.0008	0.0011	.32
Tb.N (mm^{-1})	2.554 ± 0.239	2.165 ± 0.385	3.128 ± 0.218	2.797 ± 0.276	<.0001	0.0004	.76
Tb.Th (mm)	0.040 ± 0.005	0.041 ± 0.005	0.039 ± 0.003	0.037 ± 0.004	.08	0.87	.23
Tb.Sp (mm)	0.393 ± 0.036	0.477 ± 0.097	0.317 ± 0.026	0.359 ± 0.037	<.0001	0.0012	.25
L5 vertebra							
BV/TV	0.189 ± 0.028	0.177 ± 0.013	0.253 ± 0.019	0.212 ± 0.019	<.0001	0.0004	.05
Tb.N (mm^{-1})	3.797 ± 0.513	3.580 ± 0.285	4.491 ± 0.345	4.022 ± 0.254	<.0001	0.0091	.32
Tb.Th (mm)	0.050 ± 0.003	049 ± 0.002	0.056 ± 0.002	0.053 ± 0.002	<.0001	0.0032	.02
Tb.Sp (mm)	0.227 ± 0.023	0.229 ± 0.013	0.202 ± 0.020	0.214 ± 0.012	.0013	0.25	.44

	WT: *Nmp4*$^{-/-}$				
Serum P1NP	**Preop**	**Postop$^{4\ wks}$**	**Postop$^{12\ wks}$**	***P* Values [G; T; G × T]$^{4\ wks}$**	***P* Values [G; T; G × T]$^{12\ wks}$**
	5.62 ± 1.21: 6.02 ± 1.41	5.83 ± 1.41: 4.77 ± 1.22	3.15 ± 0.65: 2.81 ± 0.76	.34; .16; .05	.95; <.0001; .36

	WT: *Nmp4*$^{-/-}$				
Serum CTX	**Preop**	**Postop$^{4\ wks}$**	**Postop$^{12\ wks}$**	***P* Values [G; T; G × T]$^{4\ wks}$**	***P* Values [G; T; G × T]$^{12\ wks}$**
	13.66 ± 2.43: 13.37 ± 1.88	12.96 ± 3.04: 13.53 ± 2.58	11.47 ± 2.24: 9.36 ± 1.22	.92; .46; .96	.14; .0003; .18

The % change body weight, uterine weight, and μCT of distal femur and L5 vertebra from WT and *Nmp4*$^{-/-}$ mice after ovx or sham operation 4-week postop. Serum bone formation (P1NP) and bone resorption (CTX) marker levels were compared in mice previous to the operation (preop) and 4 and 12 weeks after surgery (postop). The 12-week postop data were obtained from the vehicle-control treatment groups. Data are average ± SD, number of mice/experimental group = 8–14 (4 mice in WT sham uterine weight). Statistical significance was set at $P \leq .05$, and differences were determined using a two-way ANOVA.

a significant decrease in uterine weight in both genotypes (Table 1). There was no genotype × treatment interaction in either of these parameters.

Both WT and *Nmp4*$^{-/-}$ mice exhibited significant bone loss 4 weeks after ovx surgery as measured in the trabecular bone compartment of the distal femur and the L5 vertebra (Table 1). The *Nmp4*$^{-/-}$ mice exhibited a trend towards enhanced loss of bone that neared significance in the distal femur (BV/TV, genotype × treatment interaction = 0.06) (Table 1) and reached significance in the L5 vertebra (BV/TV, genotype × treatment interaction < 0.05) (Table 1). Despite this enhanced (or nearly enhanced) rate of bone loss the *Nmp4*$^{-/-}$ animals maintained more trabecular bone compared with WT mice during the first 4 weeks after ovx. The *Nmp4*$^{-/-}$ mice exhibited a decrease in the serum bone formation marker P1NP at 4-week postop and both genotypes showed significant decreases in this marker at 12-week postop in the vehicle-treated mice. A small decrease in the serum bone resorption marker CTX was observed at 12-week postop in the vehicle-treated mice.

Ovx *Nmp4*$^{-/-}$ mice show an enhanced bone gain response to PTH therapy

With a separate group of ovx mice we initiated treatment of both WT and *Nmp4*-null ovx animals with PTH (30 μg/kg · d) or vehicle control 4 weeks after surgery. The duration of hormone therapy lasted 4 weeks (8-wk postop) and 8 weeks (12-wk postop). The ovx *Nmp4*$^{-/-}$ mice showed an enhanced PTH-induced gain in femoral

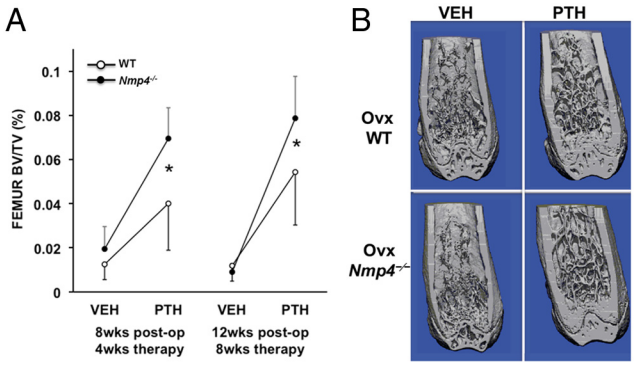

Figure 2. Disabling Nmp4 enhances PTH restorative therapy in the distal femur of ovx *Nmp4*$^{-/-}$ mice. A, Interaction plots of femoral trabecular BV/TV of ovx WT and ovx *Nmp4*$^{-/-}$ mice as determined by μCT at 4 and 8 weeks of treatment. Data are average ± SD, number of mice/experimental group = 8–9. Statistical differences were determined using a two-way ANOVA, and significance was set at $P \leq .05$. The Tukey's honest significant difference post hoc test was used to determine differences between the treatment groups. There were genotype, treatment and genotype × treatment interaction at both time points. There was no difference between the vehicle-treated WT and *Nmp4*$^{-/-}$ mice. B, μCT images showing PTH-induced improvements in distal femur trabecular architecture in ovx WT and *Nmp4*$^{-/-}$ mice after 8 weeks of treatment (12-wk postop, 24 wk of age).

Table 2. PTH-Induced Bone Gain Data

	WT		*Nmp4*$^{-/-}$		Two-Way ANOVA *P* Values		
	VEH	PTH	VEH	PTH	Genotype	Treatment	Gene × Treat
Distal femur							
4 wk							
Conn.D (mm^{-3})	3.180 ± 3.870	33.230 ± 26.730	9.681 ± 15.979	67.533 ± 14.111	.0018	<.0001	.03
SMI	3.752 ± 0.437	3.013 ± 0.384	3.472 ± 0.327	2.514 ± 0.113	.0025	<.0001	.36
Tb.N (mm^{-1})	2.100 ± 0.519	2.441 ± 0.281	2.712 ± 0.241	2.833 ± 0.224	.0002	.06	.36
Tb.Th (mm)	0.039 ± 0.010	0.042 ± 0.007	0.033 ± 0.003	0.044 ± 0.003	.54	.004	.09
Tb.Sp (mm)	0.510 ± 0.157	0.409 ± 0.051	0.370 ± 0.036	0.342 ± 0.032	.0019	.04	.24
8 wk							
Conn.D (mm^{-3})	3.123 ± 5.307	38.658 ± 14.910	0.982 ± 1.103	58.128 ± 13.570	.03	<.0001	.0064
SMI	3.808 ± 0.479	2.470 ± 0.284	3.589 ± 0.218	2.262 ± 0.141	.05	<.0001	.96
Tb.N (mm^{-1})	2.132 ± 0.297	2.164 ± 0.431	2.286 ± 0.145	2.552 ± 0.277	.02	.17	.28
Tb.Th (mm)	0.037 ± 0.006	0.048 ± 0.005	0.030 ± 0.004	0.049 ± 0.003	.12	<.0001	.02
Tb.Sp (mm)	0.476 ± 0.072	0.471 ± 0.109	0.438 ± 0.033	0.378 ± 0.045	.01	.20	.27
L5 vertebra							
4 wk							
Tb.N (mm^{-1})	3.453 ± 0.451	4.875 ± 0.587	3.891 ± 0.504	5.518 ± 0.381	.0049	<.0001	.56
Tb.Th (mm)	0.051 ± 0.002	0.049 ± 0.002	0.054 ± 0.004	0.051 ± 0.001	.04	.03	.60
Tb.Sp (mm)	0.246 ± 0.021	0.224 ± 0.030	0.229 ± 0.021	0.197 ± 0.021	.02	.0036	.52
8 weeks							
Tb.N (mm^{-1})	4.046 ± 0.917	5.648 ± 1.191	3.627 ± 0.235	5.906 ± 0.754	.79	<.0001	.26
Tb.Th (mm)	0.053 ± 0.003	0.049 ± 0.004	0.055 ± 0.001	0.054 ± 0.001	.0018	.0044	.09
Tb.Sp (mm)	0.239 ± 0.021	0.206 ± 0.037	0.256 ± 0.020	0.186 ± 0.023	.86	<.0001	.05

μCT (distal femur and L5 vertebra) from ovx WT and ovx *Nmp4*$^{-/-}$ mice after 4 and 8 weeks of PTH/VEH therapy. Data are average ± SD, number of mice/experimental group = 8–9. Statistical significance was set at $P \leq .05$, and differences were determined using a two-way ANOVA.

BV/TV and Conn.D at 4 and 8 weeks of therapy compared with their ovx WT littermates as well as an augmented gain in Tb.Th at 8 weeks (Figure 2 and Table 2). The null mice also showed an enhanced PTH response at the L5 vertebra at 8 weeks of treatment (Figure 3 and Table 2). Specifically the two-way ANOVA indicated strong genotype × treatment effects for the distal femur for both 4 and 8 weeks of therapy and for the L5 vertebra for 8 weeks of therapy (see Figures 2A and 3A); the post hoc tests concluded that the difference between the genotypes was within the hormone-treated groups. The vehicle-treated ovx WT and ovx *Nmp4*$^{-/-}$ groups showed no difference in BV/TV (Figures 2 and 3) at the end of the treatment regimens indicating that the modest enhanced loss in bone in the *Nmp4*$^{-/-}$ mice was stabilized by 4 weeks of therapy. PTH significantly elevated MAR, MS/BS, and BFR at the end of 4 weeks of treatment as shown by strong treatment effects (Table 3). However, there was no genotype effect or genotype × treatment interaction for any of these parameters (Table 3). Hormone significantly elevated serum levels of the bone formation marker P1NP and the resorption marker CTX at 8 weeks of therapy, but there was no treatment × genotype interaction for either of these parameters (Table 3).

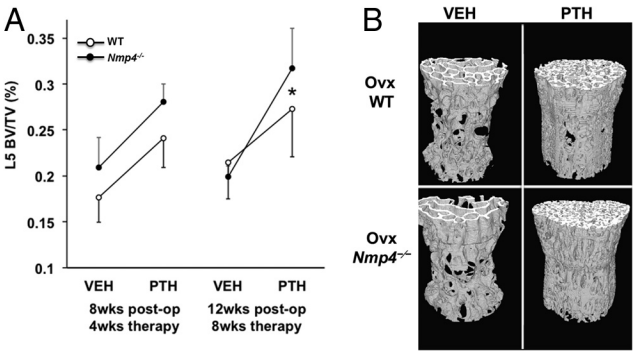

Figure 3. The exaggerated response to anabolic PTH persists in the L5 vertebra of ovx *Nmp4*$^{-/-}$ mice. A, Interaction plots of L5 vertebra BV/TV of ovx WT and ovx *Nmp4*$^{-/-}$ mice as determined by μCT at 4 and 8 weeks of treatment. Data are average ± SD, number of mice/experimental group = 8–9. Statistical differences were determined using a two-way ANOVA, and significance was set at $P \leq .05$. The LS Means Student's *t* post hoc test was used to determine differences between the treatment groups. There were genotype, treatment effects at both time points, and a genotype × treatment interaction at 8 weeks of therapy. There was no difference between the vehicle-treated WT and *Nmp4*$^{-/-}$ mice. B, μCT images showing PTH-induced improvements in L5 trabecular architecture in ovx WT and *Nmp4*$^{-/-}$ mice after 8 weeks of treatment (12-wk postop, 24 wk of age).

FACS analysis of the BM CD45^{-}/CD105^{+}/CD146^{+}/nestin^{+} osteoprogenitors revealed a significant elevation in the number of these cells in the BM obtained from the *Nmp4*$^{-/-}$ mice at the end of 4 weeks of therapy, irrespective of treatment (Figure 4A). This is consistent with our previous observation in the ovary-intact null mice (12). By the end of 8 weeks of treatment (12-wk postop) the observed increase in the number of these *Nmp4*$^{-/-}$ cells in the BM failed to reach statistical significance, but there was a significant elevation in the number of the PBL *Nmp4*$^{-/-}$ osteoprogenitors in the vehicle-treated mice (Figure 4D). The *Nmp4*$^{-/-}$ mice showed a significant elevation in CD8^{+} T cells in both the BM and the PBL throughout the entire therapy regimen (Figure 4, B and E). PTH significantly decreased the numbers of these cells in

Table 3. Histomorphometry and Serum Analyses

	WT		*Nmp4*$^{-/-}$		Two-Way ANOVA *P* Values		
	VEH	PTH	VEH	PTH	Genotype	Treatment	Gene × Treat
Dynamic histo							
MAR (μm/d)	2.28 ± 0.37	3.80 ± 0.73	2.29 ± 0.37	3.61 ± 0.40	.70	<.0001	.66
MS/BS (%)	0.41 ± 0.09	0.55 ± 0.05	0.44 ± 0.10	0.52 ± 0.06	.98	.01	.45
BFR (μm^2/μm · d)	0.95 ± 0.28	2.09 ± 0.52	1.01 ± 0.25	1.86 ± 0.22	.60	<.0001	.37
Serum							
	WT		*Nmp4*$^{-/-}$		Two-Way ANOVA *P* Values		
	VEH$^{8\ wks}$	PTH$^{8\ wks}$	VEH$^{8\ wks}$	PTH$^{8\ wks}$	Genotype	Treatment	Gene x Treat
P1NP (ng/mL)	3.147 ± 0.653	10.066 ± 2.659	2.806 ± 0.760	8.042 ± 3.304	.19	<.0001	.34
CTX (ng/mL)	11.466 ± 2.239	15.147 ± 3.518	9.361 ± 1.222	14.157 ± 1.532	.12	.0002	.56

Dynamic bone histomorphometry data of the distal femur from WT and *Nmp4*$^{-/-}$ mice treated with intermittent PTH or vehicle for 4 weeks (8-wk postop). Sera data were collected at the end of 8 weeks of treatment (12-wk postop). The parameters include MAR, MS/BS, and BFR. Data are average ± SD, number of mice/experimental group = 4–7. A two-way ANOVA was used to determine statistical differences, and significance was set at $P \leq .05$.

the BM at 8 weeks of therapy in both genotypes (Figure 4B) but had no impact on the number of these cells in the PBL (Figure 4E). Disabling Nmp4 had little to no effect on CD4$^+$ T cells, nor did treatment with PTH (Figure 4, C and F). The modest increase in BM CD4$^+$ T cells approached significance ($P < .06$) but this was not reflected in the PBL, just as we previously observed in the ovary-intact mice (12).

To determine whether the enhanced osteogenic potential of the BM could be reliably and reproducibly maintained in vitro in MSPC cultures over several passages and in the absence of supporting cells (eg, T cells), we established expanded WT and *Nmp4*$^{-/-}$ MSPCs from ovary-intact mice. The expanded *Nmp4*$^{-/-}$ MSPCs from ovary-intact mice exhibited modest but significantly enhanced proliferation compared with the WT cells (Figure 5A). Both the null and WT expanded MSPCs showed strong alkaline phosphatase expression (Figure 5B). However, the expanded *Nmp4*$^{-/-}$ MSPCs typically showed an accelerated and enhanced mineralization compared with WT cells under various concentrations of dexamethasone and ascorbic acid (Figure 5B). Finally, the expanded *Nmp4*$^{-/-}$ and WT MSPCs exhibited varying degrees of alkaline phosphatase staining while maintained in MesenCult medium, depending on the confluence of the cells and time in culture (3–9 d); however, no mineralization was observed in these control cultures (data not shown).

Genome-wide ChIP-seq/GO analysis reveals Nmp4 target genes and potential pathways of the antianabolic axis

Nmp4 is expressed in nearly all cells, yet the most singular consequence of globally disabling this protein is the enhanced mobilization of bone cells upon osteoanabolic induction (11–13, 15). As a first step in understanding the origins of this phenotype, which may have clinical significance, we needed the next information: 1) the identity of the Nmp4 target genes including "core" target genes common to multiple cell types; 2) identify common functions of these core genes to distinguish pathways that make osteoprogenitors particularly vulnerable to the effects of Nmp4; and 3) experimental confirmation of some of these pathways. To begin to understand how Nmp4 works, we set out to understand 4) whether Nmp4 targets functional regions of the genome; 5) if it binds directly to DNA or via other proteins; and 6) whether osteoanabolic agents, eg, PTH, alter Nmp4 DNA-binding along target genes.

The potential Nmp4 target genes identified by ChIP-seq in the MC3T3-E1 (vehicle-treated) cells and those established in the 3 ENCODE cell lines were compared using those genes that had 1 or more peaks associated with the TSS. A Venn diagram of these genes showed that 2114 Nmp4 core target genes were common to the 4 cell lines (Figure 6A and Supplemental Table 2). These core target genes were classified into functionally related categories using GO analysis with the DAVID tool (39). The functional annotation-clustering algorithm was applied to the target list, which is able to give a more insightful view of the relationships between annotation categories and terms compared with other analytic modules (39). The significance of group classification was defined by enrichment scores based on Fisher exact statistics (FDR $P < .05$). The DAVID-derived biological profile was further summarized using REVIGO (40). GO analysis of the core target genes designated Nmp4 as a negative regulator of cellular biosynthetic processes showing significant enrichment for genes involved in the regulation of transcription, chromatin modification, protein catabolic processes, regulation of the cell cycle, and mRNA processing/splicing (Figure 6B). Interestingly, the genes specific to any one particular cell line or specific to vehicle-treated or PTH-treated MC3T3-E1 cells did not yield a distinct bi-

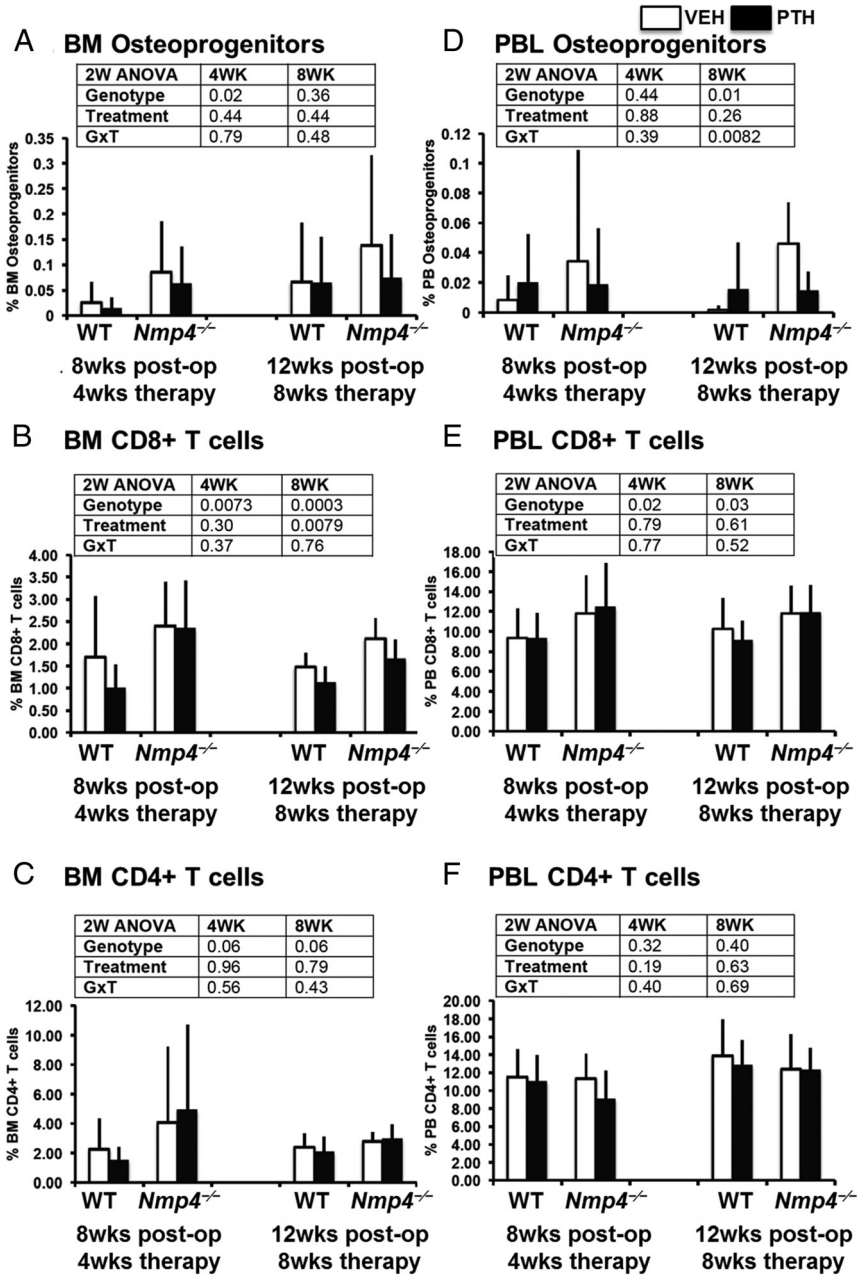

Figure 4. Ovx does not abrogate the expanded population of osteoprogenitors and $CD8^+$ T cells in $Nmp4^{-/-}$ mice. FACS analysis of BM and PBL osteoprogenitors, $CD8^+$ T cells, and $CD4^+$ T cells. A and D, The frequency of femoral BM and PBL $CD45^-/CD105^+/CD146^+/CD105^+/nestin^+$ osteoprogenitor cells in WT and $Nmp4^{-/-}$ mice at the end of 4 and 8 weeks of treatment with intermittent PTH or vehicle control. B and E, The frequency of BM and PBL $CD8^+$ T cells from the WT and $Nmp4^{-/-}$ mice. C and F, The frequency of BM and PBL $CD4^+$ T cells from the WT and null mice. Data are average ± SD, number of mice/experimental group = 8–9. Statistical differences were determined using a two-way ANOVA, and significance was set at $P \leq .05$.

ological process profile that reached statistical significance as obtained with the core target genes (data not shown). However, peak-associated genes common to the vehicle- and PTH-treated MC3T3-E1 cells yielded a profile nearly identical to that obtained with the core target genes.

Next, we probed existing datasets for enriched transcription factors within our Nmp4 core target gene list using the ENCODE ChIP-seq Significance Tool (Table 4) (41). This profile shows that Nmp4 binding in the promoter regions of its target genes predominantly cooccurs with proteins that regulate chromatin organization and with proteins that contribute to maintaining stem/progenitor pluripotency/multipotency and the poised gene state, eg, chromodomain helicase DNA binding protein 2, Swi-independent 3a, and K(lysine) acetyltransferase 2A (KAT2a) (43–45).

In an effort to gain further understanding of how Nmp4 regulates gene expression, we prepared a genome-wide functional region map of the Nmp4 binding sites for all 4 cell types as described in Materials and Methods. Most the occupancy peaks were located in or near the TSS or in intragenic regions, areas typically associated with regulatory functions (Figure 7A). To determine whether Nmp4 binds directly to DNA or can associate with the genome via other proteins we used the discovery algorithm GEM to derive the Nmp4 consensus-binding site from the MC3T3-E1 data. In support of previous studies by our lab and others the derived binding site matched the unusual homopolymeric (dA · dT) consensus sequence previously derived by cyclic amplification and electrophoretic mobility shift assay (Figure 7B) (24, 25). No other consensus sequences were identified suggesting a single and direct mode of genome association, mediated by the Cys_2His_2 DNA-binding domain (28). To determine whether PTH challenge altered Nmp4 DNA-binding along target genes we generated genome-wide Nmp4 ChIP-seq profiles using the preosteoblast cell line MC3T3-E1 treated with hPTH (1–34) or vehicle control for 1 hour. We used the 1-hour time point because we observed the most significant differences in femoral mRNA expression profiles between WT and $Nmp4^{-/-}$ mice 1 hour after injection (11). Hormone reduced Nmp4 genome-wide occupancy

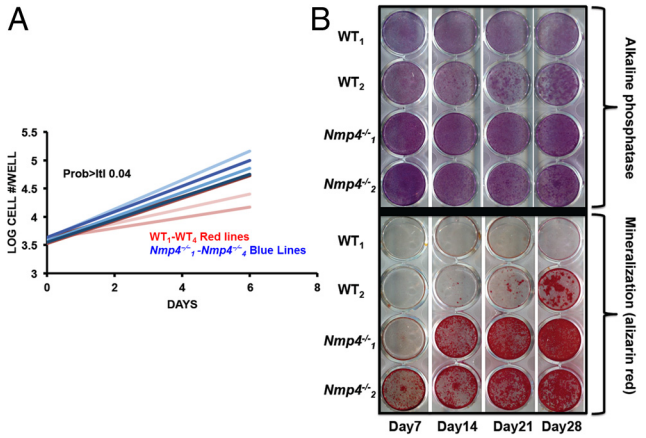

Figure 5. Expanded *Nmp4*$^{-/-}$ MSPCs exhibit enhanced proliferation and mineralization in culture. A, Comparative growth rates of expanded WT and *Nmp4*$^{-/-}$ MSPCs. Cell counts/d (n = 4 lines per genotype log10 cells/well, 3 wells/sample, average ± SD, *t* test, $t < 0.05$). Note: each "line" is derived from a single mouse. B, Alkaline phosphatase (alk phos) and alizarin red staining of a WT and *Nmp4*$^{-/-}$ MSPC cultures from day 7 to 28. See text for details.

from a total of 15 446 to 13 109 binding sites. However, at the level of the single gene there was a diversity of changes in Nmp4 occupancy, ie, PTH was observed to remove (eg, *Nid2*), induce (eg, *Ccdc53*) or have no effect on Nmp4-DNA association (eg, *Akt2* and *Arrb2*) (Figure 8; also see ChIP-quantitative PCR confirmation of Nmp4 binding; Supplemental Figure 1).

As a first step in the validation of the ChIP-seq-derived antianabolic map we interrogated 90 mRNA transcripts in nondifferentiating and osteogenic differentiating WT and *Nmp4*$^{-/-}$ expanded MSPCs at 5 different time points. The accelerated and enhanced mineralization of the *Nmp4*$^{-/-}$ MSPCs (Figure 5) is consistent with our previous observation that in response to PTH *Nmp4*$^{-/-}$ mice add more bone and add it faster than WT mice (11). Our choice of Nmp4 target genes (Supplemental Table 1) was based on our DAVID analysis. We chose both core target genes and Nmp4 target genes identified in the MC3T3-E1 preosteoblasts. DAVID also uses Kyoto Encyclopedia of Genes and Genomes (KEGG) database to map large gene lists to signaling pathways (39). For example the DAVID/KEGG profile of the Nmp4 core target genes included the target of rapamycin and insulin/IGF-1 signaling pathways (Table 5) and indeed the insulin/IGF-1→insulin receptor substrate 1→PI3K→3-phosphoinositide dependent protein kinase-1→AKT signaling response limb is common to many of the pathways listed. This is also consistent with our ingenuity pathway analysis (Supplemental Table 3). Also included were Nmp4 target genes coding for proteins involved in the ubiquitin-proteasome system, chromatin remodeling, transcription regulation, and RNA processing. Finally, we analyzed the expression of osteogenic differentiation markers.

Volcano plots (Supplemental Figure 2) identify genes that were statistically significantly up-regulated or down-regulated by at least 2-fold in the *Nmp4*$^{-/-}$ cells compared with the WT cohort on the same day of culture. Figures 9 and 10 compare the relative mRNA expression of select genes with the level of the transcript in WT cells on day 3 of culture thus providing a time-course view. The *Nmp4*$^{-/-}$ cells showed a strikingly elevated expression of the Nmp4 target gene insulin-like growth factor binding protein 2 (*Igfbp2*) mRNA and down-regulation of the target gene *Igfbp4* mRNA during the early differentiation period (Figure 9, A and B). IGFBP2 stimulates osteoblast differentiation, whereas the IGFBP4 is a potent inhibitor of Igf actions (46, 47). 3-phosphoinositide dependent protein kinase-1 (*Pdk1*, target gene) a key component of the IGF1/insulin signaling pathway (48) was up-regulated in the *Nmp4*$^{-/-}$ cells throughout the developmental time course (Figure 9C). Interestingly, neither the target genes *Igf1* nor its receptor *Igf1r* exhibited striking differences in gene expression between the 2 genotypes (data not shown). The *Nmp4*$^{-/-}$ cells exhibited an enhanced anabolic profile during the latter differentiation period as evidenced by elevated expression levels of the nontarget

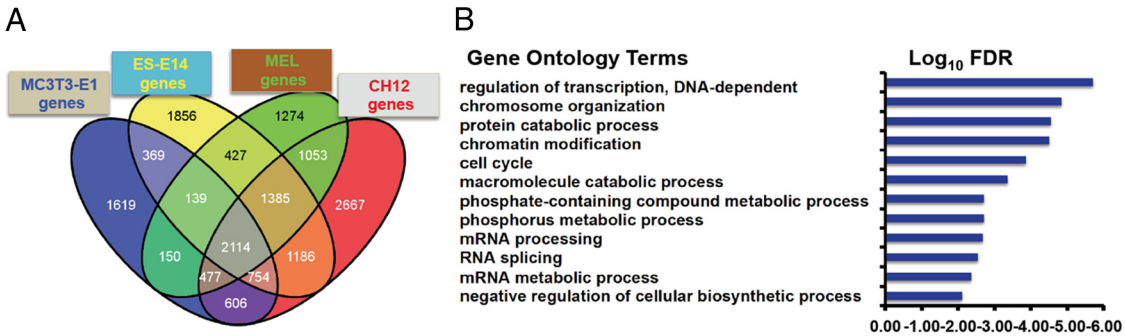

Figure 6. Nmp4 associates with core target genes common to multiple cell types and acts as a negative regulation of cellular biosynthetic processes. A, Venn diagram illustrating the shared Nmp4 target genes in the MC3T3-E1 osteoblast-like cells (vehicle treated), and the 3 ENCODE cells lines, ES-E14 (embryonic stem cells), MEL, and CH12 cells (B cell lymphomas). B, DAVID/REVIGO GO profile of Nmp4 core target genes.

Table 4. ENCODE ChIP-Seq Significance Tool Profile for Enriched TFs Within the Nmp4 Target Core Gene List

Factor	Q Value	Factor	Q Value
Nmp4	0.00E + 00	Max	0.00E + 00
CHD2	0.00E + 00	Mxi1	0.00E + 00
CTCF	0.00E + 00	NELFe	0.00E + 00
GCN5	0.00E + 00	Pol2	0.00E + 00
HCFC1	0.00E + 00	SIN3A	0.00E + 00
MAZ	0.00E + 00	TBP	0.00E + 00
p300	0.00E + 00	c-Myc	7.352e-317

TF, transcription factor; Q value, hypergeometric test; Benjamini-Hochberg (select TFs from 72 entries).

genes *Bmp2* (Figure 9D), *Pth1r* (Figure 9E), and *Bglap* (OCN) (Figure 9F).

Chemokine (C-X-C motif) (CXC) ligand 12 (*Cxcl12*) expression (target gene), also known as stromal-derived factor 1, was dramatically down-regulated in the *Nmp4*$^{-/-}$ cells throughout development (Figure 10A) and the target gene *Plaur* (urokinase plasminogen activator receptor [*uPAR*]) was up-regulated in the null cells (Figure 10B). Both genes play roles in MSPC osteogenic lineage commitment (49–52). *Spp1* (osteopontin, target gene) and thrombospondin 2 (*Thbs2*) (target gene) regulate aspects of mineralization (53, 54); the former was up-regulated in our null cell, whereas the latter was down-regulated (Figure 10, C and D). Type I collagen (*Col1a1*, target gene) expression was elevated in the *Nmp4*$^{-/-}$ cells throughout the developmental period (Figure 10E). Interestingly, we observed no substantial difference in the expression profiles of *Sp7* (osterix) (Figure 10F) or the target gene *Runx2* (data not shown), essential transcription factors for osteoblast differentiation (55).

Discussion

Our findings that the *Nmp4*$^{-/-}$ mice are not protected from ovx-induced bone loss yet maintain the amplified response to PTH therapy is a key advance necessary for further consideration of Nmp4-based treatment strategies. The ovx *Nmp4*$^{-/-}$ mice displayed an enhanced hormone-induced recovery of femoral and L5 trabecular BV/TV despite delaying treatment until 4-week postop to allow for significant bone loss. Both the ovx WT and ovx *Nmp4*$^{-/-}$ mice showed strong responses to PTH therapy. After 4 and 8 weeks of treatment the WT mice displayed a 3.2- and 4.6-fold increase in femoral BV/TV over vehicle-treated mice, respectively. However, the *Nmp4*$^{-/-}$ mice showed a 3.6- and 8.8-fold increase over the same time period resulting in a very strong genotype × treatment interaction. Differences in PTH-mediated BV/TV restoration efficacy between the WT and *Nmp4*$^{-/-}$ mice in the L5 vertebra and was less striking although statistically significant (1.3- vs 1.6-fold at 8 wk in the WT and *Nmp4*$^{-/-}$ mice, respectively). We observed similar PTH-responsive femoral and L5 profiles between younger, ova-

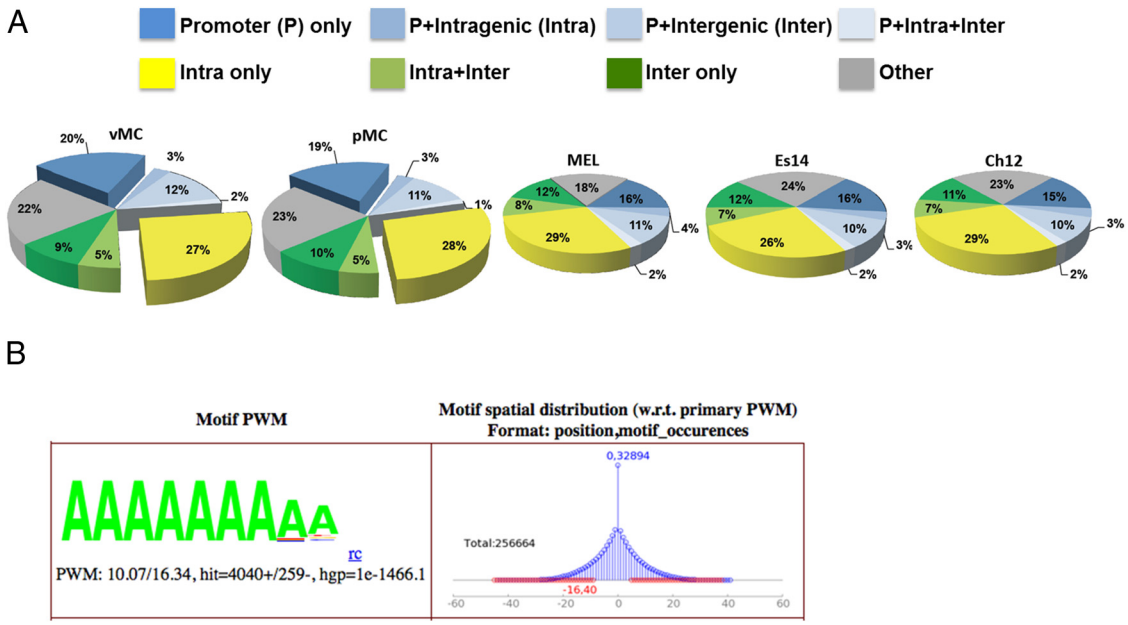

Figure 7. Nmp4 binds to AT-rich DNA typically proximal to TSS sites or within intragenic regions. A, Genome-wide mapping of the Nmp4 binding sites show that most sites are distributed in the TSS and intragenic regions of the genome. ChIP-seq analysis included vehicle-treated and PTH-treated MC3T3-E1 osteoblast-like cells (vMC and pMC, respectively) and 3 murine cell lines from the ENCODE Consortium, including ES-E14 (Es14), which are E14 undifferentiated mouse embryonic stem cells, and 2 mouse erythroleukemia cell lines (Ch12 and MEL) derived from B cell lymphomas. B, GEM analysis for the Nmp4 consensus sequence derived from MC3T3-E1 cells. A minimal k-mer width of 6 and maximum of 20 was used. The optimal position weight matrix (PWM) score for the MC3T3-E1 data was 10.07. The hypergeometric *P* value (hgp) was 1e-1466.1.

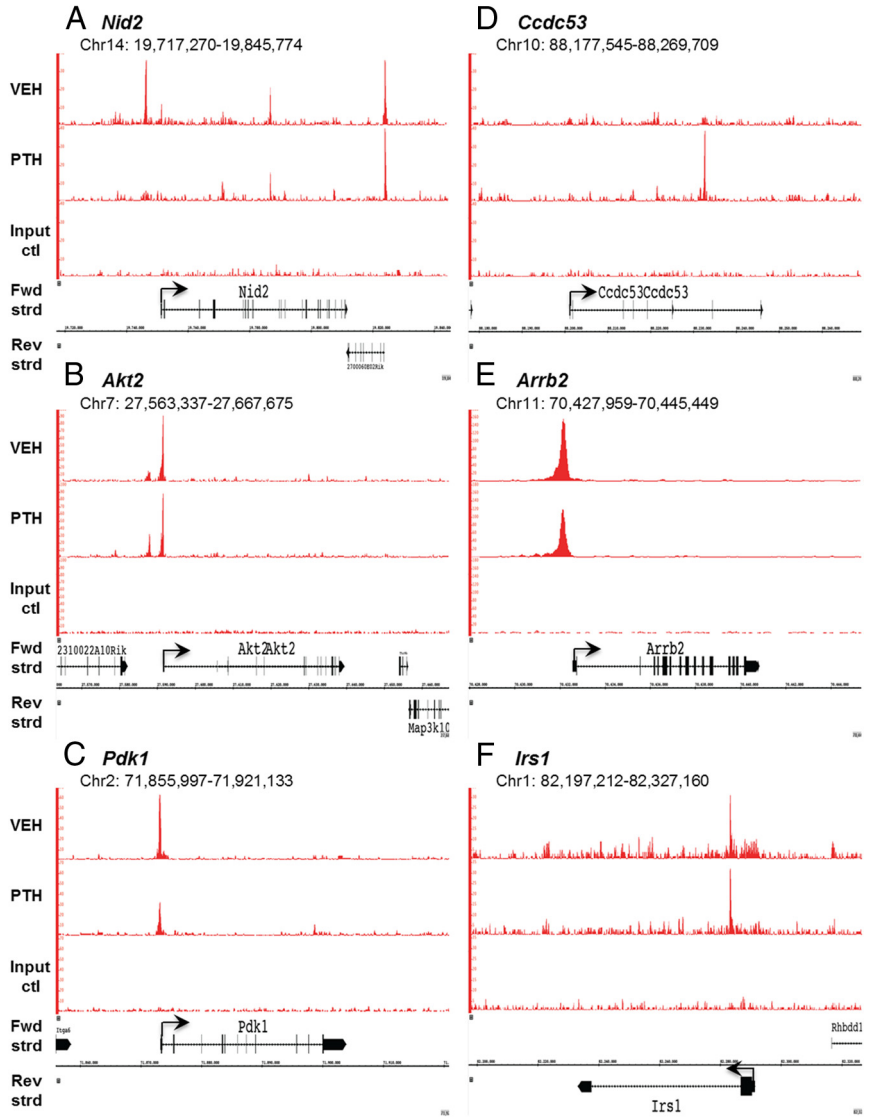

Figure 8. ChIP-seq reveals Nmp4 binding profiles at specific gene loci. Mouse MC3T3-E1 cells were seeded into 21 150-mm plates at an initial density of 50 000 cells/plate (320 cells/cm^2) and maintained in α-MEM complete medium + ascorbic acid for 14 days. Before harvest cells were treated with 25nM hPTH (1–34) or vehicle control for 1 hour. Processing for ChIP-seq analysis was performed as described in Materials and Methods. Sequences (50-nt reads, single end) were aligned to the mouse genome (mm10) using the Burrows-Wheeler algorithm. Alignments were extended in silico at their 3′-ends to a length of 150 bp, which is the average genomic fragment length in the size-selected library, and assigned to 32-nt bins along the genome. Nmp4 (Znf384) peak locations were determined using the MACS algorithm (v1.4.2) with a cutoff of $P = 1e\text{-}7$. The genomic loci including the chromosome number and nucleotide interval are indicated. Read scales are indicated on the y-axis. An arrow indicates the transcriptional start sites and direction of transcription for each of the genes; vertical boxes within the gene indicate exons. The Nmp4 ChIP-seq gene profiles include (A) *Nid2* (B) *Akt2*, (C) *Pdk1*, (D) *ccdc53*, (E) *Arrb2*, and (F) *Irs1*. The input DNA profiles were devoid of peaks.

ry-intact WT and *Nmp4*-null mice (11–13). The histomorphometry and serum data reported here tracked the PTH-induced increases in bone mass in the ovx animals showing strong treatment effects for bone formation parameters MAR, BFR, and MS/BS (at 4 wk of treatment) as well as strong increases in bone remodeling serum P1NP and CTX (at 8 wk of treatment). However, these parameters did not distinguish the genotypes in regards to the amount of bone formed over this time period as was achieved with the μCT data. Interestingly, the histomorphometry data did not distinguish the differences in PTH-induced bone formation in ovary-intact WT and *Nmp4*$^{-/-}$ mice (11). Our present observation that *Nmp4*$^{-/-}$ MSPCs exhibit an accelerated and enhanced mineralization in response to anabolic cues, ie, osteogenic medium suggests that the augmented bone formation is an early event. Similarly, we did not observe the expected ovx-induced small increase in serum CTX. Instead, the serum data of the vehicle-treated mice showed a large decrease in P1NP and a smaller decrease in CTX over the time course of the entire experiment, ie, preop vs 12-week postop. This suggests a decrease in bone remodeling in the untreated mice predominantly in the bone formation arm. A more extensive time course with earlier harvest points for histomorphometry and serum samples is required to more fully characterize the anticipated differences in WT and *Nmp4*$^{-/-}$ dynamic bone remodeling.

The most robust phenotypic characteristic of Nmp4 ablation is the exaggerated bone formation response to PTH or BMP2, which suggests that the adult mice harbor more BM MSPCs with heightened sensitivity to osteoanabolic signals. Disabling Nmp4 has no observable impact on embryonic or perinatal skeletal development. Adult MSPCs are a heterogeneous population of multipotent stem, progenitor, and stromal cells that contribute to BM homeostasis (56). In mouse BM, much of the CFU-F activity is in the nestin$^+$ cell population and in the human marrow the CD146$^+$ population (56, 57). In ovary-intact, *Nmp4*$^{-/-}$ mice, we observed a 4-fold increase in the frequency of CD45$^-$/CD105$^+$/CD146$^+$/nestin$^+$ cells irrespective of treatment (PTH vs vehicle control), which paralleled the magnitude increase in CFU-F and CFU-F$^{\text{alk phos+}}$

Table 5. DAVID Profile of KEGG Pathway Mapping

GO Term Pathways	FDR
Target of rapamycin signaling pathway	0.003
Insulin signaling pathway	0.004
Chronic myeloid leukemia	0.026
JAK-STAT signaling pathway	0.026
Neurotrophin signaling pathway	0.034

Only pathways with an FDR of $P < .05$ are listed.

cell number in culture (12). Similarly, the ovx *Nmp4*$^{-/-}$ mice exhibited an approximate 3-fold increase in the CD45^{-}/CD105^{+}/CD146^{+}/nestin^{+} cells at 8-week postop compared with the ovx WT animals.

The enhanced osteogenic potential of the *Nmp4*$^{-/-}$ BM as measured by the frequency of cells capable of becoming osteoprogenitors persists in expanded *Nmp4*$^{-/-}$ MSPC cultures over 5–10 passages and removed from the supporting CD8^{+} T cells. In culture these cells displayed a modest increase in proliferative activity and perhaps this aspect of the phenotype contributes to the observed expanded pool of osteoprogenitors in vivo. In an earlier study, Noda and coworkers (15) demonstrated that *Nmp4*$^{-/-}$ BM yielded significantly more CFU-F^{Ob} mineralizing colonies at passage P_0 than WT BM. Our present data extend these observations and show that the serially passaged Nmp4$^{-/-}$ MSPCs maintain a strikingly enhanced capacity for mineralization compared with the capacity of the WT cultures. Taken together these observations suggest that there is a cell autonomous role of Nmp4 for regulating MSPC osteogenesis.

Our -omics data combined with our low-density array results suggest that upon challenge with an anabolic cue *Nmp4*$^{-/-}$ MSPCs produce autocrine/paracrine factors that enhance the replication and differentiation of neighboring osteoprogenitors, a key early event driving the PTH anabolic response (58). We observed that once *Nmp4*$^{-/-}$ cells were transferred to osteogenic medium they expressed strikingly elevated levels of the Nmp4 target gene *Igfbp2*, a strong autocrine/paracrine factor that enhances osteogenesis (47). Consistent with our observations, overexpression of Igfbp2 in MC3T3-E1 cells accelerated the time course of differentiation and mineralization as well as increased the total number of differentiating cells. By day 6, in this previous study, Igfbp2-overexpressing cells expressed twice as much OCN as control cultures and this difference persisted (47). This is a strikingly similar phenotype to the *Nmp4*$^{-/-}$ cells. Interestingly, the expression of the Nmp4 target gene *Igfbp4* was decreased in the *null* cells. This binding protein is a strong inhibitor of osteoblast differentiation (46), and thus its suppression may further accelerate and enhance the differentiation of the null cells.

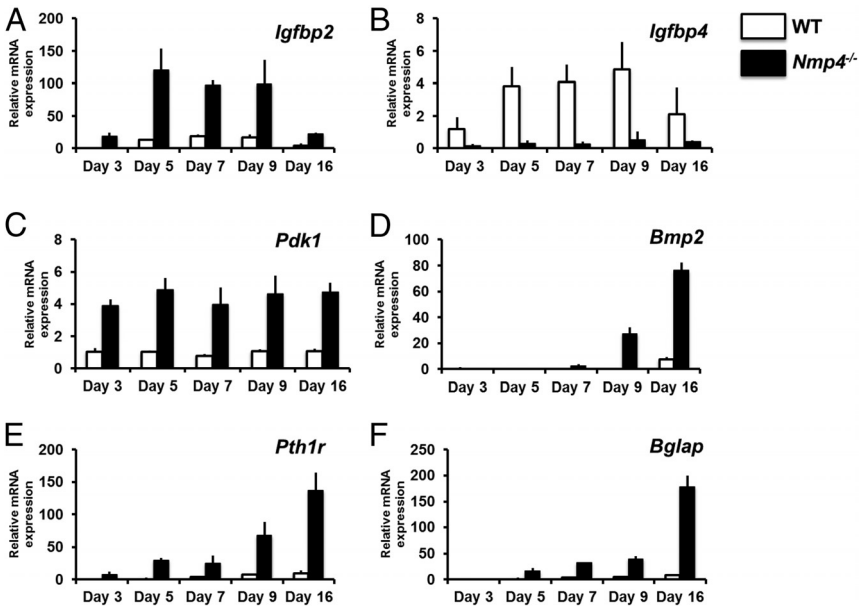

Figure 9. Comparison of mRNA expression profiles derived from nondifferentiating (d 3) and osteogenic-differentiating (d 5–16) WT and *Nmp4*$^{-/-}$ cells. All transcript levels are compared with WT day 3 providing a time course of expression. mRNA profiles (A) *Igfbp2*, (B) *Igfbp4*, (C) *Pdk1*, (D) *Bmp2*, and (E) *Pth1r* were derived from the TLDA system (Format 96a; Applied Biosystems) performed on a QuantStudio 7 Flex Real-Time PCR System and normalized with GusB. F, *Bglap* mRNA profile qRT-PCRs were performed on an Eppendorf Mastercycler RealPlex^{2} using *Rplp2* Mm03059047_gH) as the normalizer, as previously described (Robling et al [13]). Comparison of profiles using *GusB* and *Rplp2* as the normalizer showed no differences in the shape of the expression profiles.

Igf1 is a key mediator of the PTH anabolic response (59, 60), and although there was no notable alteration in the expression profiles of *Igf1* or *Igf1r* in the null cells, the expression of *Pdk1*, a target of Nmp4 and a key kinase component of the IGF1/insulin signaling pathway, was elevated. This may enhance the sensitivity of the *Nmp4*$^{-/-}$ cells to this growth factor. At the end of the 16-day culture period the *Nmp4*$^{-/-}$ cells exhibited an enhanced anabolic profile as evidenced by the elevated expressions of the nontarget Nmp4 genes *Bmp2*, *Pth1r*, and *Bglap*. Perhaps this is an autocrine/paracrine response to the earlier surge in *Igfbp2* expression. Indeed the Igf1 pathway plays a significant role in MSPC proliferation and mineralization (61, 62) and the null cells exhibited alterations in the expression not only of *Bglap* but the Nmp4 target extracellular matrix proteins

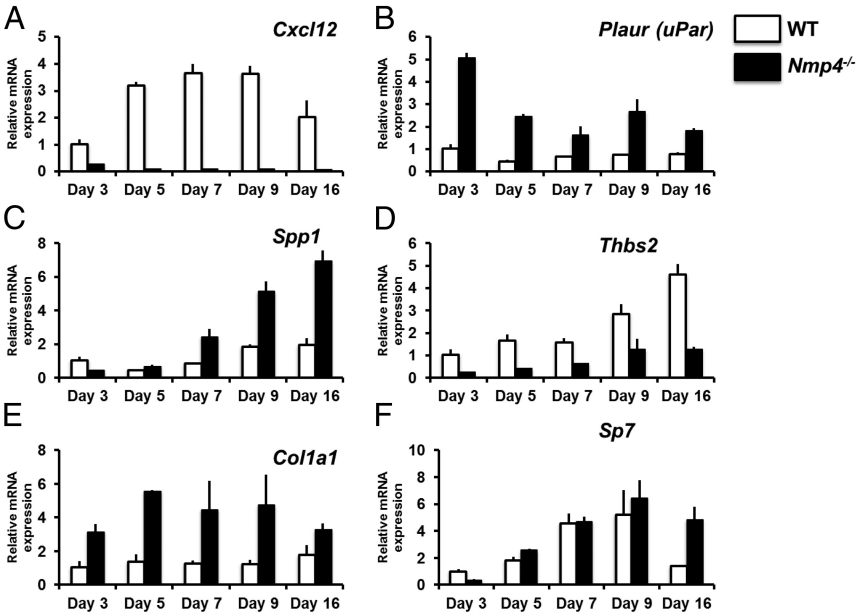

Figure 10. Comparison of mRNA expression profiles derived from nondifferentiating (d 3) and osteogenic-differentiating (d 5–16) WT and *Nmp4*$^{-/-}$ cells. All transcript levels are compared with WT day 3 providing a time course of expression. mRNA profiles (A) *Cxcl12*, (B) *Plaur*, (C) *Spp1*, (D) *Thbs2*, (E) *Col1a1* were derived from the TLDA system (Format 96a; Applied Biosystems) performed on a QuantStudio 7 Flex Real-Time PCR System and normalized with GusB. F, *Sp7* mRNA profile qRT-PCRs were performed on an Eppendorf Mastercycler RealPlex^2 using *Rplp2* (Mm03059047_gH) as the normalizer, as previously described (Robling et al [13]). The day-16 WT sample is the average of 2 replicates. Comparison of profiles using GusB and Rplp2 as the normalizer showed no differences in the shape of the expression profiles.

Col1a1, *Spp1*, and *Thbs2*. Although the molecular mechanisms underlying mineralization remain to be elucidated, *Spp1* is an anionic phosphoprotein expressed in mineralizing tissues that appears to regulate crystal size, shape, and location (54). *Thbs2* is an extracellular matrix glycoprotein that has pleiotropic effects on bone phenotype. This protein appears to suppress the MSPC osteoprogenitor pool but also supports mineralization (53, 63, 64). Therefore, whether the decrease in *Thbs2* expression in the *Nmp4*$^{-/-}$ cells impacts the observed alteration in the number of osteoprogenitors, alterations in mineralization or impacts cell phenotype in other ways remains to be determined. Finally, we observed no striking differences in the expression of the transcription regulators *Sp7* and *Runx2* between the genotypes. This suggests that disabling Nmp4 alters select aspects of the developing osteoblast phenotype.

The dramatic decrease in *Cxcl12* expression in the *Nmp4*$^{-/-}$ cells raises the question as to whether this plays a role in the observed increase in CFU-F$^{\text{alk phos+}}$ osteoprogenitors in the null mice (12, 15). CXCL12 and its receptor CXC receptor 4 (CXCR4) play key roles in maintaining the BM niche and CXCL12 is expressed by BM stromal cells and cells of the osteoblast lineage (52, 65). Ablation of the receptor CXCR4 in mature osteoblasts increased the number of CFU-F$^{\text{alk phos+}}$ osteoprogenitors recovered from these mice although the phenotype also included a decrease in BV/TV (51). Our results suggest that suppressing the expression of the CXCR4 ligand CXCL12 results in a similar impact on osteoprogenitor number but a different bone phenotype. The up-regulation of *Plaur* expression in the *Nmp4*$^{-/-}$ MSPCs may potentially contribute to the increased number of CFU-F$^{\text{alk phos+}}$ cells because abrogating the activity of this GPI-anchored receptor suppressed MSPC osteogenic differentiation (50). Finally, mutagenesis and rescuing experiments to determine whether the potential targets are truly functionally significant is the next required step for authenticating this new antianabolic network.

Further parsing of the enhanced *Nmp4*$^{-/-}$ BM osteogenic potential implicates the elevated frequency of CD8$^+$ T cells in both ovary-intact and ovx *Nmp4*$^{-/-}$ mice, although this requires functional confirmation in these models. The ovx null animals exhibited elevated numbers of CD8$^+$ T cells in both BM and PBL compartments throughout the entire treatment regimen, similar to what we previously observed in the younger ovary-intact *Nmp4*$^{-/-}$ mice, although this increase was limited to the BM (12). The elevated number of CD8$^+$ T cells is intriguing, because these cells are documented to amplify the PTH anabolic response (20, 22). MSPCs regulate T-cell proliferation and survival (66), and perhaps disabling Nmp4 derepresses this aspect of the cell-cell interaction, although this apparent alteration in proliferation/survival may be a cell autonomous feature of the *Nmp4*$^{-/-}$ T-cell phenotype. Although the elevated number of *Nmp4*$^{-/-}$ osteoprogenitors declined at 12-week postop, the higher number of *Nmp4*$^{-/-}$ CD8$^+$ T cells did not decrease. Therefore, although the augmented response to PTH might be weakened in the Nmp4$^{-/-}$ mice, it may not disappear because the persistent increased lymphocyte number might provide extra Wnt10b as a potent osteoprogenitor differentiation factor.

Why is there typically no difference between the amount of baseline trabecular bone in WT and *Nmp4*$^{-/-}$ mice despite the presence of an expanded pool of osteoprogenitors and CD8$^+$ T cells in the null BM? This phenomenon differs from the results of recent clinical trials in which neutralizing sclerostin, an inhibitor of the Wnt sig-

naling pathway and osteoblast differentiation, significantly increases baseline bone mineral density (67). Apparently disabling Nmp4 is not sufficient for driving excess bone formation but instead primes the aforementioned cells for activation by an anabolic cue. The occasionally observed elevated trabecular volume in untreated *Nmp4*$^{-/-}$ mice may be due to the sporadic local release of growth factors, eg, IGF1, IGFBP2 or BMP2. However, exogenous pharmacological doses of PTH provide a strong stimulus for triggering the response leading to the enhanced bone formation. Once activated by the anabolic cue, the *Nmp4*$^{-/-}$ cells produce the autocrine/paracrine factors that enhance the anabolic response.

Consistent with the requirement for a strong anabolic cue to trigger enhanced bone formation in the *Nmp4*$^{-/-}$ mice, disabling this transcription factor did not protect the animals from ovx-induced bone loss, indeed the initial rate of loss during the first 4 weeks after ovx was higher (L5) or nearly higher (distal femur) in the *Nmp4*$^{-/-}$ mice. These animals harbor a modestly elevated number of osteoclast progenitors (CFU-GM) (12) that upon differentiation exhibit an enhanced bone-resorbing activity in vitro (11). Therefore, a decrease in estrogen might accentuate this aspect of the phenotype. Moreover, differences in sex steroid levels may underlie why intact male *Nmp4*$^{-/-}$ mice did not lose bone under hind limb suspension (16). As mentioned, the *Nmp4*$^{-/-}$ baseline phenotype includes an occasional unprovoked enhancement in trabecular architecture, which we observed in the present study. That is to say, despite the elevated initial bone loss, the cohort of sham and ovx *Nmp4*$^{-/-}$ mice had more femoral and L5 trabecular bone compared with WT at the time of harvest (Table 3). However, there was no statistical difference between vehicle-treated animals in either the 4 or 8-week hormone therapy cohorts (Figures 2 and 3). Longitudinal studies for serum turnover markers coupled with peripheral quantitative computed tomography in live mice could be used to track the real-time dynamics of ovx-induced bone loss and subsequent therapy-induced bone gain between the WT and *Nmp4*$^{-/-}$ mice. In lieu of this, we employed a two-way ANOVA, which incorporates differences in control groups, to evaluate whether there is an interaction between genotype and treatment.

The present data also contribute to our knowledge as to how Nmp4 works at the molecular level. Nmp4 binds throughout the genome but is primarily localized to regions near the TSS and within the gene, consistent with mediating a regulatory role. GEM analysis confirmed the AT-rich homopolymeric-binding site and did not identify other consensus sequences expected only if Nmp4 also interacted with the genome indirectly via other DNA-binding proteins. Nmp4 association with the genome is responsive to PTH because hormone decreased genome-wide occupancy in the MC3T3-E1 cells after 1 hour of exposure. However, the impact of PTH on Nmp4 occupancy was gene and site-specific and hormone stimulation was observed to induce, remove, or have no effect on Nmp4 genomic occupancy. This may further augment the fine control that this transcription factor has over the regulation of osteoprogenitor and/or bone-forming capacity.

There is a critical need for osteoanabolic agents (68). We have taken a 2-pronged approach in our research to serve this clinical demand: 1) identify molecular and cellular mechanisms that could be used, for example in an adjuvant setting to promote enhanced efficacy or less frequent dosing with current osteoanabolic agents; and 2) identify innovative approaches to identify new drug targets/pathways or mechanisms of action that would provide needed substrate for the future drug discovery initiatives in bone disease, including osteoporosis. Our discovery-driven approaches have mapped a global network of Nmp4-regulated pathways potentially comprising a bone anti-anabolic axis. Further functional studies charting the hierarchy and interactions of theses network pathways will provide a novel integrated mechanism underlying the natural constraints on bone formation. We postulate that the Nmp4 antianabolic network may constitute a novel strategy to identify and reveal pharmacologically accessible pathways for adding new bone to the old skeleton.

Acknowledgments

Address all correspondence and requests for reprints to: Joseph P. Bidwell, Department of Anatomy and Cell Biology, Indiana University School of Medicine, Medical Science Building 5035, 635 Barnhill Drive, Indianapolis, IN 46202. E-mail: jbidwell@iupui.edu.

This work was supported in part by the Department of Defense Grant PR120563 (to J.P.B.), the Eli Lilly Grant 062079-00002B (to J.P.B.), and the National Institutes of Health Clinical and Translational Science Institute Predoctoral Fellowship TL1 000162 (to P.C.).

Disclosure Summary: P.C., M.B.A., Z.W., Y.S., S.H.-B., Y.H., D.H., F.M.P., A.G.R., S.J.W., F.-C.Y., and Y.L. have nothing to disclose. Eli Lilly and Company has awarded research funds to J.P.B. and M.R.A. Eli Lilly and Company funded part of this work. V.K. is an employee of Eli Lilly and Company and owns stock in this company. K.R.S., J.K.M., and Z.R.G. are employees of Eli Lilly and Company.

References

1. **Kraenzlin ME, Meier C.** Parathyroid hormone analogues in the treatment of osteoporosis. *Nat Rev Endocrinol*. 2011;7:647–656.
2. **Baron R, Hesse E.** Update on bone anabolics in osteoporosis treatment: rationale, current status, and perspectives. *J Clin Endocrinol Metab*. 2012;97:311–325.
3. **Cipriani C, Capriani C, Irani D, Bilezikian JP.** Safety of osteoanabolic therapy: a decade of experience. *J Bone Miner Res*. 2012;27:2419–2428.
4. **Yu EW, Neer RM, Lee H, et al.** Time-dependent changes in skeletal response to teriparatide: escalating vs. constant dose teriparatide (PTH 1–34) in osteoporotic women. *Bone*. 2011;48:713–719.
5. **McClung MR, Grauer A, Boonen S, et al.** Romosozumab in postmenopausal women with low bone mineral density. *N Engl J Med*. 2014;370:412–420.
6. **Padhi D, Jang G, Stouch B, Fang L, Posvar E.** Single-dose, placebo-controlled, randomized study of AMG 785, a sclerostin monoclonal antibody. *J Bone Miner Res*. 2011;26:19–26.
7. **Saag KG, Zanchetta JR, Devogelaer JP, et al.** Effects of teriparatide versus alendronate for treating glucocorticoid-induced osteoporosis: thirty-six-month results of a randomized, double-blind, controlled trial. *Arthritis Rheum*. 2009;60:3346–3355.
8. **Black DM, Greenspan SL, Ensrud KE, et al.** The effects of parathyroid hormone and alendronate alone or in combination in postmenopausal osteoporosis. *N Engl J Med*. 2003;349:1207–1215.
9. **Cosman F, Eriksen EF, Recknor C, et al.** Effects of intravenous zoledronic acid plus subcutaneous teriparatide [rhPTH(1–34)] in postmenopausal osteoporosis. *J Bone Miner Res*. 2011;26:503–511.
10. **Finkelstein JS, Wyland JJ, Lee H, Neer RM.** Effects of teriparatide, alendronate, or both in women with postmenopausal osteoporosis. *J Clin Endocrinol Metab*. 2010;95:1838–1845.
11. **Childress P, Philip BK, Robling AG, et al.** Nmp4/CIZ suppresses the response of bone to anabolic parathyroid hormone by regulating both osteoblasts and osteoclasts. *Calcif Tissue Int*. 2011;89:74–89.
12. **He Y, Childress P, Hood M Jr, et al.** Nmp4/CIZ suppresses the parathyroid hormone anabolic window by restricting mesenchymal stem cell and osteoprogenitor frequency. *Stem Cells Dev*. 2013;22:492–500.
13. **Robling AG, Childress P, Yu J, et al.** Nmp4/CIZ suppresses parathyroid hormone-induced increases in trabecular bone. *J Cell Physiol*. 2009;219:734–743.
14. **Krane SM.** Identifying genes that regulate bone remodeling as potential therapeutic targets. *J Exp Med*. 2005;201:841–843.
15. **Morinobu M, Nakamoto T, Hino K, et al.** The nucleocytoplasmic shuttling protein CIZ reduces adult bone mass by inhibiting bone morphogenetic protein-induced bone formation. *J Exp Med*. 2005;201:961–970.
16. **Hino K, Nakamoto T, Nifuji A, et al.** Deficiency of CIZ, a nucleocytoplasmic shuttling protein, prevents unloading-induced bone loss through the enhancement of osteoblastic bone formation in vivo. *Bone*. 2007;40:852–860.
17. **Nakamoto T, Shiratsuchi A, Oda H, et al.** Impaired spermatogenesis and male fertility defects in CIZ/Nmp4-disrupted mice. *Genes Cells*. 2004;9:575–589.
18. **Isern J, Martín-Antonio B, Ghazanfari R, et al.** Self-renewing human bone marrow mesenspheres promote hematopoietic stem cell expansion. *Cell Rep*. 2013;3:1714–1724.
19. **Méndez-Ferrer S, Michurina TV, Ferraro F, et al.** Mesenchymal and haematopoietic stem cells form a unique bone marrow niche. *Nature*. 2010;466:829–834.
20. **Bedi B, Li JY, Tawfeek H, et al.** Silencing of parathyroid hormone (PTH) receptor 1 in T cells blunts the bone anabolic activity of PTH. *Proc Natl Acad Sci USA*. 2012;109:5.
21. **Li JY, Walker LD, Tyagi AM, Adams J, Weitzmann MN, Pacifici R.** The sclerostin-independent bone anabolic activity of intermittent PTH treatment is mediated by T-cell-produced Wnt10b. *J Bone Miner Res*. 2014;29:43–54.
22. **Terauchi M, Li JY, Bedi B, et al.** T lymphocytes amplify the anabolic activity of parathyroid hormone through Wnt10b signaling. *Cell Metab*. 2009;10:229–240.
23. **Bidwell JP, Childress P, Alvarez MB, et al.** Nmp4/CIZ closes the parathyroid hormone anabolic window. *Crit Rev Eukaryot Gene Expr*. 2012;22:205–218.
24. **Nakamoto T, Yamagata T, Sakai R, et al.** CIZ, a zinc finger protein that interacts with p130(cas) and activates the expression of matrix metalloproteinases. *Mol Cell Biol*. 2000;20:1649–1658.
25. **Alvarez M, Thunyakitpisal P, Morrison P, Onyia J, Hock J, Bidwell JP.** PTH-responsive osteoblast nuclear matrix architectural transcription factor binds to the rat type I collagen promoter. *J Cell Biochem*. 1998;69:336–352.
26. **Shah R, Alvarez M, Jones DR, et al.** Nmp4/CIZ regulation of matrix metalloproteinase 13 (MMP-13) response to parathyroid hormone in osteoblasts. *Am J Physiol Endocrinol Metab*. 2004;287:16.
27. **Thunyakitpisal P, Alvarez M, Tokunaga K, et al.** Cloning and functional analysis of a family of nuclear matrix transcription factors (NP/NMP4) that regulate type I collagen expression in osteoblasts. *J Bone Miner Res*. 2001;16:10–23.
28. **Torrungruang K, Alvarez M, Shah R, Onyia JE, Rhodes SJ, Bidwell JP.** DNA binding and gene activation properties of the Nmp4 nuclear matrix transcription factors. *J Biol Chem*. 2002;277:16153–16159.
29. **Alvarez MB, Childress P, Philip BK, et al.** Immortalization and characterization of osteoblast cell lines generated from wild-type and Nmp4-null mouse bone marrow stromal cells using murine telomerase reverse transcriptase (mTERT). *J Cell Physiol*. 2012;227:1873–1882.
30. **Shen ZJ, Nakamoto T, Tsuji K, et al.** Negative regulation of bone morphogenetic protein/Smad signaling by Cas-interacting zinc finger protein in osteoblasts. *J Biol Chem*. 2002;277:29840–29846.
31. **Yang Z, Bidwell JP, Young SR, Gerard-O'Riley R, Wang H, Pavalko FM.** Nmp4/CIZ inhibits mechanically induced β-catenin signaling activity in osteoblasts. *J Cell Physiol*. 2010;223:435–441.
32. **Stamatoyannopoulos JA, Snyder M, Hardison R, et al.** An encyclopedia of mouse DNA elements (mouse ENCODE). *Genome Biol*. 2012;13:2012–2013.
33. **Wu X, Estwick SA, Chen S, et al.** Neurofibromin plays a critical role in modulating osteoblast differentiation of mesenchymal stem/progenitor cells. *Hum Mol Genet*. 2006;15:2837–2845.
34. **Bouxsein ML, Boyd SK, Christiansen BA, Guldberg RE, Jepsen KJ, Müller R.** Guidelines for assessment of bone microstructure in rodents using micro-computed tomography. *J Bone Miner Res*. 2010;25:1468–1486.
35. **Dempster DW, Compston JE, Drezner MK, et al.** Standardized nomenclature, symbols, and units for bone histomorphometry: a 2012 update of the report of the ASBMR Histomorphometry Nomenclature Committee. *J Bone Miner Res*. 2013;28:2–17.
36. **Li H, Durbin R.** Fast and accurate short read alignment with Burrows-Wheeler transform. *Bioinformatics*. 2009;25:1754–1760.
37. **Rosenbloom KR, Sloan CA, Malladi VS, et al.** ENCODE data in the UCSC Genome Browser: year 5 update. *Nucleic Acids Res*. 2013;41:27.
38. **Guo Y, Mahony S, Gifford DK.** High resolution genome wide binding event finding and motif discovery reveals transcription factor spatial binding constraints. *PLoS Comput Biol*. 2012;8:9.
39. **Huang da W, Sherman BT, Lempicki RA.** Systematic and integrative analysis of large gene lists using DAVID bioinformatics resources. *Nat Protoc*. 2009;4:44–57.
40. **Supek F, Bosnjak M, Skunca N, Smuc T.** REVIGO summarizes and visualizes long lists of gene ontology terms. *PLoS One*. 2011;6:18.
41. **Auerbach RK, Chen B, Butte AJ.** Relating genes to function: identifying enriched transcription factors using the ENCODE ChIP-Seq significance tool. *Bioinformatics*. 2013;29:1922–1924.

42. **Vieira Potter VJ, Strissel KJ, Xie C, et al.** Adipose tissue inflammation and reduced insulin sensitivity in ovariectomized mice occurs in the absence of increased adiposity. *Endocrinology*. 2012;153:4266–4277.
43. **Harada A, Okada S, Konno D, et al.** Chd2 interacts with H3.3 to determine myogenic cell fate. *EMBO J*. 2012;31:2994–3007.
44. **Lin W, Srajer G, Evrard YA, Phan HM, Furuta Y, Dent SY.** Developmental potential of Gcn5(−/−) embryonic stem cells in vivo and in vitro. *Dev Dyn*. 2007;236:1547–1557.
45. **Nascimento EM, Cox CL, MacArthur S, et al.** The opposing transcriptional functions of Sin3a and c-Myc are required to maintain tissue homeostasis. *Nat Cell Biol*. 2011;13:1395–1405.
46. **Miyakoshi N, Richman C, Qin X, Baylink DJ, Mohan S.** Effects of recombinant insulin-like growth factor-binding protein-4 on bone formation parameters in mice. *Endocrinology*. 1999;140:5719–5728.
47. **Xi G, Wai C, DeMambro V, Rosen CJ, Clemmons DR.** IGFBP-2 directly stimulates osteoblast differentiation. *J Bone Miner Res*. 2014;29:2427–2438.
48. **Calleja V, Laguerre M, de Las Heras-Martinez G, et al.** Acute regulation of PDK1 by a complex interplay of molecular switches. *Biochem Soc Trans*. 2014;42:1435–1440.
49. **Furlan F, Galbiati C, Jorgensen NR, et al.** Urokinase plasminogen activator receptor affects bone homeostasis by regulating osteoblast and osteoclast function. *J Bone Miner Res*. 2007;22:1387–1396.
50. **Kalbasi Anaraki P, Patecki M, Larmann J, et al.** Urokinase receptor mediates osteogenic differentiation of mesenchymal stem cells and vascular calcification via the complement C5a receptor. *Stem Cells Dev*. 2014;23:352–362.
51. **Shahnazari M, Chu V, Wronski TJ, Nissenson RA, Halloran BP.** CXCL12/CXCR4 signaling in the osteoblast regulates the mesenchymal stem cell and osteoclast lineage populations. *FASEB J*. 2013;27:3505–3513.
52. **Sugiyama T, Kohara H, Noda M, Nagasawa T.** Maintenance of the hematopoietic stem cell pool by CXCL12-CXCR4 chemokine signaling in bone marrow stromal cell niches. *Immunity*. 2006;25:977–988.
53. **Alford AI, Terkhorn SP, Reddy AB, Hankenson KD.** Thrombospondin-2 regulates matrix mineralization in MC3T3-E1 pre-osteoblasts. *Bone*. 2010;46:464–471.
54. **Hunter GK.** Role of osteopontin in modulation of hydroxyapatite formation. *Calcif Tissue Int*. 2013;93:348–354.
55. **Komori T.** Signaling networks in RUNX2-dependent bone development. *J Cell Biochem*. 2011;112:750–755.
56. **Mizoguchi T, Pinho S, Ahmed J, et al.** Osterix marks distinct waves of primitive and definitive stromal progenitors during bone marrow development. *Dev Cell*. 2014;29:340–349.
57. **Sacchetti B, Funari A, Michienzi S, et al.** Self-renewing osteoprogenitors in bone marrow sinusoids can organize a hematopoietic microenvironment. *Cell*. 2007;131:324–336.
58. **Jilka RL.** Molecular and cellular mechanisms of the anabolic effect of intermittent PTH. *Bone*. 2007;40:1434–1446.
59. **Bikle DD, Wang Y.** Insulin like growth factor-I: a critical mediator of the skeletal response to parathyroid hormone. *Curr Mol Pharmacol*. 2012;5:135–142.
60. **Elis S, Courtland HW, Wu Y, et al.** Elevated serum IGF-1 levels synergize PTH action on the skeleton only when the tissue IGF-1 axis is intact. *J Bone Miner Res*. 2010;25:2051–2058.
61. **Kumar S, Ponnazhagan S.** Mobilization of bone marrow mesenchymal stem cells in vivo augments bone healing in a mouse model of segmental bone defect. *Bone*. 2012;50:1012–1018.
62. **Xian L, Wu X, Pang L, et al.** Matrix IGF-1 maintains bone mass by activation of mTOR in mesenchymal stem cells. *Nat Med*. 2012;18:1095–1101.
63. **Hankenson KD, Bain SD, Kyriakides TR, Smith EA, Goldstein SA, Bornstein P.** Increased marrow-derived osteoprogenitor cells and endosteal bone formation in mice lacking thrombospondin 2. *J Bone Miner Res*. 2000;15:851–862.
64. **Hankenson KD, Bornstein P.** The secreted protein thrombospondin 2 is an autocrine inhibitor of marrow stromal cell proliferation. *J Bone Miner Res*. 2002;17:415–425.
65. **Jung Y, Wang J, Schneider A, et al.** Regulation of SDF-1 (CXCL12) production by osteoblasts; a possible mechanism for stem cell homing. *Bone*. 2006;38:497–508.
66. **Wang L, Zhao Y, Shi S.** Interplay between mesenchymal stem cells and lymphocytes: implications for immunotherapy and tissue regeneration. *J Dent Res*. 2012;91:1003–1010.
67. **Becker CB.** Sclerostin inhibition for osteoporosis–a new approach. *N Engl J Med*. 2014;370:476–477.
68. **Lewiecki EM.** New targets for intervention in the treatment of postmenopausal osteoporosis. *Nat Rev Rheumatol*. 2011;7:631–638.